UNIVERSITY OF LIVERPOOL

Nonlinear Power System Stabilizer based on Uncertainties and Disturbance Estimator

Thesis submitted in accordance with the requirements of the University of Liverpool for the degree of Doctor in Philosophy

by

Wenzheng Deng

March 2019

Department of Electrical Engineering and Electronics

The University of Liverpool

Acknowledgement

I would like to give my heartfelt thanks to my supervisor, Dr. L. Jiang, whose encouragement, guidance and support enabled me to develop a deep understanding of my work. Without his consistent and illuminating instructions, my research work and my life could not proceed to this stage. The skill of researching, writing and presenting he taught me will benefit me throughout my life.

I offer my regards and blessings to all of the members of Smart Grid Control and Renewable Energy Group, the University of Liverpool, especially to Dr. Liuying Li, Dr. Yaxing Ren for their invalubel gudance and help.

I would like to devote my deepest thank and love to my family and friends, who always encourage me when my project went through failures one after another. I am grateful to the Department of Electrical Engineering and Electronics at the University of Liverpool, for providing the research facilities that made it possible for me to carry out this research.

Abstract

Nowadays power system tends to integrate more renewable generations such as wind and solar power, flexible loads operating in plug-play mode, and intensively interaction with information communication technology. All those changes bring lots of challenges for the operation and control of power system, specially the fast changing of operation points, uncertainties from generation and load sides, and fast dynamics caused by power electronic devices and reduced inertia; which demand advanced control system to ensure the stable and economical operation of power system. As synchronous generators still generate the most electricity worldwide and act as the main contributor of power system stability, this thesis aims at investigating a new type of power system stabilizer (PSS) for synchronous generator to improve the overall power system stability. To deal with fast-changing unknown uncertainties and disturbances, estimation and compensation of disturbance and uncertainties in time-domain and frequency domain observer are proposed, respectively.

After recalling the conventional PSS based on lead/lag phase compensation techniques and two typical analysis methods: damping torque analysis and the modal analysis based on small-signal stability, feedback linearization control and extended-order perturbation observer (ESO) based nonlinear adaptive control have been applied to design a nonlinear PSS and ESO-PSS, state feedback and output feedback, respectively. The ESO-PSS can effectively deal with unknown states and the disturbances and is verified by simulation studies.

An uncertain and disturbance estimator (UDE) designed in frequency domain has been proposed to replace the ESO in time domain, with merits of easy implementation and embedded with the conventional lead/lag type PSS, while maintaining the capability of disturbance/nonlinearities rejection and robust to model uncertainty, and only requiring one measurement. Different feedback signals, speed/power/ acceleration power are investigated and compared in SMIB with other types of CPSSs and nonlinear PSSs respectively.

Performance of the proposed UDEPSS has been tested in the multi-machine power system for their capability of damping of inter-area oscillation. IEEE standard multi-band PSS, PSS4B, and the classical speed type and acceleration power type PSSs are compared. The Speed type UDEPSS can provide better performance than all other PSSs which has much simpler structure than the PSS4B and very good robustness to system operation points and uncertainties due to the compensation of the disturbance and uncertainties. Moreover, it only requires one measurement which make it be more practical than those ESPO based PSS which requires rotor angle measurement and high-order derivatives of the rotor speed.

Declaration

The author hereby declares that this thesis is record of work carried out in the Department of Engineering and Electronics at the University of Liverpool during the period from October 2014 to March 2019. The thesis is original in content except where otherwise indicated.

List of Figures

List of Tables

Symbols & Abbreviations

p.u.	Per unit.
AVR	Automatic voltage regulator.
SISO	Single input single output.
WAMS	Wide-area monitoring system.
UDE	Uncertainty and disturbance estimator.
SMIB	Single machine infinite bus system.
NPSS	Nonlinear power system stabilizer.
CPSS	Conventional power system stabilizer.
DTA	Damping torque analysis.
CNAC	Coordinated nonlinear adaptive control.
FLC	Feedback linearization control.
ESO	Extended-state perturbation observer.
ESPO	Extended-order state and perturbation observer.
TDC	Time delay control.
NAC	Nonlinear adaptive control.
AC	Alternating current.
FACTS	Flexible alternating current transmission systems.
PSS	Power system stabilizer.
PID	Proportional-integral-differential.

Table of Content

Chapter 1 Introduction

1.1 Background

Modern power system is one of the largest interconnected industrial systems which consists of large number of components such as generator, transformer, transmission line, circuit breaker, power electronic based devices, and different types of loads [1]. Usually the electricity is generated from large-capacity synchronous generators, increased the voltage level by transformer, connected to high-voltage transmission network and transmitted to the load center far away from the generation site, and finally reduced the voltage level and supply to the consumer via medium and low-voltage level distribution system. The transmission network is typically span national level across several hundreds and thousands of miles such as National Grid UK and China State Grid, one of the largest interconnected grids in the world [7].

Under the recent trend of making power system more environment friendly and sustainable, one of the other directions are to develop a micro-grid which composes of local and distributed energy sources such as renewable generations from wind and solar power, energy storage, combined heat, and power plant. One main advantage of the micro-grid the electricity generated will be consumed by the local end users to reduce the transmission losses. The combined heat and electricity from combined heat and power (CHP) plant in micro grid can also provide electricity and heat to local

users and thus has very high efficiency [2].

Both the large-scale power system and the micro-grid require control system to maintain its operation and stability. Control system plays an important and necessary role to reliably and efficiently operate an interconnected power system and micro-grid [2]. Power system control includes a combination of manual operator controls and automatic controls. The operators control the balance between the power generation and the load demand under normal operating conditions, and to provide electricity with satisfactory range of voltage, frequency and power quality as well, to supply the load demand [1,3,4]. This is also called system dispatch at the control center, and the main task is to schedule the generation of electricity based on the prediction of load. The automatic controls make the fast adjustments necessary to maintain the system voltage and frequency within design limits following normal load disturbances and sudden faults happening in the system.

Most large capacity synchronous generators have installed speed governing systems which automatically adjust the output of the prime mover to keep the generator speed constant, automatic voltage regulator (AVR) which adjust the generators' excitation to maintain the generator voltages constant. Moreover, because of the use of high gain negative feedback in the AVR, the generator suffers from poor damping of low frequency oscillation after load disturbance and power system fault, power system stabilizer is designed to improve the damping of the oscillation of the rotor angle (so as the output power) [16,17].

1.1.1 Power System Stability

Power system stability is like the stability of any dynamic system and has similar fundamental mathematical underpinnings. Power system stability refers to the ability of the power system to return back to a normal state of equilibrium (a given initial operating condition) after being subjected to a physical disturbance such as load disturbance and power system faults, and remain the most system variables bounded during the transient period after the disturbance [9]. Conversely, instability of power system means a condition which lose synchronism of any synchronous generator in the power system to other synchronous generators. Figure 1.1 and 1.2 show two different blackouts after power system stability problems occurred. The power system is a highly nonlinear system that operates in a constantly changing environment, loads, generator outputs and key operating parameters change continually [9]. In conventional power systems, the load is uncertain and time-varying while the generators are controlled to follow the load variations. Nowadays, with the increasing penetration of uncontrollable and intermittent renewable power generation, such as wind power and solar power generations, more uncertainties are introduced from the generation side as the output of the wind farm and the solar farm are usually operated to generate as much power as they can while depending the weather condition which sometimes is more difficulty to be predicted than the load side. With the increased uncertainties introduced from the generation side, plus the usage of information and communication technology (ICT), advanced and fast acting controls are demanded for a smart and flexible future power grid [8].

Power system stability has been recognized as an important problem for secure system operation as many major blackouts caused by power system instability have illustrated the importance of this phenomenon [10, 11].

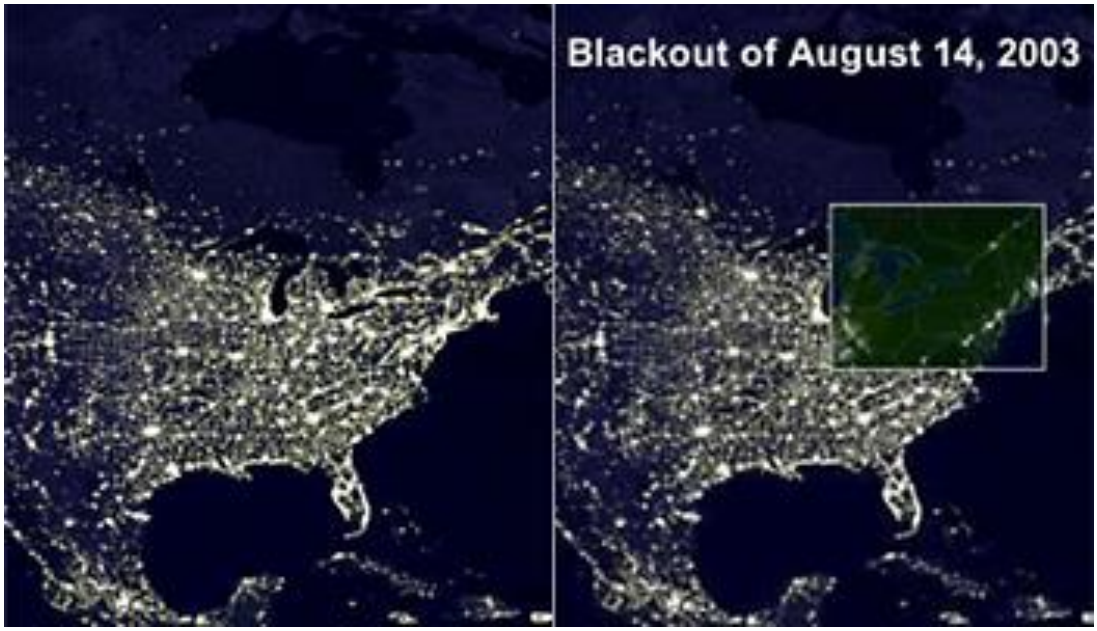

Figure 1.1: 2003 blackout in eastern Canada and the US [1]

The image dramatically illustrates the extent of the blackout on August 14, 2003, and it was found that key PSS's were either out of service or poorly tuned.

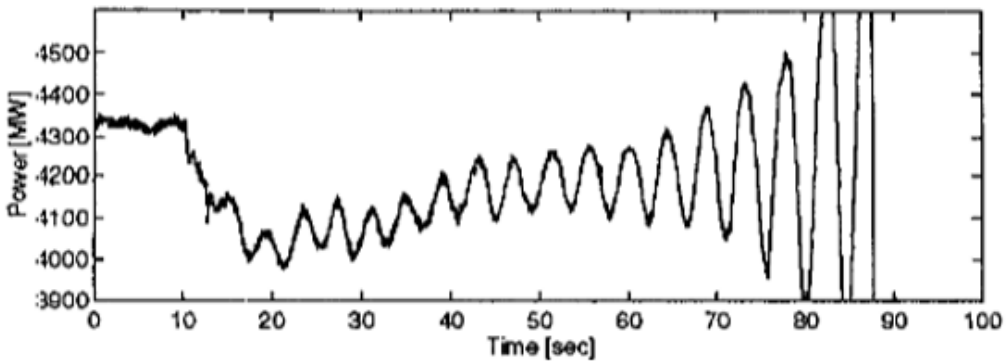

Active power on California-Oregon Intertie (COI) transmission line

(a)

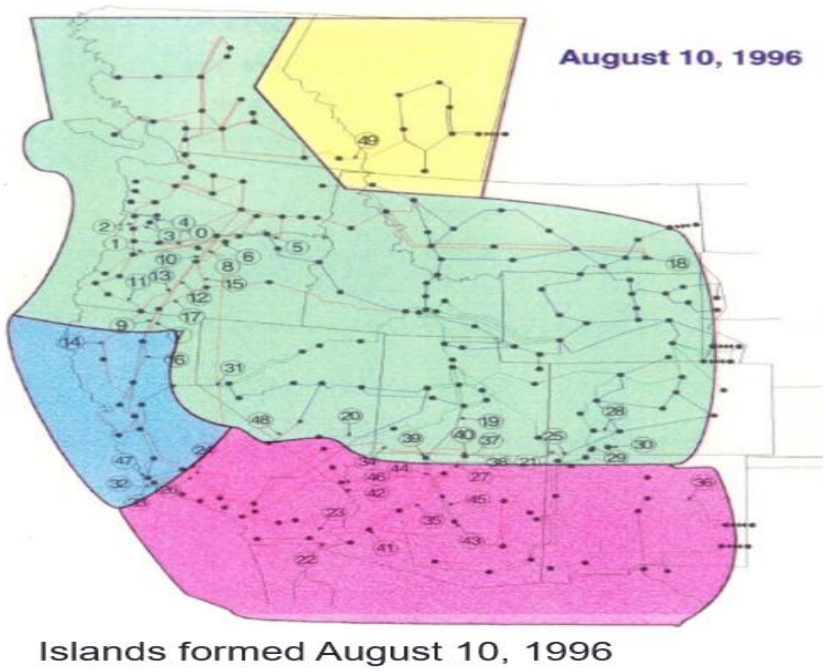

(b)

Figure 1.2: Western system coordinating council system blackout [122, 123]

The figures show that the wester system coordinating council system has been broken up into four islands with loss of 30390 MW and 7.49 million customers affected which low frequency oscillation detected.

Historically, transient instability has been the dominant stability problem on most systems. Nowadays different forms of system instability have emerged, such as voltage stability, frequency stability, sub-synchronous oscillation, low-frequency oscillation and interarea oscillations. Figure 1.3 show the classification of different power system stability. Those new stability problems are the results of the power system evolution through the continuing growth in interconnections such as (1): the use of new technologies and controls such as more power electronics devices and flexible alternating current transmission system (FACTS) and the information and communication technologies (ICT) in the closed-loop and the developed smart grid

technology with the involvement of demand-side participation; (2): the increased operation in highly stressed conditions in the electricity market environment, and the fast growing of renewable power generations [17].

Based on the guideline reference [9], power system stability can be broadly classified into rotor angle, voltage and frequency stability. Figure 1 just show the classification of different power system stability. Each of these three stabilities can be further classified into large disturbance or small disturbance, short term or long term, respectively. When subjected to a disturbance, the stability of the system depends on the initial operating condition as well as the nature of the disturbance.

Rotor angle stability refers to the ability of synchronous machines of an interconnected power system to remain in synchronism after being subjected to a disturbance. It depends on the ability to maintain/restore equilibrium between electromagnetic torque and mechanical torque of each synchronous machine in the system. Instability that may result occurs in the form of increasing angular swings of some generators leading to their loss of synchronism with other generators [9]. The change in electromagnetic torque of a synchronous machine following a perturbation can be resolved into two components. The first is synchronizing torque which in phase with rotor angle deviation and the second is damping torque which in phase with the speed deviation [4].

System stability depends on the existence of both components of torque for each of the synchronous machines. Lacking enough synchronizing torque results in aperiodic or non-oscillatory instability, whereas lack of damping torque results in

oscillatory instability (low frequency oscillation). As synchronous generators are still the main generation equipment installed worldwide, despite the fast growing of renewable generations [1, 2]. This thesis targets to design a new type of power system stabilizer to improve the rotor angle stability.

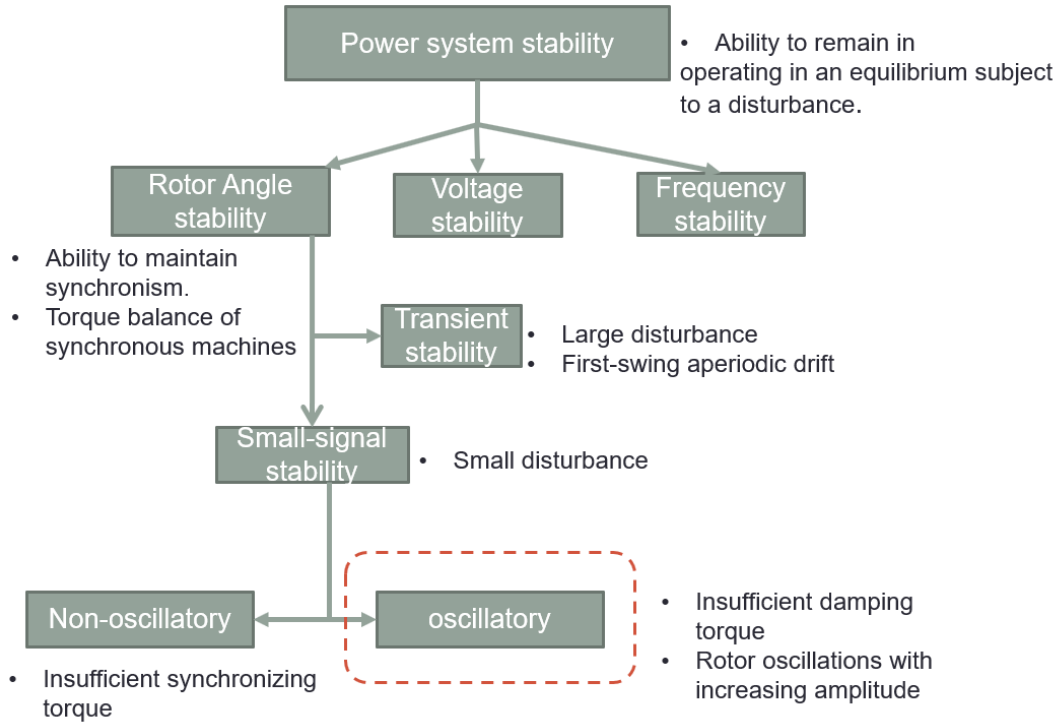

Figure 1.3: Classification of different power system stability [1]

1.1.2 Power System Stabilizer

For most utilities around the world, the power system stabilizer (PSS) installed in synchronous generator is probably the most frequently used device for resolving oscillatory stability problems. Power system stabilizers are generator control equipment which are used in excitation systems to enhance the damping of rotor oscillation caused due to small signal disturbance [17,18]. The action of a PSS is to extend the angular stability limits of a power system by providing supplemental damping to the oscillation of synchronous machine rotors through the generator excitation. A synchronous generator which equipped with power system stabilizer is show in Figure 1.4.

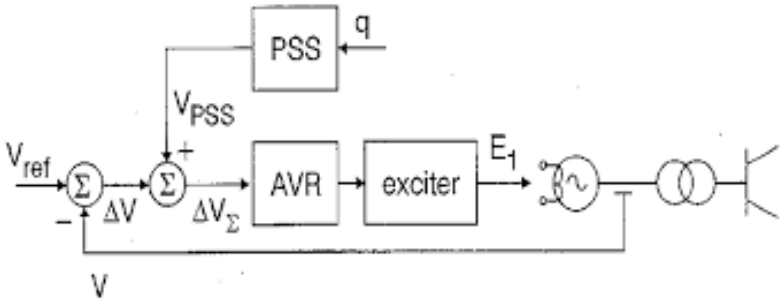

Figure 1.4: Synchronous generator equipped with Power System Stabilizer [122]

The basic function of a PSS is to extend stability limits by modulating generator excitation to provide damping to the oscillations of synchronous machine rotors relative to one another. These oscillations of concern typically occur in the frequency range of approximately 0.2 to 2.5 Hz, and insufficient damping of these oscillations may limit the ability to transmit power. To provide damping, the stabilizer must produce a component of electrical torque on the rotor which is in phase with speed variations. The basic design principle of PSS is that the PSS's transfer function must

compensate the gain/phase characteristic of the excitation system, generator, AVR and the connected power grid, such that the PSS must provide torque in phase with the speed variation. Thus, depending on the type of feedback inputs, the transfer function of PSS needs corresponding phase led/lag compensation part [18, 19].

The PSS is mainly designed based on classical control theory and frequency analysis method, and single-input and single-output (SISO) system. It is based on one frequency only (for calculation of the phase of the transfer function) and one operation point upon which the nonlinear model linearized at one operation point. It works well for single generator connected with infinite bus system (its oscillation is called local mode). However, power system is a typical nonlinear system operating at time-varying operation points. It is a challenging task to tune PSS for providing satisfactory performance at multi-machine power system [24,25]. For example, there are oscillation with even low frequency such as, inter-area mode between 0.17 and 0.25 Hz at Brazil power grid the north-south interconnection [31], on the UCTE/CENTREL interconnection in Europe at 0.36, 0.26, and even 0.19 Hz [33], and serious 0.4-Hz oscillations in several post-contingency in the 2003 blackout in eastern Canada and the U.S. grid. Thus, it is a cost and difficult task to re-tune the PSSs even for same power grid under the configuration changes and fault conditions. PSSs suffer another drawback of being liable to cause great variations in the voltage profile and they may even result in leading power factor operation and losing system stability under severe disturbances, especially those three phase faults which may occur at the generator terminals [1].

While most of the existing PSSs in nowadays systems are power acceleration analog devices based on a design dating back to 1980s, the utility was approached at the beginning of the nineties by manufactures offering a digital PSS based on the integral of accelerating power which is represented as PSS2B PSS. As known today, this modern PSS can easily be tuned as speed-based PSS, while mitigating two major operational problems which had restricted the application of the old PSS technology utilizing electrical power or terminal frequency, namely the excess VAR modulation during mechanical power reference changes for the first and adverse torsional interactions for the second [37].

Following the western U.S. interconnection blackouts in 1996 and the 2003 blackouts in eastern Canada, it was found that key PSS's were either out of service or poorly tuned [10-13]. The difficulty of tuning a proper PSSs lies in the fact that the conventional PSSs are designed in the frequency domain and use the frequency response method such as lead-lag phase compensation to damp one specific oscillation frequency. It is based on single input single output (SISO) method and tuned on the one-point linearizing model at one operation point. Thus, the PSS performance will be affected by the operation point variation and the interaction between multiple PSSs. Although PSS was introduced and extensively used a long time ago and despite its inherent simplicity, it may still be one of the most misunderstood and misused pieces of generator control equipment [37]. Performance and limitations have been compared for PSS4B, PSS2B and CSSs (speed type PSS and acceleration type PSS) in [37].

Lots of optimization and advanced control methods have been proposed to improve the performance of the PSS, such as optimal control and eigenvalue assignment [27, 61]. Since these techniques do not consider the presence of system uncertainties like system nonlinear characteristics, variation of system configuration due to unpredictable disturbances, loading conditions into consideration in the system modelling, the robustness of these PSSs against uncertainties cannot be guaranteed [29,30,54,55, 59,65]. Advanced control method based on robust control theory was another developed method to improve power system stability, and it was proved that this kind of PSS has much better controller characteristics (less settle time and overshoot) and appropriate control systems against disturbance compared with conventional controllers [29,30,59]. However, in advanced control methods, system efficiency maybe greatly reduced by changing operating point and the presence of oscillation is also one of the main disadvantages of this classic methods. Moreover, the robustness of the system to slow down the response time of the system will lead to high cost as well.

Artificial Intelligence based methods, such as Genetic Algorithm /Particle swarm optimization (PSO) Algorithm [67,74], rule-based bacteria foraging [62], neural network [68], fuzzy control [70,72, 75-77] , dynamic programming [69], self-tuning adaptive control [79], system identification based control [71] have been applied to improve the robustness and find out the optimal parameters. Synchronous generator still plays a dominant role for generating most of electricity in the world despite of the fast developing of renewable generations. PSS designed for power system with

renewable energy have been carried out, such as largescale PV plant [85], and wind farms [86].

Another problem of the classical PSS is it is designed mainly for damping the local-mode oscillation, i.e. single generator oscillates against the infinite bus system. Inter-area oscillation at the frequency below 1 HZ has become a main concern towards to the expand and interconnection of large generators in different area. The capability of the PSS using the local signal as the feedback inputs to damp the inter-area oscillation is limited [33, 34, 47]. Multi-band PSS4B's performance to damp the inter-area oscillation has been studied in [48]. Wide-area damping control based on the usage of the remote target signal as the feedback input signal has been proposed to provide the damping to the inter-area mode directly, with the cost of communication network for transmitting the remote signal and also possible reality and stability problem caused by the communication networks [90-94].

Wide-area damping control uses the measurements obtained from wide-area monitoring system (WAMS) [89-94]. Providing time synchronized data of power system operating states, WAMS will play a crucial role in the smart grid protection and control. WAMS helps insure efficient energy transmission as well as reliable and optimal grid management. As the key enabler of a smart grid, numerous sensors such as phasor measurement units transmit real-time dynamic data to power system control centers so that monitoring and control of the whole system is possible. One of the most common applications of phasor measurement units (PMUs) is power system monitoring, especially for monitoring wide-area disturbances and low frequency

electromechanical oscillations. PMUs are a solution to increase observability in monitoring systems and provide additional insight of power system dynamics [90]. Though the WAMS based controllers provide many advantages comparing to the local-signals based controllers, especially for providing damping of those inter-area oscillations which is not observable and thus un-controllable from the local controllers, the usage of communication networks for transmitting of remote signals from the RTU (Remote Terminal Unit) require additional costs and most importantly, cause additional disturbances into the control-loop, such as the latency of networks and data drop-outs, which will reduce the overall system stability and reliability [87-94].

1.1.3 Disturbance Observer Based Control Design

Most of the well-developed control theories, either in the frequency domain or in the time domain, deals with systems whose mathematical representations are completely known. However, in many practical situations especially power systems, the parameters of the system are either poorly known or operate in environments where unpredictable large system parameter variations and unexpected disturbances are possible. Several solutions based on advanced control techniques have been developed so far. One of the primary methods is adaptive control [7]. In adaptive control, the structure of the controller is selected a priori, usually proportional-derivative (PD) or proportional-integral-derivative (PID) type controller. The controller gains are then updated using a recursively estimated parameters of the plant so that the plant output closely follows the desired response. Another control theory

is time delay control (TDC) [98]. Based on the assumption that a continuous signal remains unchanged during a small enough period, the past observation of uncertainties and disturbances is used to modify the control action directly, rather than to adjust controller gains, such as gain scheduling or to identify system parameters. However, TDC inherently requires that all the states and their derivatives be available for feedback. This imposes very strict limitations on the practical application. Another inherent drawback is that oscillations always exist in the control signal. An assumption in the frequency domain was used to propose an alternative control strategy to obtain similar performance to TDC. The major part of the controller is called an uncertainty and disturbance (UDE) [108] and has been applied to power electronics [109-111]. UDE is one type of disturbance observer and same-order, reduced-order disturbance observers have been summarized in book [6]. The main idea of UDE and disturbance observer (DO) is to employ a low-pass unity gain and proper filter to estimate the unknown disturbances and parameter uncertainties in the frequency range of interests, i.e. assuming the cut-off frequency of the UDE/DO is higher than the system frequency. Auto disturbance rejection control employs an extend-order nonlinear disturbance observer to estimate the nonlinearities and disturbances and then cancelled in the control law [103-105]. In [97], an extend-order perturbation observer is proposed to estimate the whole system nonlinearities and disturbances and then employ the real-time estimate of perturbation to achieve an adaptive feedback linearization control. An extend-order liner Luenberger observer or slide-mode observer are proposed, rather than the nonlinear DO in active disturbance rejection

control (ARDC) and has been approved with same merit as the ADRC but a better and easier for stability analysis and controller gain design. This thesis will use UDE to estimate the disturbance and uncertainties and compensate it to design a UDE-PSS which can deal with the nonlinearities and operation points variations.

1.2 Research motivations and objectives

The contribution of PSS for improving power system stability still have great potential and needs more investigations. Main problems of the PSSs are summarized as below. The first one is that their design and tuning are carried out based on one operation point and the linearized model based on that operation point is used. Their performance may be degraded when the power system operates at a different operation point caused either by the load disturbances, scheduling/dispatch of the whole power system, or by disturbance caused by faults happening at the system. Secondly, the conventional frequency domain-based design, such as lead-lag compensator type PSS, can only easily be designed and analyzed in a single machine infinite bus system (SMIB) and it is difficulty to extend them to multi-machine large-scale system. In other words, the interaction between different generators cannot be handled effectively. Finally, with the increased development of renewable energy generation from wind and solar power, those intermittent and time-varying generations together with demand-side response technology which include direct controllable load will further shift the whole power system operating at different operation points.

The objective of this research work is to improve the overall stability of the power system, by designing a new type of nonlinear power system stabilizer based on an auxiliary Uncertainties and Disturbance Estimator (UDE). The UDE-based PSS is designed and analyzed in frequency domain and has replaced the time-domain extended-order perturbation observer to a same order observer. Via designing of a new type of nonlinear power system stabilizer based on local signals feedback and estimation of external dynamics of the whole power system, we aim to (1) inherent the simplicity of the classical PSS-type controller which are designed in frequency domain; and (2) consider the nonlinearity during the design stage to provide adaptive capability to time-varying operation points and unknown disturbances caused by fault, which requires fewer tuning efforts than the conventional PSSs which are designed and tuned around one operation point. The designed UDE-based PSS will be compared with the conventional lead-lag type PSS (including PSS2B and PSS4B) and the perturbation based nonlinear adaptive PSS [97].

1.3 Contributions of the thesis

A nonlinear PSS is designed based on the feedback linearizing control and extended-order perturbation observer based nonlinear adaptive control. The design is based on the fourth-order model of single machine infinite bus system, and the PSS output is added into the input of the AVR together with the terminal voltage deviation signal.

The proposed nonlinear power system stabilizer (NPSS) is carried out on the frequency domain and only required one measurement added to the currently industrial used conventional CPSS. The proposed NPSS is easily implemented as no derivate of states are needed, compared with the nonlinear perturbation observer-based methods. The perturbation estimation is used to improve the robustness and adaptive capability of the CPSS. The proposed NPSS doesn't require the remote signal for additional tuning as the Wide area damping controller.

Then a UDE is designed by using different feedback signals speed and acceleration power and replace the extended state perturbation observer (ESPO) in nonlinear adaptive control (NAC) PSS. Finally, a UDE-PSS is designed by using the speed and the acceleration power as the only required measurement, which composes of a UDE and a PID-type forward controller. Effectiveness of the UDE-PSS is tested at the benchmark two-area four generators system, which shows the superior performance than the conventional type PSSs and the multi-band PSSs (PSS4B), in terms of robustness, easy tuning of parameters and improved stability margin. The proposed new decentralized PSS targets to solve the challenge tuning burden of the conventional PSSs and the coordination of PSSs tuning in multi-machine power system.

1.4 Thesis Structure

Chapter 1: Background

In this chapter, the development and main power system stability problems are pointed out firstly followed by the introduction of power system stability and power system stabilizer including the reasons for new power system stability problems and the basic knowledge and theory of power system stabilizer. Secondly, the theory of disturbance observer-based control design is stated. Finally, the research motivations, objectives and contributions of the thesis is summarized.

Chapter 2: System Model & Conventional PSS Design

The model of single synchronous generator connected with infinite bus is given for the design of PSS at the following chapter. Design methods of conventional PSS based on phase compensation and damping torque analysis are reviewed. Small signal stability analysis of single machine infinite bus (SMIB) with and without PSS are carried out to show the effectiveness of the PSS, supported by the simulation results to verify the effectiveness of the model.

Chapter 3: Nonlinear PSS Based on Feedback Linearization Control

This chapter has investigated the design of nonlinear PSS based feedback linearizing control and extend-order perturbation observer, based on the 4^{th}-order model of a SMIB system. The main difference of this chapter with reference [97] is that the PSS contributed its output to the input of the AVR, together with the terminal

voltage deviation signal, rather than contribute the excitation voltage in parallel with the AVR in [1]. Comparison of the feedback linearization control (FLC) PSS, extended state observer (ESO) PSS with the CPSS have been carried out, to illustrate the advantages and disadvantages of the ESO based PSS.

Chapter 4: PSS based on Frequency Domain Unified Disturbance Estimator

Conventional lead-lag-type Power System Stabilizer (CPSS) developed in frequency domain has been recalled, and then a perturbation estimator designed in frequency domain has been augmented on to the CPSS, and results in a Nonlinear PSS which can deal with the model uncertainties originating from the shift of operation points, external disturbances from the grid faults, and parameters uncertainties. Initial simulation tests have been done to verify the performance of the proposed NPSS, compared with the CPSS.

Chapter 5: Performance evaluation in multi-machine power system

Performance of the proposed UDEPSS has been tested in the multi-machine power system for their capability of damping of inter-area oscillation. IEEE standard multi-band PSS, PSS4B, and the classical speed type and acceleration power type PSSs are compared. The Speed type UDEPSS can provide better performance than all other PSSs which has much simpler structure than the PSS4B and very good robustness to system operation points and uncertainties due to the compensation of the disturbance and uncertainties. Moreover, it only requires one measurement which

make it be more practical than those ESPO based PSS which requires rotor angle measurement and high-order derivatives of the rotor speed.

Chapter 6: Conclusion

This chapter summaries the whole thesis and point out possible future work.

Chapter 2 System Model & Conventional PSS Design

In this chapter, firstly the model of a single synchronous generator connected to infinite bus system is presented followed by the linearized model which around one operation point. Conventional design of PSS based on Damping Torque Analysis and Phase Compensation have been recalled and demonstrated for the purpose of comparing with the nonlinear PSS which designed at the following chapters. Simulation results are presented to verify the correctness of the model.

2.1 Linearized Model of Single-Machine Infinite-Bus System

The single-machine infinite-bus (SMIB) power system is an approximative description of a real power system. The generator is connected to an infinite bus via a transformer and two parallel transmission lines. A third-order simplified model which is called one axis on E'_q - model, is adopted for the nonlinear compensation design of power system stabilizer (PSS). As the regulation of generator terminal voltage is controlled by the Automatic Voltage Regulator (AVR), which is equipped to most modern generators for excitation control. Note that the PSS's output has been applied to the input of the AVR and take actions on the excitation system.

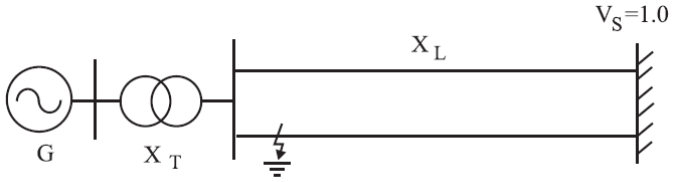

Figure 2.1: The single-machine infinite-bus power system

The whole system dynamics are described as follows:

$$\begin{cases} \dot{\delta} = \omega_0(\omega - 1) \\ \dot{\omega} = \frac{1}{M}[P_m - P_t - D(\omega - 1)] \\ \dot{E'}_q = \frac{1}{T'_{d0}}\left(-E_q + E_{fd}\right) \\ \dot{E'}_{fd} = \frac{1}{T_A}E'_{fd} + \frac{K_A}{T_A}(V_{ref} - V_t + u_{pss}) \end{cases} \tag{2.1}$$

where

$$\begin{cases} P_t = \frac{E'_q V_b}{X'_{d\Sigma}} \sin\delta - \frac{V^2_b}{2}\frac{X_q - X'_d}{X'_{d\Sigma}X_{q\Sigma}} \sin 2\delta \\ E'_q = \frac{E'_q X_{d\Sigma}}{X'_{d\Sigma}} - \frac{V_b}{2}\frac{(X_d - X'_d)\cos\delta}{X'_{d\Sigma}} \\ E_{fd} = E_{fd0} + E'_{fd} \\ V_{td} = \frac{X_q V_b \sin\delta}{X_{q\Sigma}}, \quad V_{tq} = \frac{X'_d V_b \cos\delta}{X'_{d\Sigma}} + \frac{X_t E'_q}{X'_{d\Sigma}}, \quad V_t = \sqrt{V^2_{td} + V^2_{tq}} \end{cases} \tag{2.2}$$

and δ denotes the relative rotor angle, in rad; ω the generator speed, in rad/s; ω_0 the system speed, in rad/s; E_q and E'_q the transient voltage and voltage behind the quadrature-axis, respectively; P_m the mechanical power input from the prime mover and assumed to be constant, in p.u.; T'_{d0} the direct axis transient short circuit time constant of the generator, in seconds; X_d, X'_d the synchronous and transient impedances in the d-axis, respectively; X_q the synchronous impedance in the q-axis; $X'_{d\Sigma} = X'_d + X_t, X_{q\Sigma} = X_q + X_t$, $X_{d\Sigma} = X_d + X_t$, X_t the impedances of the transformer line, respectively; u the excitation control, in p.u.; V_t and V_{ref} the generator terminal voltage and its reference value, respectively; K_a and T_a the control output and time constant of the AVR, respectively; E_{fd} the initial excitation voltage.

System (2.1) and (2.2) can be linearized at the steady-state operating point $(\delta_0, \omega_0, E'_{q0}, E'_{fd0})$ as follows:

$$\begin{cases} \Delta\dot{\delta} = \omega_0 \Delta\omega \\ \Delta\dot{\omega} = \frac{1}{M}\left(-\Delta P_t - D\Delta\omega\right) \\ \Delta\dot{E'}_q = \frac{1}{T'_{d0}}\left(-\Delta E_q + \Delta E'_{fd}\right) \\ \Delta\dot{E'}_{fd} = -\frac{1}{T_A}\Delta E'_{fd} - \frac{K_A}{T_A}\left(\Delta V_t - u_{pss}\right) \end{cases} \tag{2.3}$$

and

$$\begin{cases} \Delta P_t = K_1\Delta\delta + K_2\Delta E'_q \\ \Delta E_q = K_3\Delta E'_q + K_4\Delta\delta \\ \Delta V_t = K_5\Delta\delta + K_6\Delta E'_q \end{cases} \tag{2.4}$$

where

$$\begin{aligned} K_1 &= \frac{E'_{q0}V_b}{X'_{d\Sigma}}\cos\delta_0 - \frac{V^2_b\left(X_q - X'_d\right)}{X'_{d\Sigma}X_{q\Sigma}}\cos 2\delta_0 \\ K_2 &= \frac{V_b}{X'_{d\Sigma}}\sin\delta_0 \\ K_3 &= \frac{X_{d\Sigma}}{X'_{d\Sigma}} \\ K_4 &= \frac{(X_d - X'_d)V_b\sin\delta_0}{X'_{d\Sigma}} \\ K_5 &= \frac{V_{td0}}{V_{t0}}\frac{X_qV_b\cos\delta_0}{X_{q\Sigma}} - \frac{V_{tq0}}{V_{t0}}\frac{V_{b0}X'_d\sin\delta_0}{X'_{d\Sigma}} \\ K_6 &= \frac{V_{tq0}}{V_{t0}}\frac{X_t}{X'_{d\Sigma}} \end{aligned} \tag{2.5}$$

The linearized model can be obtained as

$$\begin{cases} \Delta\dot{\delta} = \omega_0 \Delta\omega \\ \Delta\dot{\omega} = \frac{1}{M}\left(-K_1\Delta\delta - K_2\Delta E'_q - D\Delta\omega\right) \\ \Delta\dot{E'}_q = \frac{1}{T'_{d0}}\left(-K_3\Delta E'_q - K_4\Delta\delta + \Delta E'_{fd}\right) \\ \Delta\dot{E'}_{fd} = -\frac{1}{T_A}\Delta E'_{fd} - \frac{K_A}{T_A}\left(K_5\Delta\delta + K_6\Delta E'_q - u_{pss}\right) \end{cases} \tag{2.6}$$

System (2.6) is called the Phillips-Heffron model of the SMIB system and its block diagram is shown as follows:

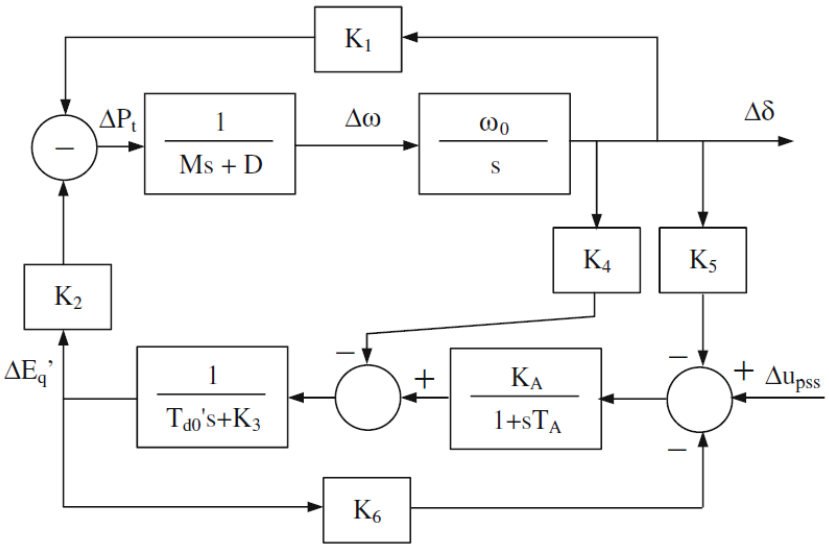

Figure 2.2: SMIB System's Phillips-Heffron Model [1]

The system (2.6) can also be represented in a state-space form as

$$\dot{X} = AX + B\Delta u_{pss} \tag{2.7}$$

where

$$X = \begin{bmatrix} \Delta\delta \\ \Delta\omega \\ \Delta E'_q \\ \Delta E'_{fd} \end{bmatrix} \quad A = \begin{bmatrix} 0 & \omega_0 & 0 & 0 \\ -\frac{K_1}{M} & -\frac{D}{M} & -\frac{K_2}{M} & 0 \\ -\frac{K_4}{T'_{do}} & 0 & -\frac{K_3}{T'_{do}} & \frac{1}{T'_{do}} \\ -\frac{K_A K_5}{T_A} & 0 & -\frac{K_A K_6}{T_A} & -\frac{1}{T_A} \end{bmatrix} \quad B = \begin{bmatrix} 0 \\ 0 \\ 0 \\ \frac{K_A}{T_A} \end{bmatrix} \tag{2.8}$$

2.2 Damping Torque Analysis [4]

The damping torque analysis (DTA) was introduced based on the Heffron-Phillips model for a SMIB power system to test excitation control's effect, such as AVR, on power system small-signal stability firstly [1, 2]. It was developed since the comprehension that the electromechanical oscillation loop's dynamic of a SMIB decides power oscillations' damping in the SMIB power system [3, 4].

From the first two first-order differential equation of system (2.6), we get

$$M\Delta\ddot{\delta} + D\Delta\ddot{\delta} + \omega_0\Delta P_t = 0 \tag{2.9}$$

Substituting equation (2.4), then we have

$$\Delta\ddot{\delta} + \frac{D}{M}\Delta\dot{\delta} + \frac{\omega_0 K_1}{M}\Delta\delta + \frac{\omega_0 K_2}{M}\Delta E'_q = 0 \tag{2.10}$$

$K_2\Delta E'_q$ is one part of ΔP_t, which is called electromagnetic torque and represented as ΔT. So, Eq. (2.10) can be rewritten as

$$\Delta\ddot{\delta} + \frac{D}{M}\Delta\dot{\delta} + \frac{\omega_0 K_1}{M}\Delta\delta + \frac{\omega_{0\Delta T}}{M} = 0 \tag{2.11}$$

The block diagram of Eq. (2.11) can be represented in Figure 2.3.

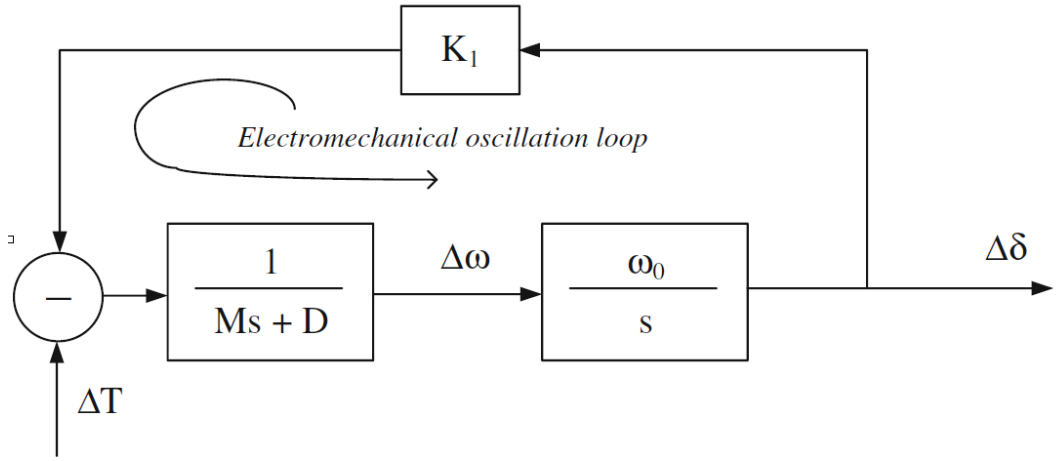

Figure 2.3: Electromechanical Oscillation Loop [4]

In Figure 2.2, the upper part is the linearized rotor motion equation and the lower part is formed from the mathematical description of dynamic of the field winding of generator and the AVR. Figure 2.3 shows the upper part of the model which is called the electromechanical oscillation loop. ΔT is the input signal or an electric torque. Firstly, assume $\Delta T = 0$, the electromechanical oscillation loop can be indicated as follows:

$$\Delta\ddot{\delta} + \frac{D}{M}\Delta\dot{\delta} + \frac{\omega_0 K_1}{M}\Delta\delta = 0 \tag{2.12}$$

The equation (2.12) only considered the dynamic characteristics of the generator rotor

and ignored the dynamic characteristics of the excitation system and the automatic voltage controller. This equals to the situation that E'_q is constant. Solve the Eq. (2.12), we can get

$$\Delta\delta(t) = ae^{-\frac{D}{2M}t}cos\omega_{NOF}t + b \tag{2.13}$$

In Eq. (2.13), a and b are constants; $\omega_{NOF} = \frac{1}{2}\sqrt{(\frac{D}{M})^2 - \frac{4\omega_0 K_1}{M}}$. ω_{NOF} is natural oscillation angle frequency of generator power angle.

The Eq. (2.13) descripted that the generator rotates or decelerates the rotor in the event of small disturbances, the rotor angular displacement changes which leads to the dynamic process of generator output active power fluctuation. Obviously, when $\frac{D}{2M}$ is small enough or negative value, the rotor movement of the generator presents a weak damping or divergence oscillation. This results in low frequency oscillation. This indicates that the low frequency oscillation damping of the SMIB system is decided by the value of $\frac{D}{M}$.

Decompose ΔT as two components as

$$\Delta\mathrm{T} = T_d\Delta\omega + T_s\Delta\delta \tag{2.14}$$

Eq. (2.10) becomes

$$\Delta\ddot{\delta} + (\frac{D}{M} + \frac{T_d}{M})\Delta\dot{\delta} + (\frac{\omega_0 K_1}{M} + \frac{\omega_0 T_s}{M})\Delta\delta = 0 \tag{2.15}$$

From the Eq. (2.15), $T_d\Delta\omega$ affects the low frequency oscillation damping of the system while $T_s\Delta\delta$ help synchronous operation of the rotor and no influence to the system damping. So, $T_d\Delta\omega$ is called damping torque and $T_s\Delta\delta$ is called synchronous torque.

The low frequency oscillation of generator output power is accordance to rotor angular

displacement fluctuation ($\Delta\delta$), and the damping of $\Delta\delta$ is decided by the angular velocity proportional term$\Delta\omega$. The influence of the generator excitation system and the automatic voltage controller on the rotor motion is considered as the contribution to the torque of the generator electromechanical oscillation circuit, and the torque will be decomposed into two parts which include damping torque and synchronous torque. The damping torque decides the damping of rotor motion oscillation and the synchronous damping decide the capability of generator synchronization [1, 2]. This is the basic theory of Damping Torque Analysis (DTA).

The following section will analysis the effect of the excitation system. From Figure 2.2, when the effect of PSS ($\Delta u_{pss} = 0$) is not considered, we have

$$(\mathrm{M}s^2 + Ds + \omega_0 K_1)\Delta\delta_s = -\omega_0 \Delta T(s) \tag{2.16}$$

$$\Delta\mathrm{T(s)} = F_{delta}(s)\Delta\delta(s) \tag{2.17}$$

$F_{delta}(s)$ is the transfer function from $\Delta\delta_s$ to $\Delta\mathrm{T(s)}$, which represents the contribution of torque. Combining two equations above gives

$$[\mathrm{M}s^2 + Ds + \omega_0 K_1 + \omega_0 F_{delta}(s)]\Delta\delta_s = 0 \tag{2.18}$$

Thus, the system characteristic equation is as follows

$$\mathrm{M}s^2 + Ds + \omega_0 K_1 + \omega_0 F_{delta}(s) = 0 \tag{2.19}$$

The (2.19) equation's solution is the eigenvalue of the system matrix or the pole of the transfer function, which relate to the dynamics of generator electromechanical oscillation: $\overline{\lambda_s} = \xi_s \pm \mathrm{j}\omega_s$. The real part of the electromechanical oscillation mode decides the damping of low frequency power system oscillation which represents the system's oscillation stability.

Substitute In complex frequency domain, it should have

$$\mathrm{M}\bar{\lambda_s}^2 + D\bar{\lambda_s} + \omega_0 K_1 + \omega_0 F_{delta}(\bar{\lambda_s}) = 0 \tag{2.20}$$

$$\Delta\mathrm{T}(\bar{\lambda_s}) = F_{delta}(\bar{\lambda_s})\Delta\delta(\bar{\lambda_s}) \tag{2.21}$$

Also, in the complex frequency domain, the first equation in system (2.6) $\mathrm{s}\Delta\delta = \omega_0\Delta\omega, s = \xi_s \pm \mathrm{j}\omega_s$, we have

$$\Delta\omega(\bar{\lambda_s}) = \frac{\xi_s}{\omega_0}\Delta\delta(\bar{\lambda_s}) + j\frac{\omega_s}{\omega_0}\Delta\delta(\bar{\lambda_s}) \tag{2.22}$$

And in complex frequency domain, the electromagnetic torque can be decomposed as

$$\Delta\mathrm{T}(\bar{\lambda_s}) = T_{s1}\Delta\delta(\bar{\lambda_s}) + T_{d1}\Delta\omega(\bar{\lambda_s}) \tag{2.23}$$

From Eq. (2.21), (2.22) and (2.23), it can be obtained that

$$F_{delta}(\bar{\lambda_s})\Delta\delta(\bar{\lambda_s}) = T_{s1}\Delta\delta(\bar{\lambda_s}) + T_{d1}\frac{\xi_s}{\omega_0}\Delta\delta(\bar{\lambda_s}) + jT_{d1}\frac{\omega_s}{\omega_0}\Delta\delta(\bar{\lambda_s}) \tag{2.24}$$

That is

$$F_{delta}(\bar{\lambda_s}) = T_{s1} + T_{d1}\frac{\xi_s}{\omega_0} + jT_{d1}\frac{\omega_s}{\omega_0} \tag{2.25}$$

Then we have

$$\begin{cases} T_{d1} = \frac{\omega_0}{\omega_s} Im\left[\overline{F_{delta}}(\bar{\lambda_s})\right] \\ T_{s1} = Re\left[\overline{F_{delta}}(\bar{\lambda_s})\right] - \frac{T_{d1}\epsilon_s}{\omega_0} \end{cases} \tag{2.26}$$

Eq. (2.26) shows that in complex frequency domain, it's feasible to decompose the electromagnetic torque into damping torque and synchronous torque.

Substitute Eq. (2.23) into Eq. (2.16), we have

$$\mathrm{M}\bar{\lambda_s}^2 + (D + T_{d1})\bar{\lambda_s} + \omega_0 K_1 + \omega_0 T_{s1} = 0 \tag{2.27}$$

From Eq. (2.27), the damping ratio can be obtained as

$$\xi_s = -\frac{D+T_{d1}}{2M} \tag{2.28}$$

Combing with Eq. (2.23), $T_{d1}\Delta\omega(\bar{\lambda_s})$ truly influences the real part of the electromechanical oscillation mode (system's oscillation stability) while the damping

torque influences the damping of the system low frequency oscillation only.

2.3 Design of PSS using Phase Compensation Method

From Figure 2.2, considering the contribution of torque from the PSS, we have electromagnetic torque as following

$$\Delta \mathrm{T} = F_{delta}(\mathrm{s})\Delta\delta + F_{pss}(\mathrm{s})\Delta u_{pss} \tag{2.29}$$

where $F_{delta}(\mathrm{s})$ is the transfer function from $\Delta\delta$ to $\Delta \mathrm{T}$ and $F_{pss}(\mathrm{s})$ is the transfer function from Δu_{pss} to $\Delta \mathrm{T}$. The electromagnetic torque provided by PSS is

$$\Delta \mathrm{T}_{pss} = F_{pss}(\mathrm{s})\Delta u_{pss} \tag{2.30}$$

From Fig.2.2, the forward channel transfer function of Δu_{pss} to $\Delta \mathrm{T}_{pss}$ is

$$F_{pss}(\mathrm{s}) = K_2 \frac{\frac{1}{K_3+sT'_{d0}}\frac{K_A}{1+sT_A}}{1+K_6\frac{1}{K_3+sT'_{d0}}\frac{K_A}{1+sT_A}} = K_2 \frac{K_A}{(K_3+sT'_{d0})(1+sT_A)+K_6K_A} \tag{2.31}$$

Note that the PSS's output has been added at the excitation system from the input port of the AVR, together with the voltage deviation signal. Let PSS's transfer function be $G_{pss}(\mathrm{s})$, that is, $\Delta u_{pss} = G_{pss}(\mathrm{s})\Delta\omega$, then the electromagnetic torque provided by power system stabilizer is

$$\Delta \mathrm{T}_{pss} = F_{pss}(\mathrm{s})G_{pss}(\mathrm{s})\Delta\omega \tag{2.32}$$

For an oscillation mode $\bar{\lambda_s} = \xi_s \pm \mathrm{j}\omega_{s,}$ the electromagnetic torque provided by the PSS is

$$\overline{F_{pss}}(\bar{\lambda_s})\overline{G_{pss}}(\bar{\lambda_s})\Delta\omega = \Delta T_{pss} \tag{2.33}$$

The principle of the PSS is to provide an additional torque contribution in phase with the deviation of speed, i.e. $\Delta\omega$, that is phase of $\overline{F_{pss}}(\bar{\lambda_s})\overline{G_{pss}}(\bar{\lambda_s})$ should be zero by designing the $\overline{G_{pss}}(\bar{\lambda_s})$.

To provide maximum damping torque, the parameters of the PSS will be properly adjusted to ensure that all electromagnetic torque is proportional to generator speed deviation, that is

$$\Delta T_{pss} = D_{pss}\Delta\omega \tag{2.34}$$

where the damping coefficient $D_{pss} > 0$, thus all electromagnetic torque provided by the PSS is positive damping torque, which can provide the highest benefit to improve the stability of system.

However, before designing power system stabilizer, the closed - loop electromechanical oscillation mode of the system $\overline{\lambda_s} = \xi_s \pm \mathrm{j}\omega_s$ is unknown. Also we usually don't want to change the natural frequency or only a small influence of the natural frequency, thus we use the system's open - loop electromechanical oscillation mode $\overline{\lambda_g} = \xi_g \pm \mathrm{j}\omega_g$to replace $\overline{\lambda_s} = \xi_s \pm \mathrm{j}\omega_s \cong \mathrm{j}\omega_g$, as the real part is very small. So, the electromagnetic torque provided by the PSS as

$$\begin{aligned}\overline{F_{pss}}(j\omega_g)\overline{G_{pss}}(j\omega_g)\Delta\omega &= \Delta T_{pss} \\ &= Re\left[\overline{F_{pss}}(j\omega_g)\overline{G_{pss}}(j\omega_g)\right]\Delta\omega - \frac{\omega_g}{\omega_0} Im\left[\overline{F_{delta}}(j\omega_g)\overline{G_{pss}}(j\omega_g)\right]\Delta\delta \\ &= T_{pssd}\Delta\omega + T_{psss}\Delta\delta\end{aligned} \tag{2.35}$$

where, $T_{pssd}\Delta\omega$ is the damping torque and $T_{psss}\Delta\delta$ is the synchronous torque.

Phase compensation method sets PSS's parameters to ensure the phase of its transfer function can compensate the phase of its forward channel's transfer function's phase, so it can provide positive damping torque for generator electromechanical oscillation. If $\overline{F_{pss}}(j\omega_g)$ and $\overline{G_{pss}}(j\omega_g)$ can be written as

$$\overline{F_{pss}}(j\omega_g) = F_{pss}\angle\phi\,,\ \overline{G_{pss}}(j\omega_g) = G_{pss}\angle\gamma \tag{2.36}$$

The phase compensation method requires

$$\begin{cases} T_{pssd} = F_{pss}G_{pss}\cos(\phi+\gamma) = D_{pss} \\ T_{psss} = F_{pss}G_{pss}\sin(\phi+\gamma) = 0 \end{cases} \tag{2.37}$$

This can be achieved by setting

$$\gamma = -\phi, G_{pss} = \frac{D_{pss}}{F_{pss}} \tag{2.38}$$

Usually the transfer function of a lead-lag type PSS is:

$$G_{pss}(s) = K\frac{1+s*T_2}{1+s*T_1} * \frac{1+s*T_4}{1+s*T_3} = K_1\frac{1+s*T_2}{1+s*T_1} * K_2\frac{1+s*T_4}{1+s*T_3} \tag{2.39}$$

where $K = K_1K_2$.

Parameters of the PSS then can be set to satisfy

$$\begin{cases} K_1\frac{1+j\omega_g*T_2}{1+j\omega_g*T_1} = \frac{D_{pss}}{F_{pss}}\angle -\frac{\emptyset}{2} \\ K_2\frac{1+j\omega_g*T_4}{1+j\omega_g*T_3} = 1.0\angle -\frac{\emptyset}{2} \end{cases} \tag{2.40}$$

Eq. (2.40) can be used to determine PSS's parameters to ensure the designed PSS can always provide pure positive damping torque for generator electromechanical oscillation loop.

Based on equation (2.39), converting the SMIB with PSS to state space model, the feedback signal of the PSS is generator rotating speed deviation:

$$\Delta u_{pss} = G_{pss}(s)\Delta\omega = K_1\frac{1+s*T_2}{1+s*T_1} * K_2\frac{1+s*T_4}{1+s*T_3} * \Delta\omega \tag{2.41}$$

Define a new state variable as

$$\Delta x_1 = K_2\frac{1+s*T_4}{1+s*T_3} * \Delta\omega \tag{2.42}$$

$$s\Delta x_1 = -\frac{1}{T_3}\Delta x_1 + \frac{K_2}{T_3}(T_4 s\Delta\omega + \Delta\omega) \tag{2.43}$$

$$= -\frac{1}{T_3}\Delta x_1 + \frac{K_2}{T_3}\left(\frac{T_4}{M}\left(-K_1\Delta\delta - K_2\Delta E'_q - D\Delta\omega\right) + \Delta\omega\right)$$

$$= -\frac{1}{T_3}\Delta x_1 + \frac{K_2}{T_3}\left(-\frac{T_4}{M}K_1\Delta\delta - \frac{T_4}{M}K_2\Delta E'_q + \left(1 - \frac{T_4}{M} * D\right)\Delta\omega\right)$$

$$\Delta u_{pss} = K_1\frac{1+s*T_2}{1+s*T_1} * \Delta x_1 \tag{2.44}$$

$$s\Delta u_{pss} = -\frac{1}{T}\Delta u_{pss} + \left(\frac{K_{1pss}}{T_1} - \frac{1}{T_3}\frac{K_{1pss}T_2}{T_1}\right)\Delta x_1 + \frac{K_1}{T_1}\frac{K_2T_2}{T_3}\left[-\frac{T_4}{M}K_1\Delta\delta - \frac{T_4}{M}K_2\Delta E'_q + (1 - \frac{T_4}{M} * D)\Delta\omega\right] \tag{2.45}$$

Adding (2.44) and (2.45) into system (2.8), the new SMIB system's closed-loop state equation can be obtained as:

$$\dot{X}' = A'X' + B'\Delta u_{pss} \tag{2.46}$$

$$X' = \begin{bmatrix} \Delta\delta \\ \Delta\omega \\ \Delta E'_q \\ \Delta E'_{fd} \\ \Delta x_1 \\ \Delta u_{pss} \end{bmatrix}$$

$$A' = \begin{bmatrix} 0 & \omega_0 & 0 & 0 & 0 & 0 \\ -\frac{K_1}{M} & -\frac{D}{M} & -\frac{K_2}{M} & 0 & 0 & 0 \\ -\frac{K_4}{T'_{d0}} & 0 & -\frac{K_3}{T'_{d0}} & \frac{1}{T'_{d0}} & 0 & 0 \\ -\frac{K_AK_5}{T_A} & 0 & -\frac{K_AK_6}{T_A} & -\frac{1}{T_A} & 0 & \frac{K_A}{T_A} \\ -\frac{K_{2pss}*K_1*T_4}{M*T_3} & \frac{K_{2pss}}{T_3*\left(1-D*\frac{T_4}{M}\right)} & -\frac{K_{2pss}*K_2*T_4}{M*T_3} & 0 & -\frac{1}{T_3} & 0 \\ \frac{K_{1pss}*T_2}{T_1} * \frac{-K_{2pss}*K_1*T_4}{M*T_3} & \frac{K_{2pss}}{T_3*\left(1-D*\frac{T_4}{M}\right)} * \frac{K_{1pss}*T_2}{T_1} & \frac{K_{1pss}*T_2}{T_1} * \frac{-K_{2pss}*K_2*T_4}{M*T_3} & 0 & \frac{K_{1pss}}{T_1} - \frac{K_{1pss}*T_2}{T_1*T_3} & \frac{-1}{T_1} \end{bmatrix}$$

$$B' = \begin{bmatrix} 0 \\ 0 \\ 0 \\ \frac{K_A}{T_A} \\ 0 \\ \frac{-1}{T_1} \end{bmatrix} \tag{2.47}$$

2.4 Case studies

2.4.1 Modal analysis

Firstly, results of [4] is recalled as the part of thesis case study and then the lead-lag design is followed. The parameters of a SMIB are given as following [2, 3]:

X_d=1.18, X_q=1.0, X_{ad}=1.0, X_f=1.13, X'_d=$X_d - \frac{x^2_{ad}}{X_f}$=0.295, M=7, D=0, T'_{d0}=5.004, X_t=0.3. The AVR parameters are: K_a=50, T_a=0.05s.

The system normal operation conditions are: P_{t0}=0.8, V_{t0}=1.05, V_{b0}=1.0. When the system steady-state operation point is $(\delta_0, \omega_0, E'_{q0}, E'_{fd0})$ = (0.7591, 314.1593, 1.0850, 0), the open-loop model of the system without PSS can be obtained based on system (2.8) as:

$$\begin{bmatrix} \Delta\dot{\delta} \\ \Delta\dot{\omega} \\ \Delta\dot{E}'_q \\ \Delta\dot{E}'_{fd} \end{bmatrix} = \begin{bmatrix} 0 & 314.1593 & 0 & 0 \\ -0.1821 & 0 & -0.1652 & 0 \\ -0.2046 & 0 & -0.4970 & 0.1998 \\ -13.3278 & 0 & -435.3836 & -20 \end{bmatrix} \begin{bmatrix} \Delta\delta \\ \Delta\omega \\ \Delta E'_q \\ \Delta E'_{fd} \end{bmatrix} \quad (2.48)$$

Eigenvalues of system (2.48) are:

$$\overline{\lambda_{1,2}} = -0.2305 \pm \mathrm{j}7.0230\,, \overline{\lambda_3} = -11.5726, \overline{\lambda_4} = -8.7491$$

Note that $\overline{\lambda_{1,2}} = -0.2305 \pm \mathrm{j}7.0230$ is the system's electromechanical oscillation mode and two dominant poles, other two poles have much faster dynamics (i.e., the abstract real part is 10 times bigger). We need to determine the power system stabilizer's parameters K_1, K_2, T_2, T_4 to satisfy that the transfer function of the PSS can compensate the phase of the forward channel transfer function

$E(\mathrm{s}) = \frac{K_2 K_3}{K_3 T_{d0} T_A S + (K_3 T_{d0} + T_A) S + 1 + K_3 K_6 K_A}$.

The open-loop electromechanical oscillation mode of the system is $\overline{\lambda_g} = -0.2350 \pm$

j7.0230, the desired target pole is $\overline{\lambda_s} = -0.7100 \pm \text{j}6.9826,$ in which the damp ratio will be increased from 0.0328 to 0.1. Based on procedure described above, the PSS is designed as:

$$G_{pss}(s) = K_1 \frac{1+s*T_2}{1+s*T_1} * K_2 \frac{1+s*T_4}{1+s*T_3} = 2.0877 * \frac{1+s*0.3710}{1+s*0.09} * 0.3654 * \frac{1+s*0.3710}{1+s*0.09}. \quad (2.49)$$

where $\text{K} = K_1K_2$ =0.7628, $T_2 = 0.3710s$, $T_4 = 0.3710s$. $K_1 = 2.0877$, $K_2 = 0.3654$.

Based on system (2.46) and (2.47) , the closed-loop state equation can be obtained as following:

$$\begin{bmatrix} \Delta\dot{\delta} \\ \Delta\dot{\omega} \\ \Delta\dot{E'}_q \\ \Delta\dot{E'}_{fd} \\ \Delta\dot{x}_1 \\ \Delta\dot{u}_{pss} \end{bmatrix} = \begin{bmatrix} 0 & 314.1593 & 0 & 0 & 0 & 0 \\ -0.1821 & 0 & -0.1652 & 0 & 0 & 0 \\ -0.2046 & 0 & -0.4970 & 0.1998 & 0 & 0 \\ -13.3278 & 0 & -435.3836 & -20 & 0 & 1000 \\ -0.3 & 4.5 & -0.3 & 0 & -11.1111 & 0 \\ -3.2 & 45.4 & -2.9 & 0 & 86.4 & -11.1111 \end{bmatrix} \begin{bmatrix} \Delta\delta \\ \Delta\omega \\ \Delta E'_q \\ \Delta E'_{fd} \\ \Delta x_1 \\ \Delta u_{pss} \end{bmatrix} \quad (2.50)$$

System's eigenvalues are as following:

$$\overline{\lambda_1} = -19.1503\,, \overline{\lambda_{2,3}} = -0.7134 \pm j6.9337,$$

$$\overline{\lambda_{4,5}} = -8.1327 \pm j6.4424, \overline{\lambda_6} = -6.1625$$

With the designed PSS, the system's closed-loop electromechanical oscillation mode are $\overline{\lambda_{2,3}} = -0.7134 \pm j6.9337$, which has been nearly move to $\overline{\lambda_s} = -0.7100 \pm$ j6.9826. Simulation results of SMIB with and without PSS is shown in the Fig. 2.4, in which we can observe the natural frequency and the damping effect improvement.

Robustness to operation points variation

The previous design is based on the system's steady-state operation point P_{t0} =0.5. When the operation point changes, i.e. P_{t0} ranges from 0.3 to 1.2, and the designed PSS ($G_{pss}(s) = K_1 \frac{1+s*T_2}{1+s*T_1} * K_2 \frac{1+s*T_4}{1+s*T_3} = 2.0877 * \frac{1+s*0.3710}{1+s*0.09} * 0.3654 * \frac{1+s*0.3710}{1+s*0.09}$) based

on P_{t0}=0.5 is applied, dominant poles of different operation point can be obtained and shown in Table 2.1. The corresponding damping ratio of each dominant poles can also be calculated by using MATLAB.

Results from Table 1 shows that when the operation point is P_{t0} =0.5, the damping ratio of the system is 0.102. When the operation point moves from 0.5 to 0.8 (from nominal load to heavy load), the damping ratio of the system is decreasing step by step while the damping ratio is increasing when the operation point reduces from 0.5 to 0.1 (from nominal load to light load). This indicates that the stability of the power system is influenced by the operation point change. Note this influence is not obvious, next step will find a case with special set of parameters which can demonstrate more obvious degradation of the damping ratio against the operation points.

Table 2.1. Changing of dominant poles & damping ratio of different operation points

P_{t0}	Dominant Poles	Damping Ratio	Change of damping ratio
0.1	-0.6615±6.3495i	0.103	0.98%
0.2	-0.6733±6.4369i	0.104	1.96%
0.3	-0.6885±6.5729i	0.104	1.96%
0.4	-0.7026±6.7440i	0.104	1.96%
0.5	-0.7134±6.9337i	0.102	0
0.6	-0.7221±7.1260i	0.101	-0.98%
0.7	-0.7321±7.3075i	0.0997	-2.25%
0.8	-0.7474±7.4687i	0.0996	-2.35%

2.4.2 PSS design based on pole assignment in open-loop system

It's not necessary to configure closed-loop pole for designing PSS like the example showed above. Instead, we can also use the electromechanical oscillation angle frequency of the open loop system to design PSS by using the phase compensation method which shows from Eq. (2.39) to Eq. (2.40). For the example in 4.1, $j\omega_g = j6.5817$,

$$\overline{F_{pss}}(j\omega_g) = K_2 \frac{K_A}{(K_3+\lambda_s T'_{d0})(1+\lambda_s T_A)+K_6 K_A} = 0.2096 - \mathrm{j}0.421 \tag{2.51}$$

Now we still set $D_{pss} = 8.7244$. Assume the transfer function of the PSS is as

$$G_{pss}(s) = K_1 \frac{1+s*T_2}{1+s*T_1} * K_2 \frac{1+s*T_4}{1+s*T_3} \tag{2.52}$$

In the equation we can set $T_1 = 0.09\mathrm{s}$, $T_3 = 0.09\mathrm{s}$.

Design PSS and set the parameter by using the method showed from Eq. (2.51) to Eq. (2.52), it can have

$$\begin{cases} K_1 \frac{1+\lambda_s*T_2}{1+\lambda_s*T_1} = 8.3529\angle 34.8142^\circ \\ K_2 \frac{1+\lambda_s*T_4}{1+\lambda_s*T_3} = 1.0\angle 34.7142^\circ \end{cases} \tag{2.53}$$

Then we can get $\mathrm{K} = K_1K_2$=0.9308, $T_2 = 0.3410s$, $T_4 = 0.4402s$. $K_1 = 2.4829$, $K_2 = 0.3749$.

The designed PSS: $G_{pss}(s) = K_1 \frac{1+s*T_2}{1+s*T_1} * K_2 \frac{1+s*T_4}{1+s*T_3} = 2.4829 * \frac{1+s*0.3410}{1+s*0.09} * 0.3749 * \frac{1+s*0.4402}{1+s*0.09}$.

From those above, the new system's close-loop state equation can be obtained from system (2.46)-(2.47) as following:

$$\begin{bmatrix} \Delta\dot{\delta} \\ \Delta\dot{\omega} \\ \Delta\dot{E'}_q \\ \Delta\dot{E'}_{fd} \\ \Delta\dot{x}_1 \\ \Delta\dot{u}_{pss} \end{bmatrix} = \begin{bmatrix} 0 & 314.1593 & 0 & 0 & 0 & 0 \\ -0.1821 & 0 & -0.1652 & 0 & 0 & 0 \\ -0.1046 & 0 & -0.4970 & 0.1998 & 0 & 0 \\ -12.8278 & 0 & -498.2836 & -20 & 0 & 1000 \\ -0.2 & 4.7 & -0.1 & 0 & -11.1111 & 0 \\ -7.2 & 13.67 & -2.6 & 0 & 235.7 & -11.1111 \end{bmatrix} \begin{bmatrix} \Delta\delta \\ \Delta\omega \\ \Delta E'_q \\ \Delta E'_{fd} \\ \Delta x_1 \\ \Delta u_{pss} \end{bmatrix} \quad (2.54)$$

Let's calculate its eigenvalue as following:

$$\overline{\lambda_1} = -19.6435\,, \overline{\lambda_{2,3}} = -0.7787 \pm j6.8886,$$

$$\overline{\lambda_{4,5}} = -7.7893 \pm j7.2330, \overline{\lambda_6} = -6.2871$$

So, when we designed the power system stabilizer, the system's closed-loop electromechanical oscillation mode has been nearly moved to $\overline{\lambda_s} = -0.7100 \pm$ j6.9826.

Comparing the results with case 1's performance, it shows that by using the phase compensation method to design PSS in the open loop system, the electromechanical oscillation mode of the system has also been moved to the required point.

Change of operation point (Robustness to operation points)

The previous system's steady-state operation point is P_{t0} =0.5. When the operation point changes, i.e. P_{t0} ranges from 0.3 to 1.2, and the designed PSS ($G_{pss}(s) = K_1\frac{1+s*T_2}{1+s*T_1} * K_2\frac{1+s*T_4}{1+s*T_3} = 2.4829 * \frac{1+s*0.3410}{1+s*0.09} * 0.3749 * \frac{1+s*0.4402}{1+s*0.09}$) based on P_{t0}=0.5 is applied, Table 2.2 shows dominant poles of different operation point. The corresponding damping ratio of each dominant poles can also be calculated by using MATLAB.

Table 2.2. Changing of dominant poles & damping ratio of different operation points

P_{t0}	Dominant Poles	Damping Ratio	Change of damping ratio
0.1	-0.7435±6.2773i	0.118	5.35%
0.2	-0.7525±6.3697i	0.117	4.46%
0.3	-0.7633±6.5129i	0.116	3.57%
0.4	-0.7724±6.6919i	0.115	2.67%
0.5	-0.7787±6.8886i	0.112	0
0.6	-0.7838±7.0858i	0.110	-1.78%
0.7	-0.7919±7.2692i	0.108	-2.57%
0.8	-0.8069±7.4287i	0.108	-2.57%
0.9	-0.8319±7.5571i	0.109	-2.67%
1.0	-0.8676±7.6496i	0.113	0.89%

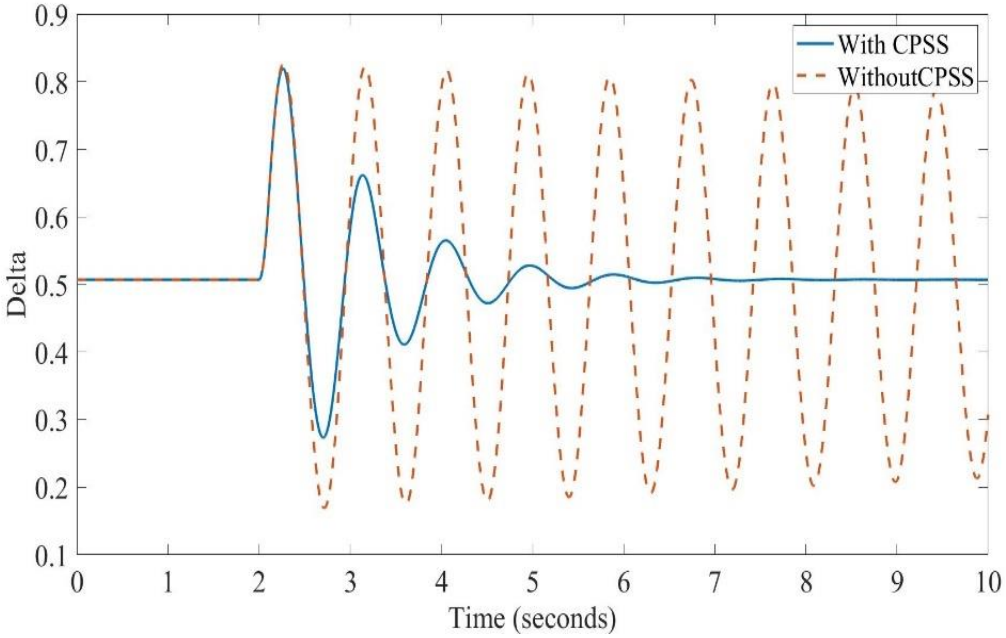

Fig. 2.4 Rotor angle response of SMIB with and without PSS

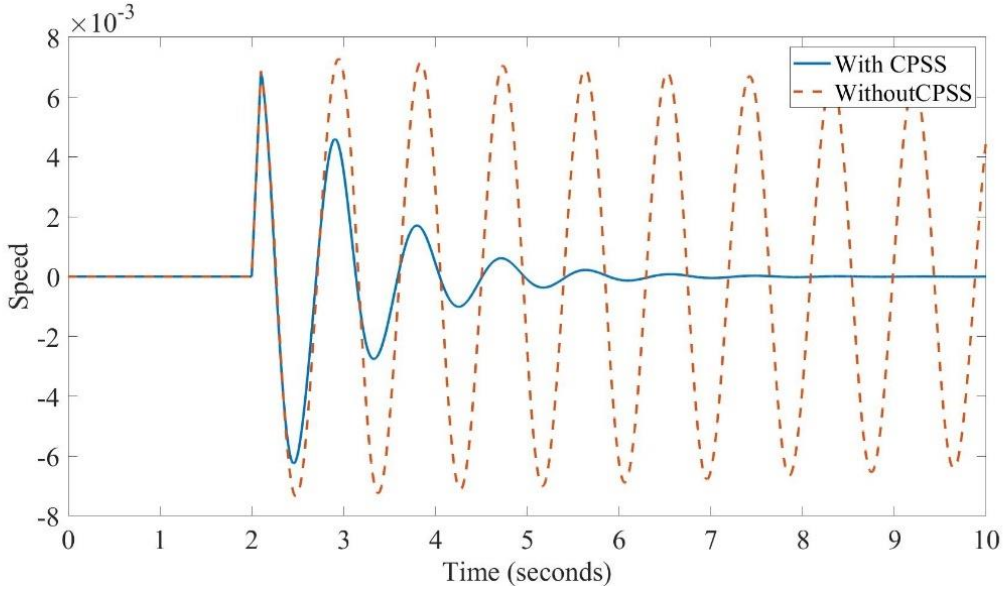

Fig. 2.5 Speed response of SMIB with and without PSS

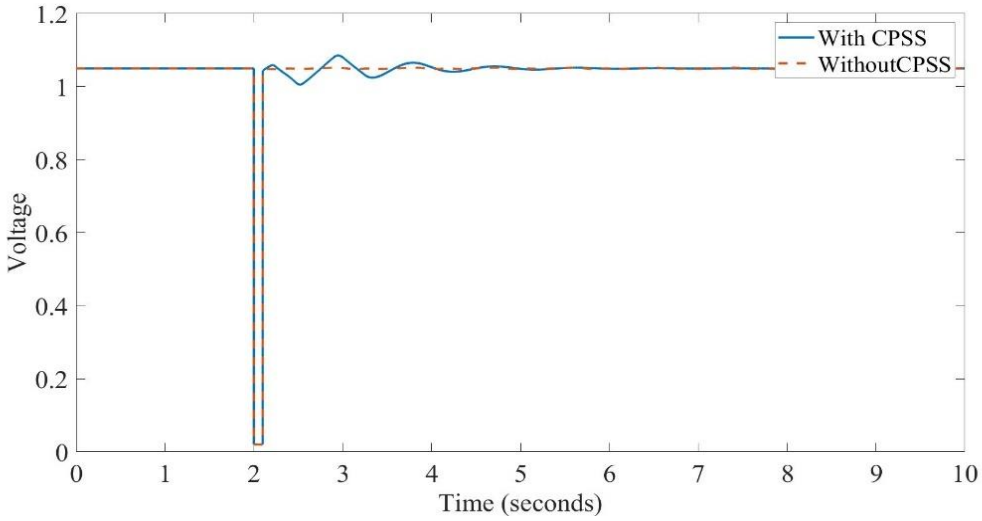

Fig. 2.6 Voltage response of SMIB with and without PSS

2.5 Conclusion

The model of single synchronous generator connected with infinite bus is given for the design of PSS at this chapter. Design methods of conventional PSS based on phase compensation and damping torque analysis are viewed. Small signal stability analysis of SMIB with and without PSS are carried out to show the effectiveness of the PSS, supported by the simulation results to verify the effectiveness of the model.

Chapter 3 Extended-state Perturbation Observer based Nonlinear PSS

3.1 Introduction

This chapter will investigate the design of nonlinear PSS based on accurate feedback linearizing control at first, then based on an extend-state perturbation observer (ESO) based nonlinear adaptive control. The design is based on the 4-th order model of the single machine infinite bus system and the designed NPSS will be used to compare the frequency domain UDE-PSS, and conventional PSS based on lead/lag phase compensator, Speed type PSS and acceleration Power type PSS. Note that Chapter 3.2 is repeated section of Chapter 2.1.

3.2 Nonlinear Model of Single Machine Infinite Bus System

Here the model presented in Chapter 2.1 will be recalled for the purpose of nonlinear system design. A single machine infinite bus system is shown in Fig 3.1 which is used to carry out the design of nonlinear PSS (NPSS). The synchronous generator is modelled as a third order E'_q – model. Most of the modern generators are equipped with an Automatic Voltage Regulator (AVR) because the regulation of generator terminal voltage is also a significant point of the generator excitation control. Dynamics of the whole system including the AVR are described as follows:

$$\begin{cases} \dot{\delta} = \omega_0(\omega - 1) \\ \dot{\omega} = \frac{1}{M}[P_m - P_t - D(\omega - 1)] \\ \dot{E'}_q = \frac{1}{T'_{d0}}\left(-E_q + E_{fd}\right) \\ \dot{E'}_{fd} = \frac{1}{T_A}E'_{fd} + \frac{K_A}{T_A}(V_{ref} - V_t + u_{pss}) \end{cases} \tag{3.1}$$

Where

$$\begin{cases} P_t = \frac{E\prime_q V_b}{X\prime_{d\Sigma}} \sin\delta - \frac{V^2_b}{2}\frac{X_q - X'_d}{X\prime_{d\Sigma}X_{q\Sigma}} \sin 2\delta \\ E_q = \frac{E\prime_q X_{d\Sigma}}{X\prime_{d\Sigma}} - \frac{V_b}{2}\frac{(X_d - X'_d)\cos\delta}{X\prime_{d\Sigma}} \\ E_{fd} = E_{fd0} + E'_{fd} \\ V_{td} = \frac{X_q V_b \sin\delta}{X_{q\Sigma}}, \ V_{tq} = \frac{X\prime_d V_b \cos\delta}{X\prime_{d\Sigma}} + \frac{X_t E\prime_q}{X\prime_{d\Sigma}}, \ V_t = \sqrt{V^2_{td} + V^2_{tq}} \end{cases} \tag{3.2}$$

and δ denotes the relative rotor angle, in rad; ω the generator speed, in rad/s; ω_0 the system speed, in rad/s; E_q and E'_q the transient voltage and voltage behind the quadrature-axis, respectively; P_m the mechanical power input from the prime mover and assumed to be constant, in p.u.; T'_{d0} the direct axis transient short circuit time constant of the generator, in seconds; X_d, X'_d the synchronous and transient impedances in the d-axis, respectively; X_q the synchronous impedance in the q-axis; $X'_{d\Sigma} = X'_d + X_t, X_{q\Sigma} = X_q + X_t$, $X_{d\Sigma} = X_d + X_t$, X_t the impedances of the transformer line, respectively; u the excitation control, in p.u.; V_t and V_{ref} the generator terminal voltage and its reference value, respectively; K_a and T_a the control gain and time constant of the AVR, respectively; E_{fd} and E_{fd0} the field excitation voltage and its initial value, respectively.

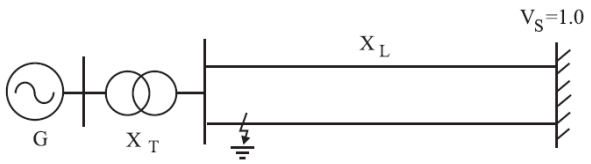

Figure 3.1: The single-machine infinite-bus power system

3.3 Input-Output Linearization Approach

Most feedback linearization approaches are based on input-output linearization or state-space linearization. In the state-space linearization approach, the goal is to linearize the map between the transformed inputs and the entire vector of transformed state variables. This objective is achieved by deriving artificial outputs (y) that yield a feedback linearized model with state dimension $r = n$. A linear controller is then synthesized for the linear input-state model. However, this approach may fail to simplify the controller design task because the map between the transformed inputs and the original outputs (y) generally is nonlinear.

In the input-output feedback linearization approach, the objective is to linearize the map between the transformed inputs (u) and the actual outputs (y) and then a linear controller is designed for the linearized input-output model which can be represented by equation (3.3) and equation (3.4) with $r \leq n$. Input-Output linearization techniques are restricted to process in which these so-called zero dynamics are stable. But in comparison with state-space linearization, input-output linearization is preferable for most process control applications because for some processes, it is possible to simultaneously linearize the input-state and input-output maps because the original outputs yield a linear model with dimension $r = n$. Consider the single-input-single-output system

$$\dot{x} = f(x) + g(x)u \tag{3.3}$$

$$y = h(x) \tag{3.4}$$

where f, g , and h are sufficiently smooth in a domain $D \subset \mathcal{R}^n$. The mappings

$f: D \to \mathcal{R}^n$ and $g: D \to \mathcal{R}^n$ are called vector fields on D.

Derive conditions which allow us to transform the system such that the input output map is linear.

The derivative $\dot{y}$ is given by

$$\dot{y} = \frac{\partial h}{\partial x}[f(x) + g(x)u] = \mathcal{L}_f h(x) + \mathcal{L}_g h(x)u \tag{3.5}$$

where

$$\frac{\partial h}{\partial x} f(x) = \mathcal{L}_f h(x) \tag{3.6}$$

is called the Lie Derivative of h with respect to f.

then

$$\mathcal{L}_g \mathcal{L}_f h(x) = \frac{\partial(\mathcal{L}_f h)}{\partial x} g(x) \tag{3.7}$$

$$\mathcal{L}^0{}_f h(x) = h(x) \tag{3.8}$$

$$\mathcal{L}^2{}_f h(x) = \mathcal{L}_f \mathcal{L}_f h(x) = \frac{\partial(\mathcal{L}_f h)}{\partial x} f(x) \tag{3.9}$$

$$\mathcal{L}^k{}_f h(x) = \mathcal{L}_f \mathcal{L}_f{}^{k-1} h(x) = \frac{\partial(\mathcal{L}_f{}^{k-1} h)}{\partial x} f(x) \tag{3.10}$$

If $\mathcal{L}_g h(x)u = 0$ then $\dot{y} = \mathcal{L}_f h(x)$ (independent of u).

Computing the second derivative as:

$$y^{(2)} = \frac{\partial(\mathcal{L}_f h)}{\partial x}[f(x) + g(x)u] = \mathcal{L}^2{}_f h(x) + \mathcal{L}_g \mathcal{L}_f h(x)u \tag{3.11}$$

If $\mathcal{L}_g \mathcal{L}_f h(x)u = 0$ then $\dot{y}^{(2)} = \mathcal{L}^2{}_f h(x)$ (independent of u).

Repeating this process, it follows that if

$$\mathcal{L}_g \mathcal{L}_f{}^{i-1} h(x) = 0, \quad i = 1, 2, \ldots, \rho - 1 \tag{3.12}$$

$$\mathcal{L}_g \mathcal{L}_f{}^{\rho-1} h(x) \neq 0 \tag{3.13}$$

then u dose not appear in y, $\dot{y}$, …, $y^{(\rho-1)}$ and

$$y^{(\rho)} = \mathcal{L}^{\rho}{}_f h(x) + \mathcal{L}_g \mathcal{L}_f{}^{\rho-1} h(x) u \tag{3.14}$$

Therefore, by setting

$$u = \frac{1}{\mathcal{L}_g \mathcal{L}_f{}^{\rho-1} h(x)} \left[-\mathcal{L}^{\rho}{}_f h(x) + v \right] \tag{3.15}$$

the system is input output linearizable and reduces to

$$y^{(\rho)} = v \quad \rightarrow chain\ of\ \rho\ integrators \tag{3.16}$$

The basic approach of input-output linearization is simply to differentiate the output function y repeatedly until the input u appears, and the design u to cancel the nonlinearity. v is the control of the linear system and ρ is the relative degree, u is the nonlinear feedback control. Based on the above procedure the SISO system is said to have relative degree ρ. Note that (3.15) is existed when $\mathcal{L}_g \mathcal{L}_f{}^{\rho-1} h(x) \neq 0, for\ all\ x$.

3.4 Design of Feedback Linearizing Control based PSS

By defining state variables as:

$$x = [x_1\ x_2\ x_3\ x_4]^{\intercal} = [\delta - \delta_0\ \ \omega_0(\omega - 1)\ \ E'_q\ \ E'_{fd}\ ]^{\intercal} \tag{3.17}$$

The state equations of system (3.1) can be rewritten in a matrix form a

$$\dot{x} = f(x) + g(x)u$$

$$f(x) = \begin{bmatrix} x_2 \\ \frac{1}{M}\left[P_m - P_t - D\frac{x_2}{\omega_0}\right] \\ \frac{1}{T'_{d0}}\left(-E_q + E_{fd}\right) \\ \frac{1}{T_A}x_4 + \frac{K_A}{T_A}\left(V_{ref} - V_t\right) \end{bmatrix};\ g(x) = \begin{bmatrix} 0 \\ 0 \\ 0 \\ \frac{K_A}{T_A} \end{bmatrix};\ u = u_{pss} \tag{3.18}$$

$$y = h(x) = x_1 \tag{3.19}$$

For system (3.18) with the chosen output (3.19), we have

$$\mathcal{L}_g h(x) = 0$$

$$\mathcal{L}_f h(x) = x_2$$

$$\mathcal{L}_g \mathcal{L}_f h(x) = 0$$

$$\mathcal{L}^2{}_f h(x)/\omega_0 = \frac{1}{M}\left[P_m - P_t - D\frac{x_2}{\omega_0}\right]$$

$$\mathcal{L}_g \mathcal{L}^2{}_f h(x) = 0$$

$$\mathcal{L}^3{}_f h(x)/\omega_0 = -\frac{1}{M} * \left(\frac{E'_q * V_b * \cos\delta}{X'_{d\Sigma}} - \frac{V^2{}_b * (X_d - X'_d) * \cos 2\delta}{X'_{d\Sigma} X_{q\Sigma}}\right) * x_2$$

$$-\frac{D}{M^2} * \left(P_m - P_t - D * \frac{x_2}{\omega}\right) - \left[\frac{V_b * \sin\delta}{M * X'_{d\Sigma}} * \frac{1}{T'_{d0}} * (E_{fd} - E_q)\right]$$

$$\mathcal{L}^4{}_f h(x)/\omega_0$$

$$= \left[-\frac{x_2}{M} * \left(\frac{-E'_q * V_b * \sin\delta}{X'_{d\Sigma}} + \frac{V^2{}_b * (X_d - X'_d) * \sin 2\delta}{X'_{d\Sigma} X_{q\Sigma}}\right) + \frac{D}{M^2}\right.$$

$$\left. * \left(\frac{E'_q * V_b * \cos\delta}{X'_{d\Sigma}} - \frac{V^2{}_b * (X_d - X'_d) * \cos 2\delta}{X'_{d\Sigma} X_{q\Sigma}}\right) - \frac{1}{M} * \frac{V_b * \cos\delta}{X'_{d\Sigma}}\right.$$

$$\left. * \frac{(E_{fd} - E_q)}{T'_{d0}}\right] * x_2 + \frac{D^2\left(P_m - P_t - \frac{D * x_2}{\omega_0}\right)}{M^3 * \omega_0}$$

$$+ \left[-\frac{x_2}{M} * \frac{V_b * \cos\delta}{X'_{d\Sigma}} + \frac{D}{M^2} * \frac{V_b * \cos\delta}{X'_{d\Sigma}} + \frac{1}{M} * \frac{V_b * \sin\delta}{X'_{d\Sigma}} * \frac{X_{d\Sigma}}{X'_{d\Sigma}}\right.$$

$$\left. * \frac{1}{T'_{d0}}\right] * f_3 + \left(-\frac{1}{M} * \frac{V_b * \sin\delta}{X'_{d\Sigma}} * \frac{1}{T'_{d0}}\right)$$

$$* f_4$$

$$\mathcal{L}_g \mathcal{L}^3{}_f h(x) = -\omega_0 * \frac{V_b * \sin\delta}{M * X'_{d\Sigma}} * \frac{1}{T'_{d0}} * \frac{K_A}{T_A}$$

As $\mathcal{L}_g \mathcal{L}^3{}_f h(x) \neq 0, \forall\delta \neq k\pi, k = 0,1,2 \ldots,$ the system has relative degree of 4.

The 4th-order derivative of y with respect to time could be obtained as

$$\frac{d^4 y}{dt^4} = a(x) + b(x)u_{pss} \tag{3.20}$$

where

$$a(x) = \mathcal{L}^4{}_f h(x) \tag{3.21}$$

$$b(x) = \mathcal{L}_g \mathcal{L}^3{}_f h(x) \tag{3.22}$$

Define new states $z_1 = y,\ z_2 = \dot{y},\ z_3 = \ddot{y},\ z_4 = \dddot{y}$, system (3.20) can be represented as

$$\begin{cases} \dot{z}_1 = z_2 \\ \dot{z}_2 = z_3 \\ \dot{z}_3 = z_4 \\ \dot{z}_4 = a(x) + b(x)u_{pss} \end{cases} \tag{3.23}$$

Let

$$v = a(x) + b(x)u_{pss} \ ,$$

and system (3.23) becomes

$$\begin{bmatrix} \dot{z}_1 \\ \dot{z}_2 \\ \dot{z}_3 \\ z_4 \end{bmatrix} = \begin{bmatrix} 0 & 1 & 0 & 0 \\ 0 & 0 & 1 & 0 \\ 0 & 0 & 0 & 1 \\ 0 & 0 & 0 & 0 \end{bmatrix} * \begin{bmatrix} z_1 \\ z_2 \\ z_3 \\ z_4 \end{bmatrix} + \begin{bmatrix} 0 \\ 0 \\ 0 \\ v \end{bmatrix} \tag{3.24}$$

$$v = -kz = [-k_1 \ -k_2 \ -k_3 \ - \ k_4] * \begin{bmatrix} z_1 \\ z_2 \\ z_3 \\ z_4 \end{bmatrix} \tag{3.25}$$

which v is the control of the linear system (3.24). So, we can obtain the feedback linearization-based control of the system (3.23) as

$$u_{pss} = \frac{v - a(x)}{b(x)} \tag{3.26}$$

which only valid when $b(x) \neq 0$, that is $\delta \neq k\pi, k = 0, 1, 2, \ldots$.

3.5 Extended-state Disturbance Observer Based Nonlinear PSS

3.5.1 Perturbation Definition & Perturbation Observer

Assume all system nonlinearities and control gain functions of system (3.14) are unknown. For the simplification of formulations, define the system perturbation as

$$\Psi(x,u,t) = \mathcal{L}^{\rho}{}_{f}h(x) + (\mathcal{L}_g\mathcal{L}_f{}^{\rho-1}h(x) - b_0)u \tag{3.27}$$

where b_0 is the nominal value of $\mathcal{L}_g\mathcal{L}_f{}^{\rho-1}h(x)$ which will be decided then.

Then the system (3.14) can be rewritten as

$$y^{(\rho)} = \Psi(x,u,t) + b_0 u \tag{3.28}$$

If $y^{(\rho)}$ can be estimated, then the perturbation can be obtained by

$$\widehat{\Psi}(x,u,t) = \hat{y}^{(\rho)} - b_0 u \tag{3.29}$$

The original idea of this kind of perturbation estimation stems from the time delay control [98], in which the time-delayed values of control input and the derivatives of state variables at the previous time steps are used to cancel nominal nonlinear dynamics and uncertainties.

In the control scheme applied in this chapter, the perturbation is estimated by an extended-order nonlinear observer based on the track-differentiator [98].

In the time delay control, the derivatives of state variables are always calculated by numeric differential method, such as backward difference algorithm. It is well known that the numeric differentiator will magnify the measurement noise. In the past years, high gain observers have played an important role in the design of a nonlinear output

feedback controller for nonlinear systems. They are mainly used to estimate the derivatives of the output. In this section, an extended-order high gain observer proposed in [97] is designed to estimate the system states and perturbation.

Define a *fictitious state (extend order)* to represent the system perturbation, refine new states $z_1 = y,\ z_2 = y^{(1)},\quad z_\rho = y^{(\rho-1)}, z_{\rho+1} = y^{(\rho)}$, the state equation of system (3.14) may be represented as

$$\begin{cases} \dot{z}_1 = z_2 \\ \cdots \\ \dot{z}_\rho = z_{\rho+1} + b_0 u \\ \dot{z}_{\rho+1} = \dot{\Psi}(\cdot) \\ y = z_1 \end{cases} \tag{3.30}$$

where $\dot{\Psi}(\cdot)$ Is the derivative of $\Psi(\cdot)$.

The system (30) can be rewritten in a matrix form:

$$\begin{cases} \dot{Z} = A_1 Z + B_3 u + B_1 \dot{\Psi}(\cdot) \\ y = C_1 Z \end{cases} \tag{3.31}$$

where

$$Z = \begin{bmatrix} z_1 \\ z_2 \\ \cdots \\ z_\rho \\ z_{\rho+1} \end{bmatrix}, A_1 = \begin{bmatrix} 0 & 1 & \ldots & \ldots & 0 \\ 0 & 0 & 1 & \ldots & 0 \\ \vdots & & & & \vdots \\ 0 & 0 & 0 & \ldots & 1 \\ 0 & 0 & 0 & \ldots & 0 \end{bmatrix}_{(\rho+1)\times(\rho+1)},$$

$$B_3 = \begin{bmatrix} 0 \\ 0 \\ \vdots \\ 1 \\ 0 \end{bmatrix}_{(\rho+1)\times 1}, B_1 = \begin{bmatrix} 0 \\ 0 \\ \vdots \\ 0 \\ 1 \end{bmatrix}_{(\rho+1)\times 1}, and\ C_1 = \begin{bmatrix} 1 \\ 0 \\ \vdots \\ 0 \\ 0 \end{bmatrix}^T_{(\rho+1)\times 1}$$

The following assumptions are made on system (3.31).

A1 b_0 is chosen to satisfy: $\left|\frac{b(x)}{b_0} - 1\right| \leq \theta < 1$, where θ is a positive constant.

A2 The function $(x, u, t) : R^n \times R \times R^+ \to R$ and $\dot{\Psi}(x, u, t) : R^n \times R \times R^+ \to R$ are locally Lipschitz in their arguments over the domain of interest and globally bounded in x:

$$|\Psi(x,u,t)| \leq \gamma_1, \left|\dot{\Psi}(x,u,t)\right| \leq \gamma_2,$$

where γ_1 and γ_2 are positive constants. In addition, $\Psi(0,0,0) = 0$ and $\dot{\Psi}(0,0,0) = 0$.

Assumption **A2** guarantees that the origin is an equilibrium point of the open-loop system.

Two cases will be discussed in the following section. When the all states $z_1, z_2, \cdots, z_\rho$ are available, a perturbation observer is designed to estimate the perturbation by using z_ρ as the measurement $y = z_\rho$. When z_1 is the only available state $y = z_1$, a state and perturbation observer is designed to estimate all other states and the perturbation. Accordingly, a state-feedback and a output-feedback NAC are obtained respectively.

3.5.2 Extended-state Perturbation Observer

Assuming all states $z_\rho, i = 1, \ldots, \rho$ are available and taking z_ρ as a measurement, a high-gain track differentiator is designed as

$$\begin{cases} \dot{\hat{z}}_\rho = \hat{z}_{\rho+1} + h_1\left(z_\rho - \hat{z}_\rho\right) + b_0 u \\ \dot{\hat{z}}_{\rho+1} = h_2(z_\rho - \hat{z}_\rho) \end{cases} \tag{3.32}$$

where h_1 and h_2 are gains of the high gain observer. Throughout this section, $\tilde{z}_i = z_i - \hat{z}_i$ refers to the estimation error of z_i whereas $\hat{z}_i$ symbolizes the estimated quantity of z_i. The estimation error $\tilde{z}_i = z_i - \hat{z}_i, i = \rho, \rho + 1$, satisfies the equation

$$\begin{cases} \dot{\tilde{z}}_\rho = -h_1\tilde{z}_\rho + \tilde{z}_{n+1} \\ \dot{\tilde{z}}_{\rho+1} = -h_2\tilde{z}_\rho + \dot{\Psi}(\cdot) \end{cases} \tag{3.33}$$

The above error dynamic can be represented in a matrix form as

$$\dot{\tilde{z}}_{po} = A_{po} z_{po} + B_{po}\dot{\Psi}(\cdot) \tag{3.34}$$

where $\tilde{z}_{po} = [\tilde{z}_n,\ \tilde{z}_{n+1}]^T$, and

$$A_{po} = \begin{bmatrix} -h_1 & 1 \\ -h_2 & 0 \end{bmatrix}, B_{po} = \begin{bmatrix} 0 \\ 1 \end{bmatrix},$$

where A_{po} is a Hurwitz matrix.

Based on [97], the estimation error of the system (3.34) is summarized as below:

Consider system (3.30) and design a high gain perturbation observer (3.32). If assumptions **A1**~**A2** hold, then given any constant δ_{po}, the gain H_{po} can be chosen such that the error $\tilde{z}_{po}$ of the perturbation observer (3.32), from any initial value $\tilde{z}_{po}(0)$, converges exponentially to the neighborhood

$$\left\| \tilde{z}_{po} \right\| \leq \delta_{po} \tag{3.35}$$

3.5.3 Extended-order State and Perturbation Observer

In this section, the output is chosen as $\mathrm{y} = z_1$ and a (ρ +1) th-order state observer is designed to estimate the system states and perturbation. The state estimate $\hat{z}_1$ of system (3.31) is obtained using the observer as

$$\dot{\hat{Z}} = A_1\hat{Z} + B_3 + H\left(y - C_1\hat{Z}\right) \tag{3.36}$$

The observer gain H is chosen as:

$$\mathrm{H} = \begin{bmatrix} \frac{\alpha_1}{\epsilon} \\ \frac{\alpha_2}{\epsilon^2} \\ \vdots \\ \frac{\alpha_\rho}{\epsilon^\rho} \\ \frac{\alpha_{\rho+1}}{\epsilon^{\rho+1}} \end{bmatrix}, \tag{3.37}$$

where ϵ is a positive constant, $0 < \epsilon < 1$, to be specified and the positive constants $\alpha_i, i = 1,2,\cdots,\rho+1,$ are chosen such that the roots of

$$s^{\rho+1} + \alpha_1 s^\rho + \cdots + \alpha_\rho s + \alpha_{\rho+1} = 0 \tag{3.38}$$

are in the open left-half complex plan, where s is the Laplace operator.

Defining the estimation error as $\tilde{z}_e = z_e - \hat{z}_e$, the error dynamics of observer (3.36) becomes

$$\dot{\tilde{z}}_e = (A_1 - HC_1)\tilde{z}_e + B_1\dot{\Psi}(\cdot) \tag{3.39}$$

For the purpose of analysis, replace the observer error dynamics by the equivalent dynamics of the scaled estimation error

$$\eta_i = \frac{\tilde{z}_i}{\epsilon^{\rho+1-i}}, \qquad 1 \le i \le \rho + 1.$$

Hence, we have $\hat{z}_e = z_e - D(\epsilon)\eta$, where

$$\eta = [\eta_1, \eta_2 \dots, \eta_{n+1}]^T,$$

$$D(\epsilon) = diag[\epsilon^{\rho+1}, \dots, 1]_{(\rho+1)\times(\rho+1)}$$

Then the error dynamics of observer (3.39) can be represented as

$$\dot{\eta} = D^{-1}(\epsilon)(A_1 - HC_1)D(\epsilon)\eta + D^{-1}(\eta)B_1\dot{\Psi}(\cdot) = \frac{1}{\epsilon}A_{10}\eta + B_1\dot{\Psi}(\cdot) \tag{3.40}$$

where

$$A_{10} = \begin{bmatrix} -\alpha_1 & 1 & \dots & \dots & 0 \\ -\alpha_2 & 0 & 1 & \dots & 0 \\ \vdots & & & & \vdots \\ -\alpha_\rho & 0 & 0 & \dots & 1 \\ -\alpha_{\rho+1} & 0 & 0 & \dots & 0 \end{bmatrix}$$

is Hurwitzian.

3.5.4 Design of ESO Based Control

The estimate of perturbation $\hat{z}_{\rho+1}$ is used to realize the feedback linearization of the nonlinear system (3.31). After the unknown system nonlinearities and uncertainties are cancelled by the perturbation estimate, a linear state feedback controller is designed for the equivalent linear system. The complete control is designed as follows:

$$\begin{cases} u = \dfrac{v}{b_0} - \dfrac{\tilde{z}_{\rho+1}}{b_0} \\ v = -KZ \end{cases} \tag{3.41}$$

where $K = [\, k_1,\ k_2 \cdots\ k_n]^T$ is the linear feedback controller gains, which make the matrix $A_0 = A - BK$ be Hurwitzian.

Using the estimates of states and perturbation, an output feedback linearization control law is designed for the nonlinear system (3.31). The complete control is designed the same as that represented by equation (3.41) except that the true states are replaced with the estimated states:

$$\begin{cases} u = \dfrac{v}{b_0} - \dfrac{\tilde{z}_{\rho+1}}{b_0} \\ v = -K\hat{Z} \end{cases} \tag{3.42}$$

where $K = [\, k_1,\ k_2 \cdots\ k_n]^T$ is the linear feedback controller gains, which make the matrix $A_0 = A - BK$ be Hurwitzian. Note that the analysis of the closed-loop system under the perturbation observer and the controller is given in [97].

3.6 Design of ESO Based PSS (ESO_PSS)

Based on system (3.23), choose $y = z_4$, design a 2rd-order perturbation observer based on (3.32) as:

$$\begin{cases} \dot{\hat{z}}_4 = \hat{z}_5 + h_1(z_4 - \hat{z}_4) + b_0 u_{pss} \\ \dot{\hat{z}}_5 = h_2(z_4 - \hat{z}_4) \end{cases} \tag{3.43}$$

and then the state – feedback ESO-PSS can be obtained from (3.41) as:

$$\begin{cases} u = \dfrac{v}{b_0} - \dfrac{\tilde{z}_5}{b_0} \\ v = -KZ \end{cases} \tag{3.44}$$

Similarly, $y = z_1$, a 5th–order state and perturbation observer can be designed based

on system (3.36) as:

$$\begin{cases} y = z_1 \\ \dot{\hat{z}}_1 = \hat{z}_2 + h_1(z_1 - \hat{z}_1) \\ \dot{\hat{z}}_2 = \hat{z}_3 + h_2(z_1 - \hat{z}_1) \\ \dot{\hat{z}}_4 = \hat{z}_3 + h_3(z_1 - \hat{z}_1) + b_0 u_{pss} \\ \dot{\hat{z}}_5 = h_5(z_1 - \hat{z}_1) \end{cases} \tag{3.45}$$

and then the output – feedback ESO-PSS can be obtained from (3.42) as:

$$\begin{cases} u = \dfrac{v}{b_0} - \dfrac{\tilde{z}_5}{b_0} \\ v = -K\hat{Z} \end{cases} \tag{3.46}$$

Note that a fifth order SPO is difficult to be implemented in practice due to the ultra-high gains used. In next chapter, a unified disturbance estimator (UDE) based on frequency domain will be investigated, in which the UDE only requires the same-order derivatives of system state equation and can be designed on output based only.

3.7 Simulation Results

The structure of the nonlinear PSS connected to the generator excitation system together with an AVR and PSS is shown in Figure 3.2

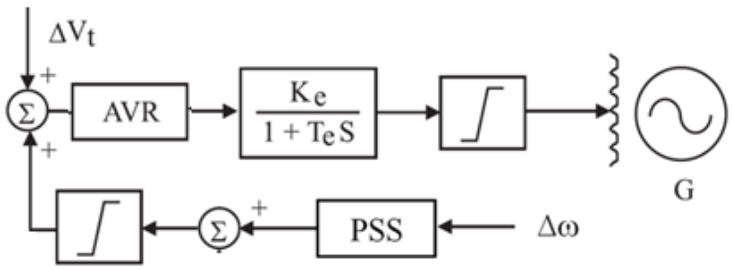

Figure 3.2 Excitation system with AVR and PSS

Simulation studies have been undertaken on a single-machine infinite-bus

power system as shown in Figure 2.1, based on same parameters given in Chapter 2. The performances of the controller are investigated with a three-phase-to-ground short-circuit fault occurring at the sending end of the transmission lines. The fault happens at 2 second and last for 0.1s, then the fault is cleared.

Pole placement technique is used to design the linear control v. Let p as the chosen pole, then $K = [\,k_1,\ k_2 \cdots\ k_n]^T = [\,p^4,\ 4p^3, 6p^2, 4p]^T$. Here $p = 12$. Note the FLCPSS and the ESOPSS use the same v. The PSS's output is limited by ±0.125 p.u.

3.7.1 Comparison of performance of FLCPSS with CPSS

Simulation results of FLCPSS are shown in Figure 3.3 to Figure 3.6, which illustrate that the performance of FLCPSS is much better than that of the CPSS. Pole location is a key parameter of the FLCPSS, in which a large value may result in unnecessary very large control gain and sensitive to measurement noise, while a small value may result in worse performance than the CPSS and even unstable system. Pole value ranges within [6, 8, 10, 12] are tested and results are shown in Figure 3.7. Note the FLCPSS gain better performance with a relatively aggressive and larger control output than the CPSS, as shown in Fig. 3.6 and also a worse voltage performance in Fig. 3.5.

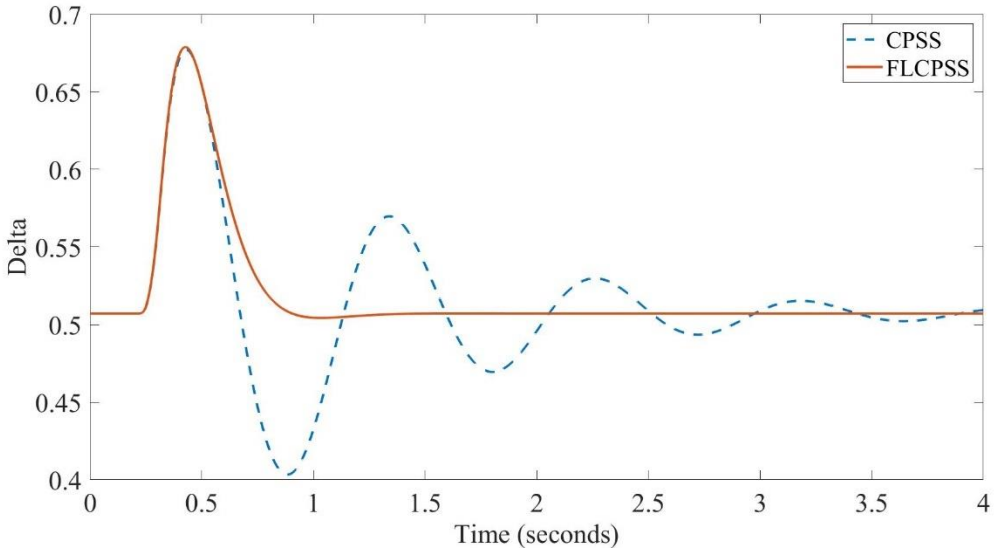

Figure 3.3 Rotor angle response of FLCPSS

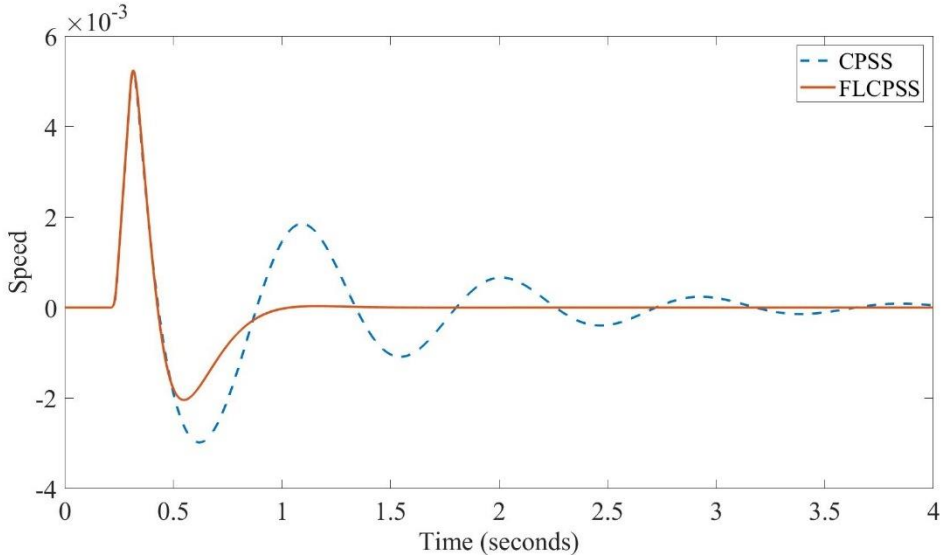

Figure 3.4 Rotor speed response of FLCPSS

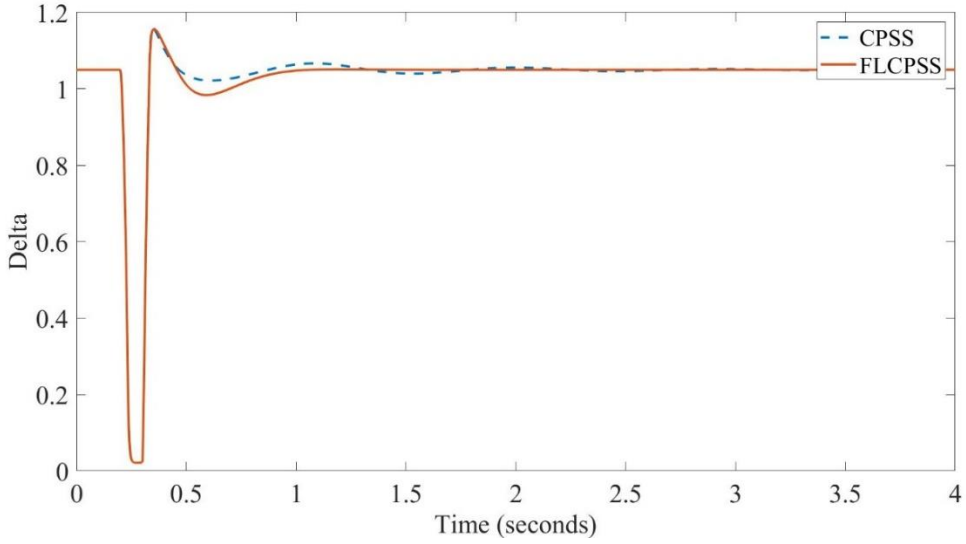

Figure 3.5 Voltage response of FLCPSS

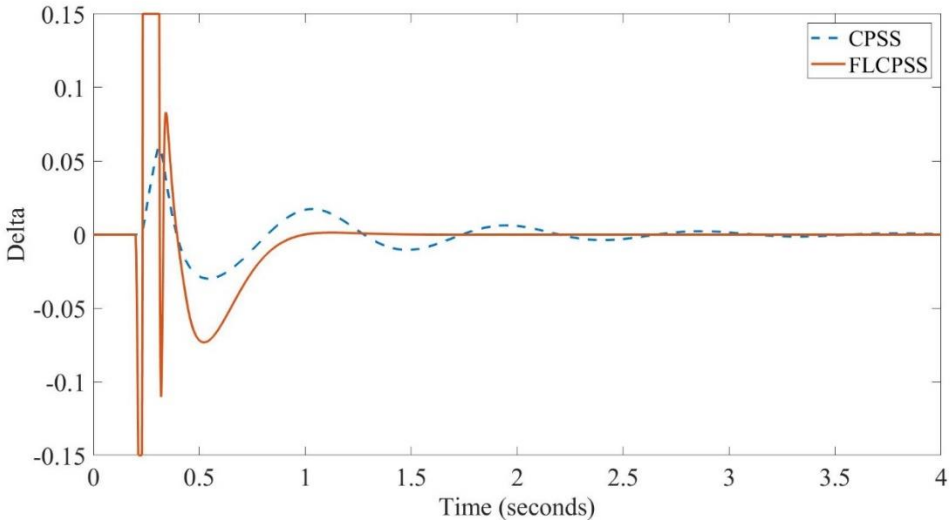

Figure 3.6 Control output of FLCPSS

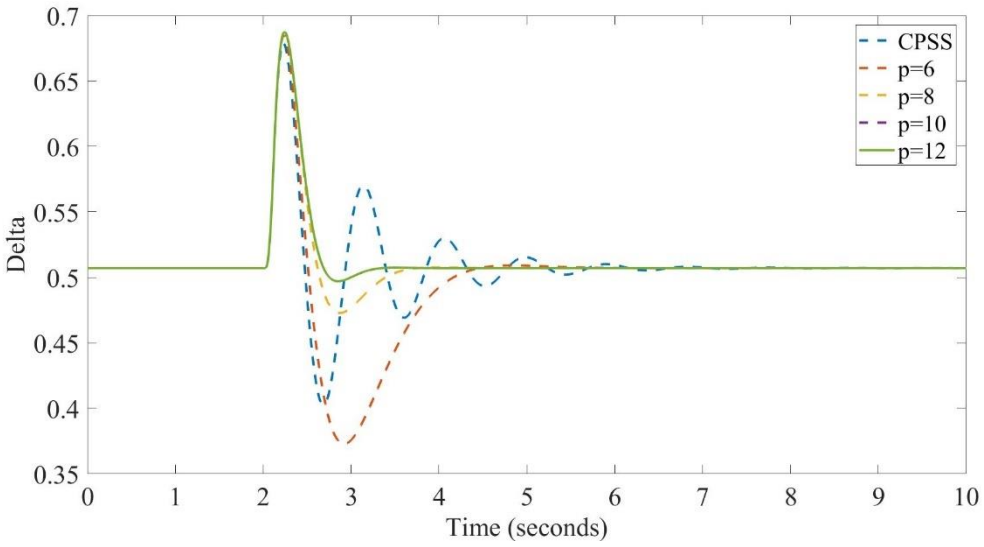

Figure 3.7 Performance comparison with different poles' value for FLCPSS

3.7.2 Performance of ESOPSS

Response of the ESOPSS is shown in Fig. 3.8. Note that ESOPSS can provide almost the same performance as the FLCPSS Note that ESOPSS does not require the accurate nonlinear model and utilize the ESO to estimate the nonlinearities and then compensate it in real time. The FLCPSS however requires the accurate nonlinear model and thus it can provide better performance, but it can predict that the weak robustness to parameter uncertainties.

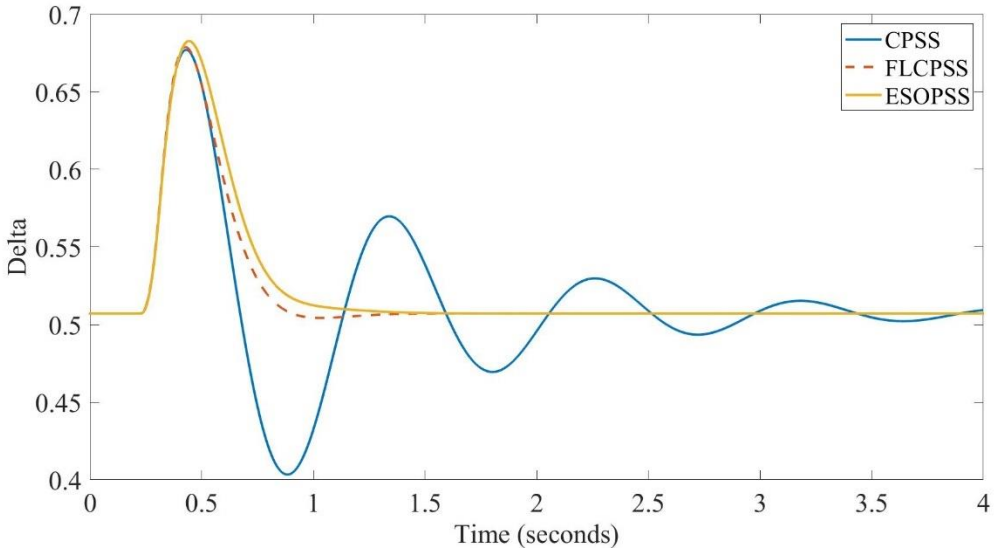
CPSS
FLCPSS
ESOPSS
Delta
Time (seconds)
0.7
0.65
0.6
0.55
0.5
0.45
0.4
0
0.5
1
1.5
2
2.5
3
3.5
4

(a)

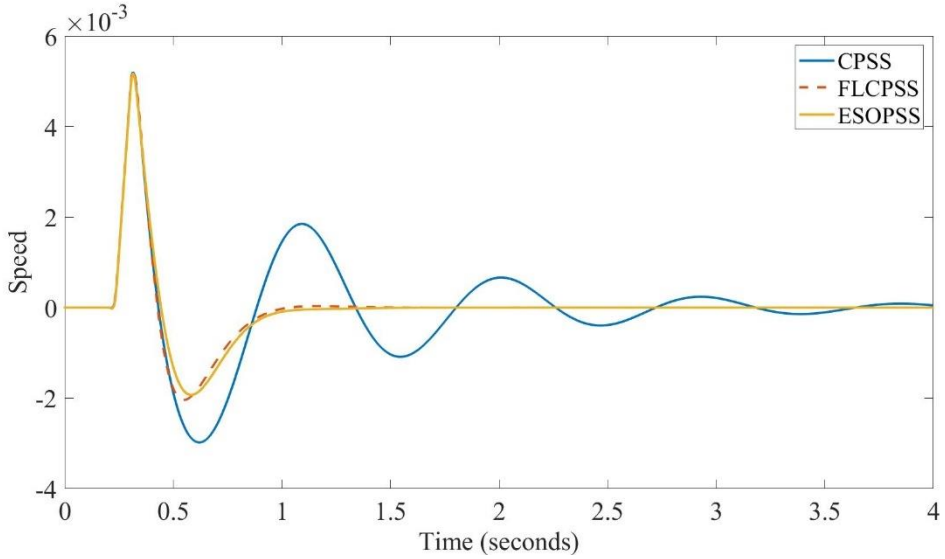
×10-3
CPSS
FLCPSS
ESOPSS
Speed
Time (seconds)
6
4
2
0
-2
-4
0
0.5
1
1.5
2
2.5
3
3.5
4

(b)

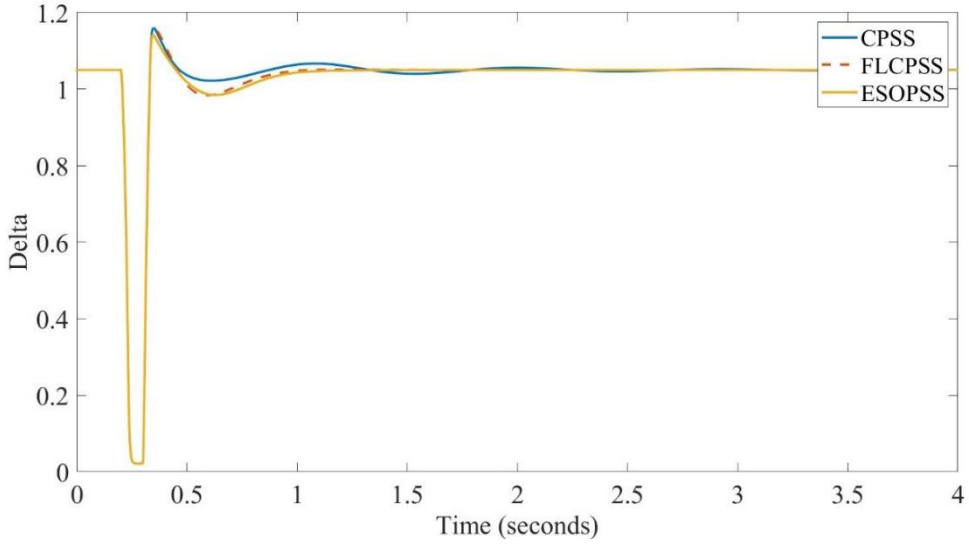

(c)

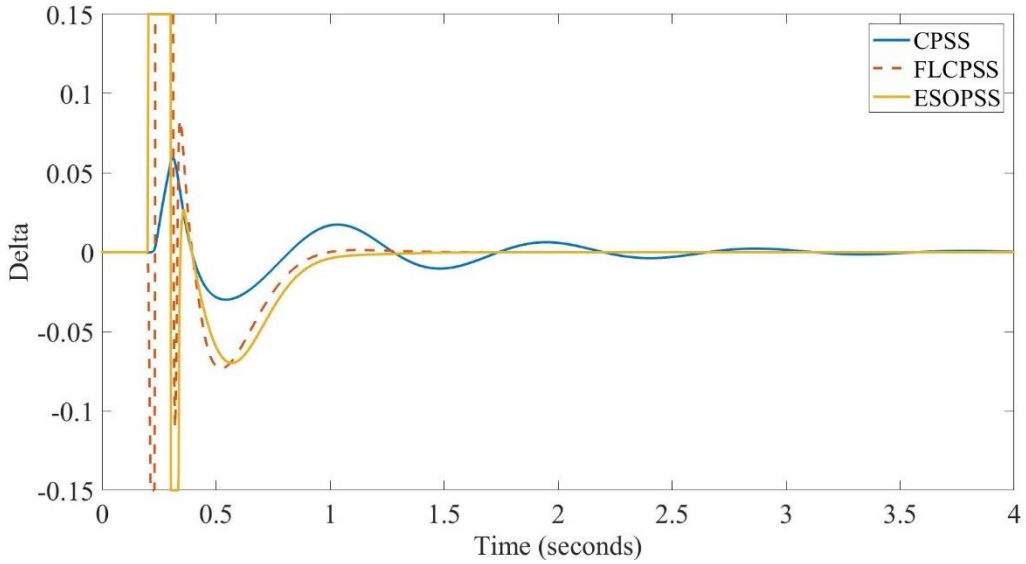

(d)

Figure 3.8 Response of ESOPSS (a) Rotor angle; (b) Speed; (c) Terminal voltage Vt;

(d) Control

3.7.3 Performance of the ESPO

If we assume all states are measurable in the system (23), i.e., $z_1 = y,\ z_2 = \dot{y},\ z_3 = \ddot{y},\ z_4 = \dddot{y}$ are all available, then choose $z_4 = \dddot{y}\ as\ measurement,$ a

second-order extended state PO is designed as: pole=20 and $\epsilon = 0.01$, that is $\alpha_1 = 2 * p = 40, \alpha_2 = p * p = 400$. The response of the PO is shown in Fig. 3.9. If only $z_1 = y$ is available, a fifth order SPO should be designed to estimate the state and the perturbation [97]. However, this will result in an extremely large gain to prevent its applicability in practice. In fact, this is the main disadvantage of the ESO, especially the high gain-based observer. Here for an illustration purpose, a third order SPO is designed with $z_3 = \ddot{y}$ as the measurement, with the same pole =20, and and $\epsilon = 0.01$. The 3-rd SPO's output is shown in Fig. 3.10. Note that both observers cannot provide accurate estimate of the a(x) (assuming all nonlinearities are unknown), but the closed-loop performance of the ESOPSS still is acceptable. The main reason is that the estimate can at least partially compensate the real uncertainties and also the second reason is the closed-loop control can provide correct function.

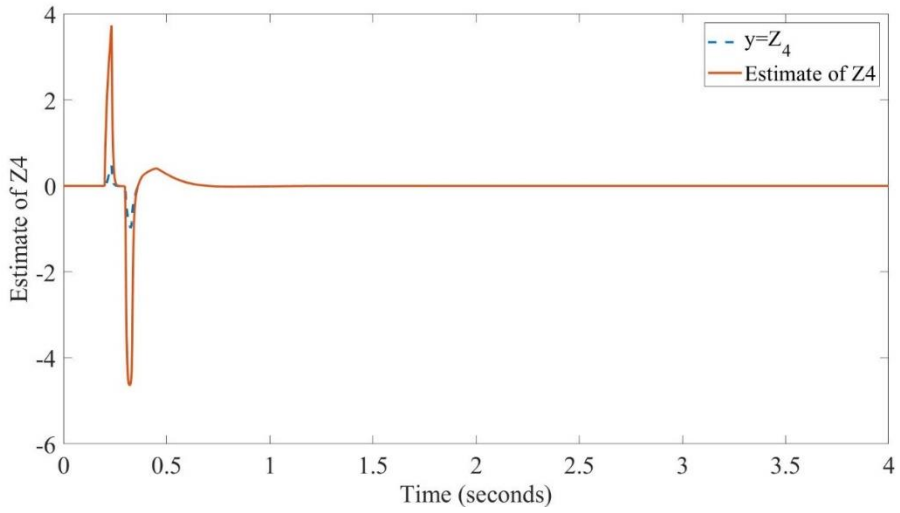

(a)

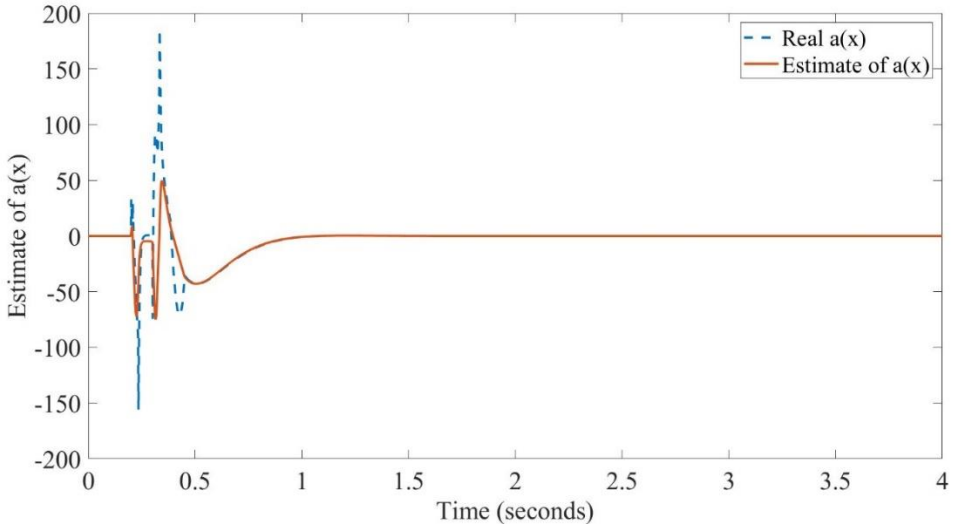

(b)

Figure 3.9 Response of second-order PO with $z_4 = \ddot{y}$ as the available measurement.

(a) Z4 and its estimate; (b) Real a(x) and its estimate

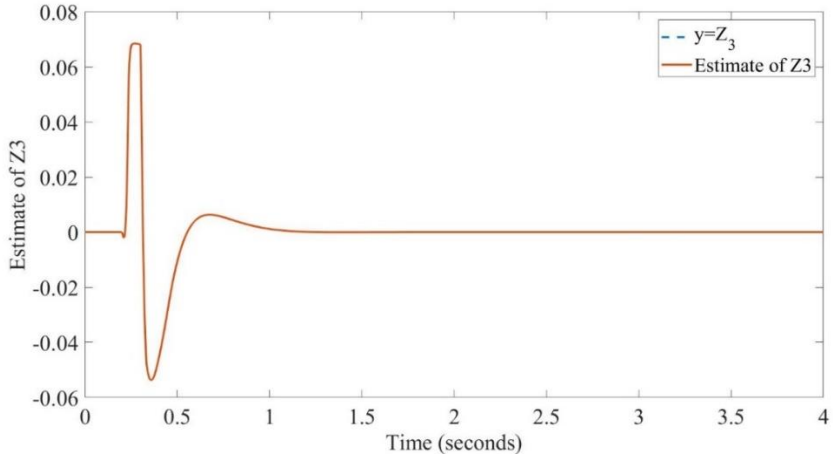

(a)

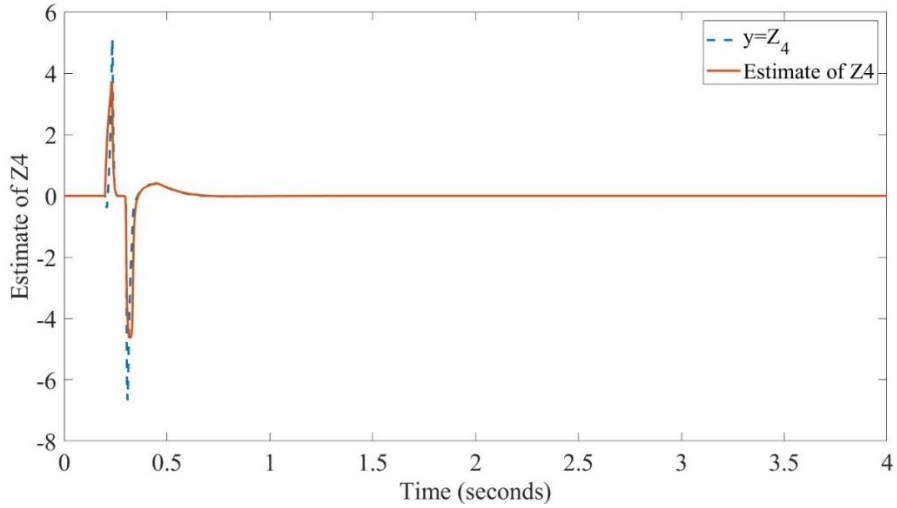

(b)

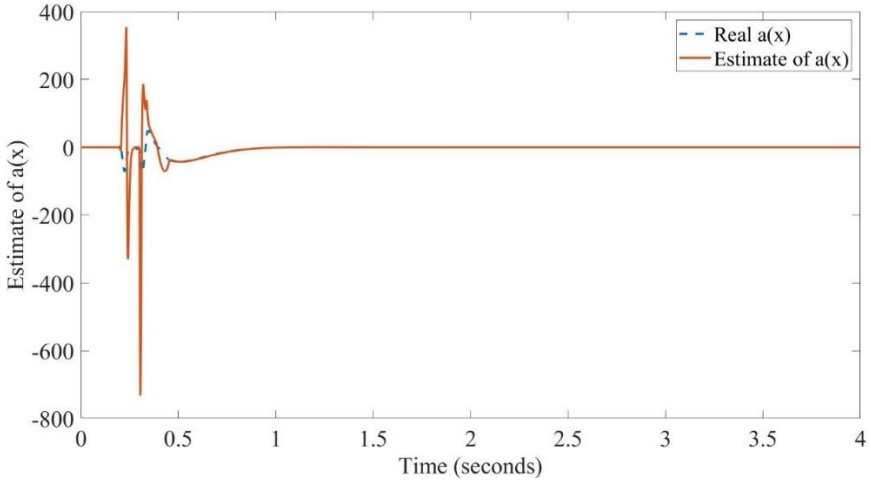

(c)

Figure 3.10 Response of second-order PO with as the available measurement $z_3 = \ddot{y}$.

(a) Z3 and its estimate; (b) Z4 and its estimate; (c) Real a(x) and its estimate

3.7.4 Robustness test

The robustness of the controller is evaluated in the cases of the variation of the system operation conditions. From the results, it can be seen that the nonlinear PSS (NPSS) including FLC and ESOPSS, have a better performance than the CPSS and without using PSS. After the fault transmission line been cut off after 0.1s, the total reactance

of the transmission line is half its initial value. Thus, the system operation point is changed because of the fault, as seen in the rotor angle response from its initial value 0.681 to 1.2 in Figure 3.10 (a). Beside the rotor angle, all other state variables, such as angular frequency, terminal voltage and generator power is stabilized to its initial value in steady state. With the use of the nonlinear compensator, the rotor angle, angular frequency, and generator power oscillation are eliminated with less than half the clear time in CPSS.

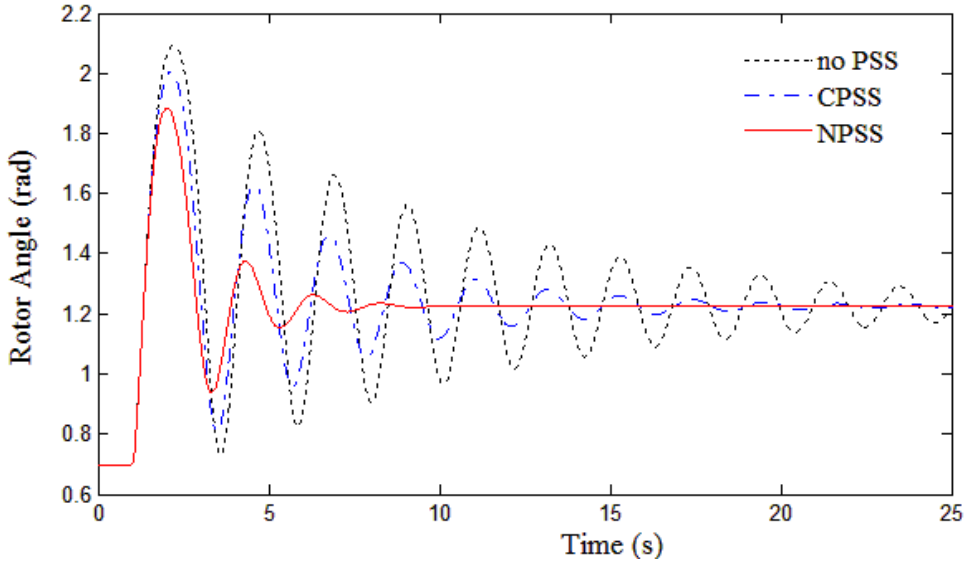
Rotor Angle (rad)
Time (s)
no PSS
CPSS
NPSS
2.2
2
1.8
1.6
1.4
1.2
1
0.8
0.6
0
5
10
15
20
25

(a)

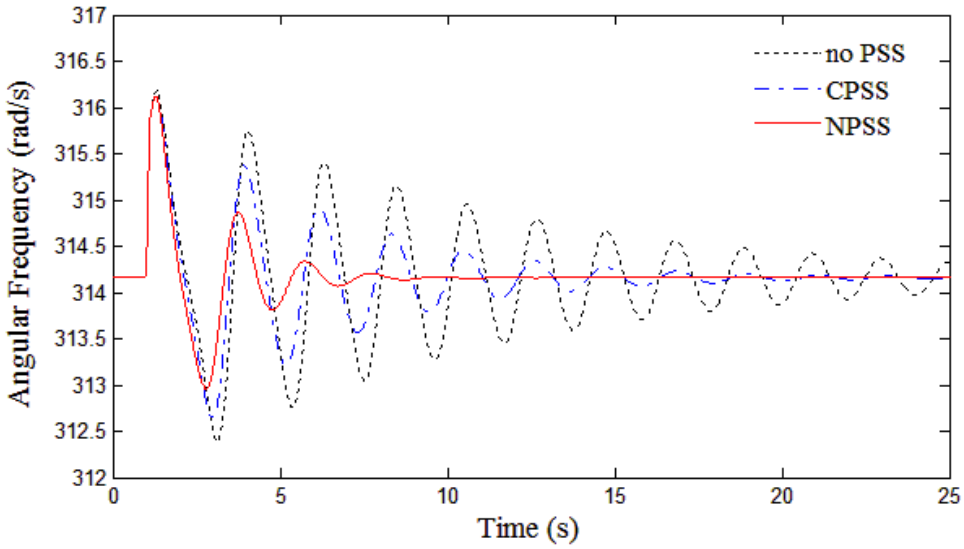
Angular Frequency (rad/s)
Time (s)
no PSS
CPSS
NPSS
317
316.5
316
315.5
315
314.5
314
313.5
313
312.5
312
0
5
10
15
20
25

(b)

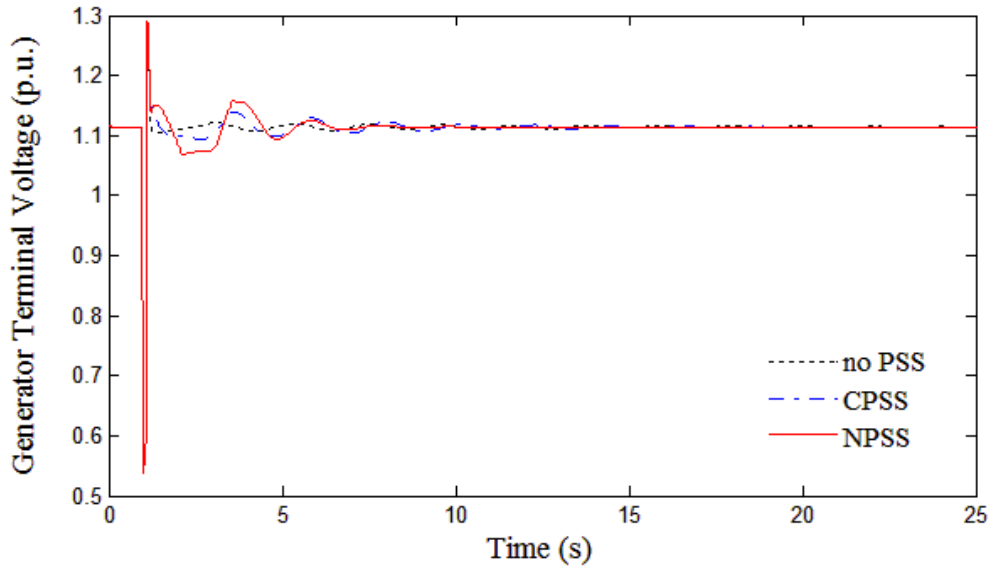

(c)

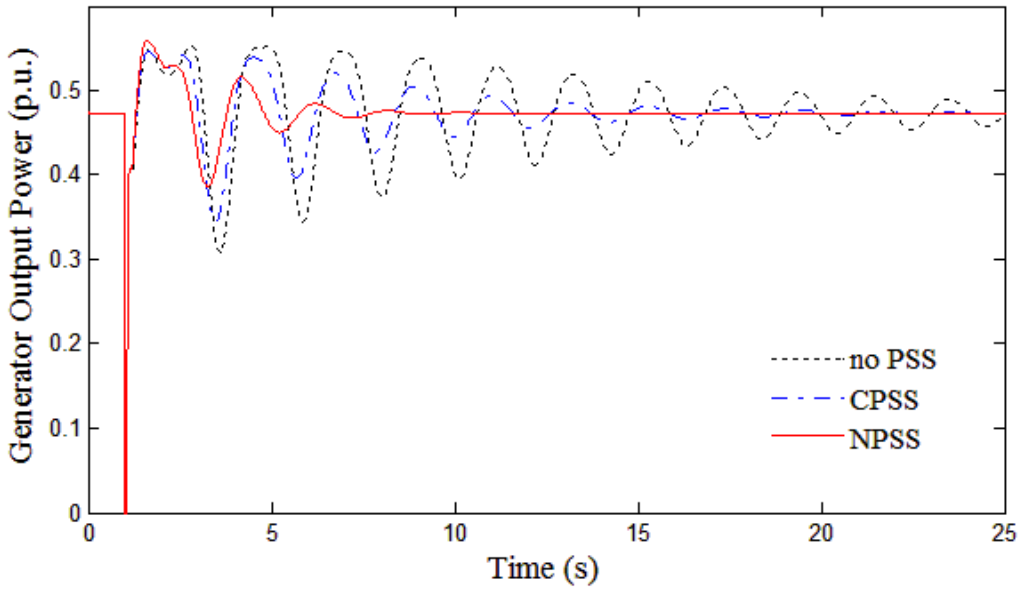

(d)

Figure3.11: Simulation results comparison between different PSS under transmission line short-circuit fault. (a) Rotor angle in rad; (b) Angular frequency in rad/s; (c) Generator terminal voltage in p.u.; and (d) Generator output power in p.u.

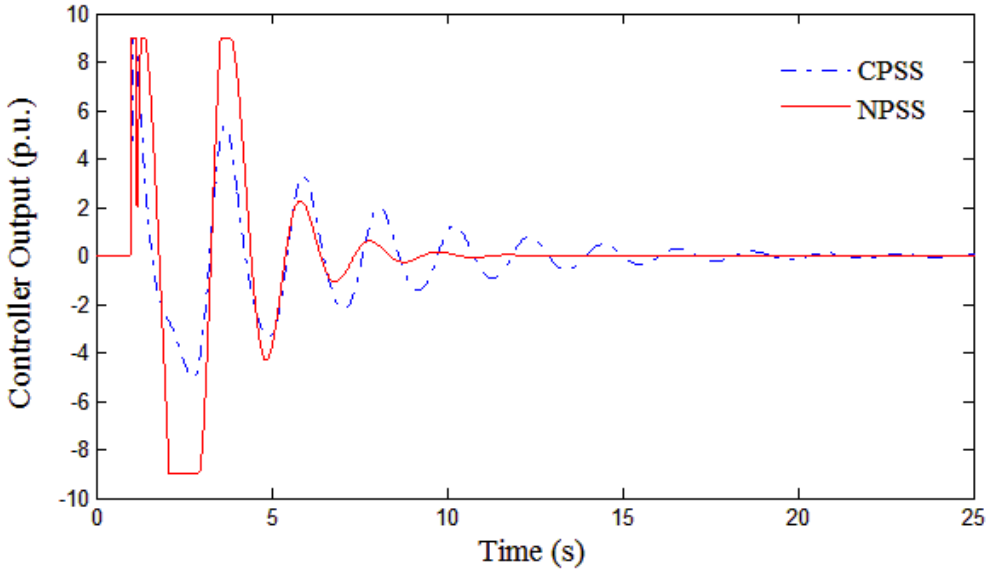

Figure 3.12: Controller output comparison between CPSS and NPSS under transmission line short-circuit fault.

To compare with the control efficiency under the same performance, the CPSS control gain can be increased to improve its performance. Figure 3.12 shows the comparison results of the control performance under the same condition with increase the control gain of CPSS to the 10 times its initial value. Then the control performance of NPSS and CPSS are almost the same, with a much quicker clear time in oscillation.

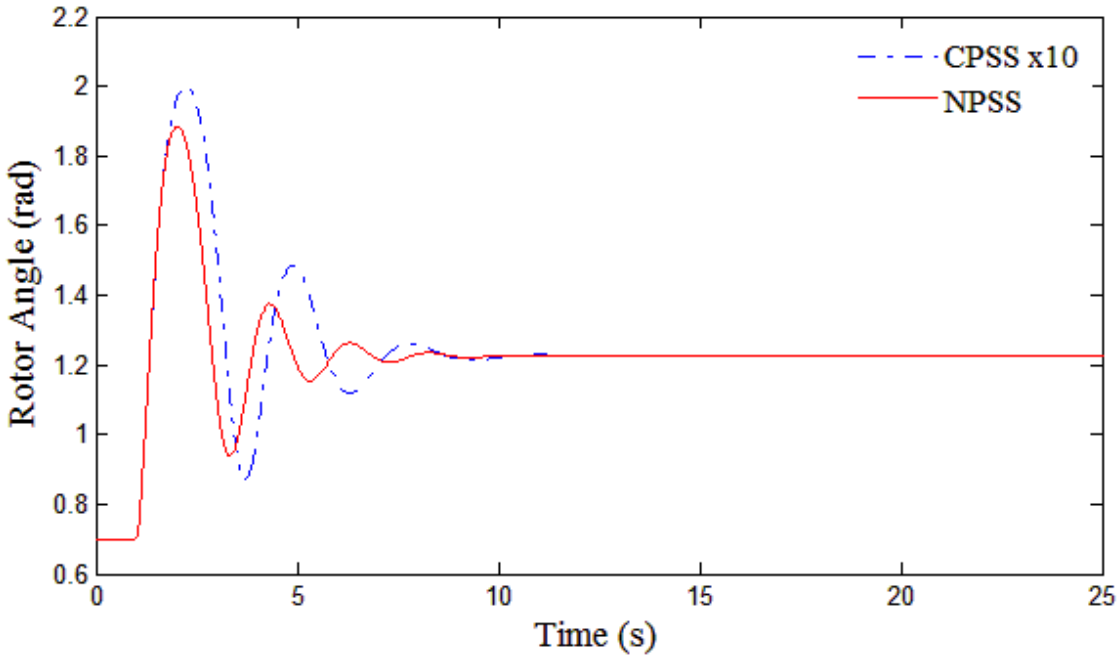

(a)

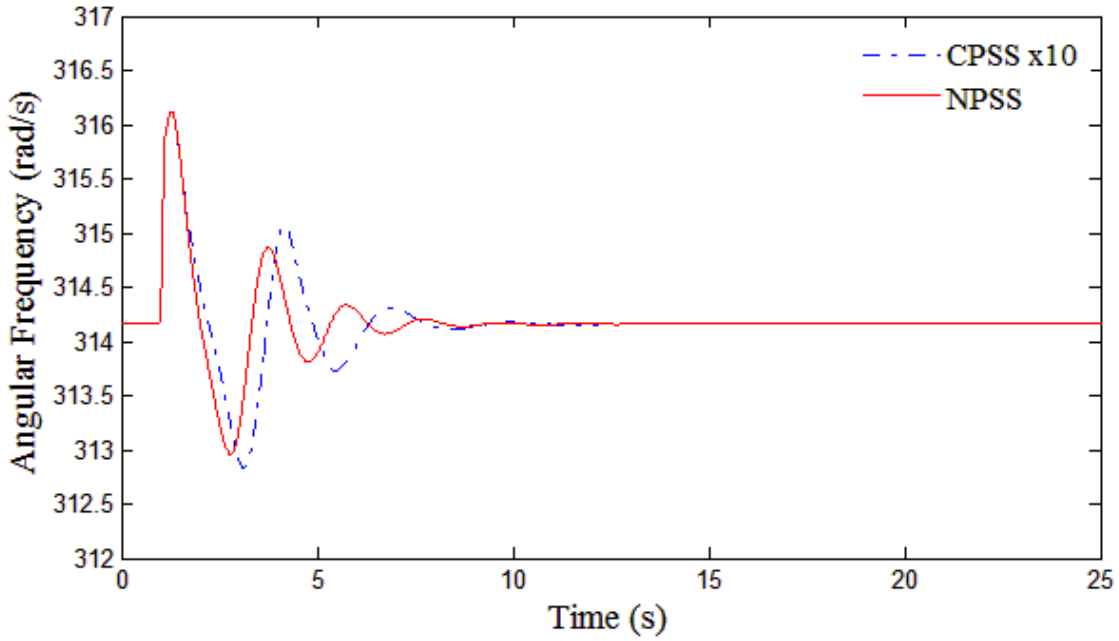
CPSS x10
NPSS
Angular Frequency (rad/s)
Time (s)
317
316.5
316
315.5
315
314.5
314
313.5
313
312.5
312
0
5
10
15
20
25

(b)

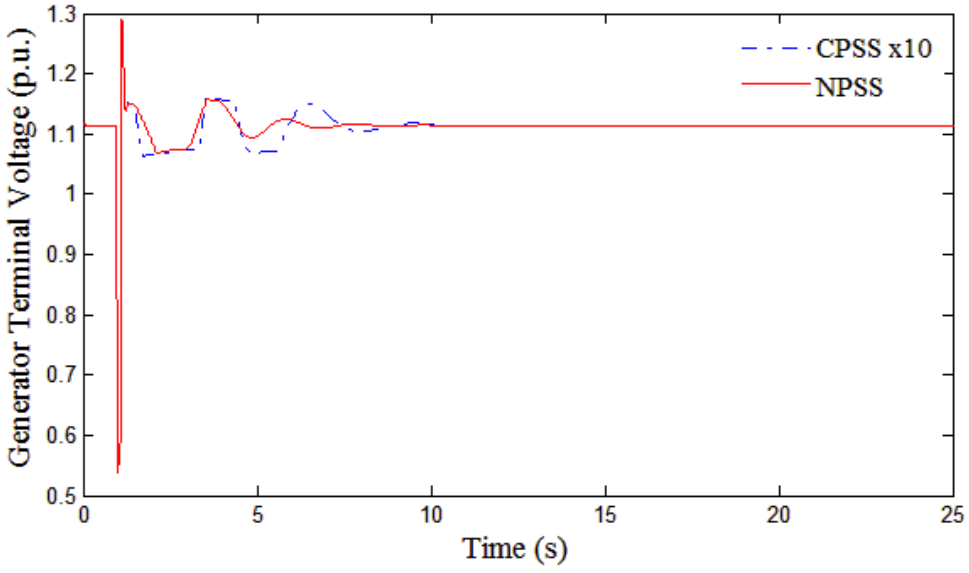
CPSS x10
NPSS
Generator Terminal Voltage (p.u.)
Time (s)
1.3
1.2
1.1
1
0.9
0.8
0.7
0.6
0.5
0
5
10
15
20
25

(C)

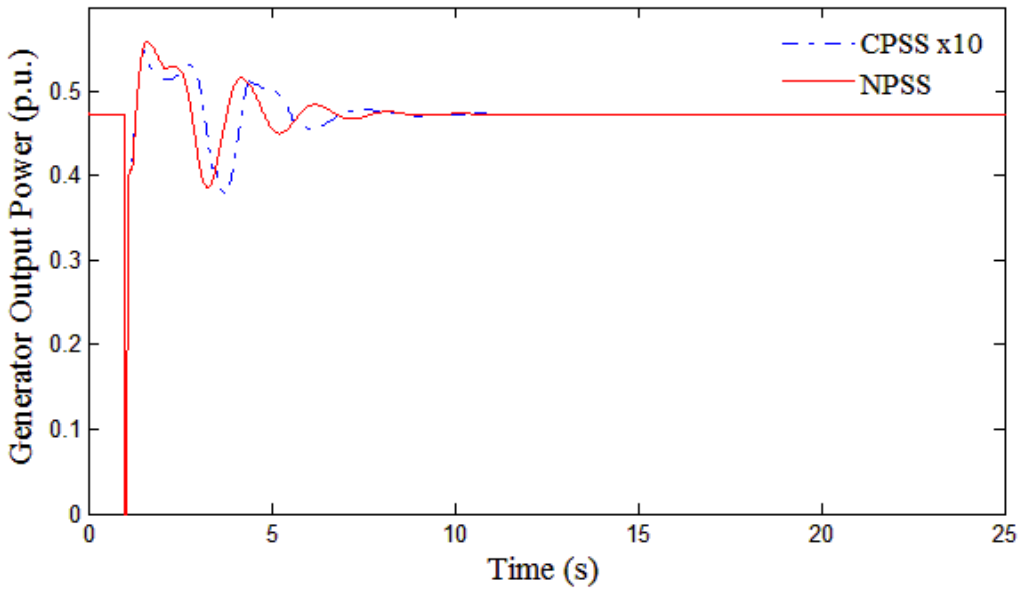

(d)

Figure 3.13: Simulation results comparison between CPSS with 10 times control gain and NPSS under transmission line short-circuit fault. (a) Rotor angle in rad; (b) Angular frequency in rad/s; (c) Generator terminal voltage in p.u.; and (d) Generator output power in p.u.

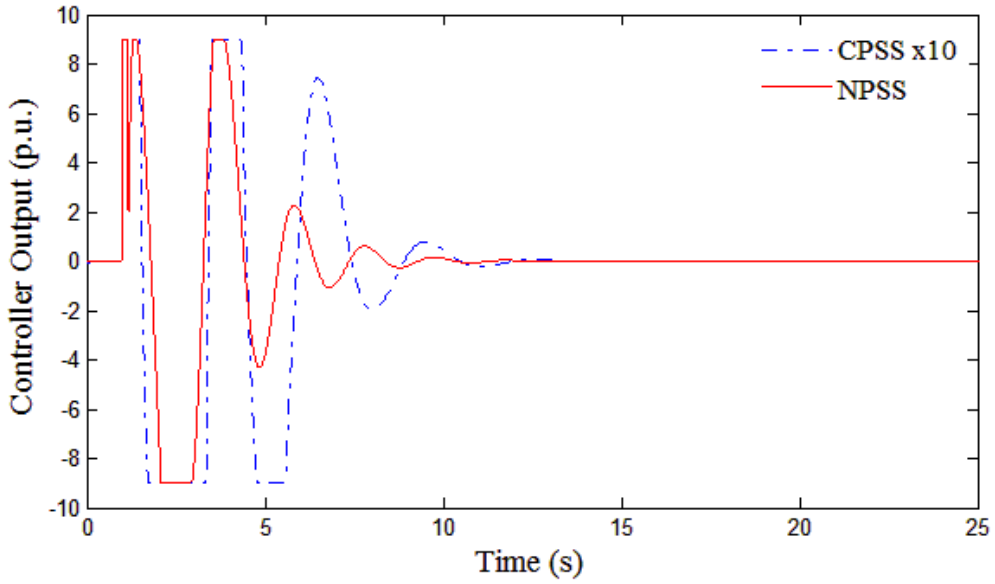

Figure 3.14: Controller output comparison between CPSS with 10 times control gain and NPSS under transmission line short-circuit fault.

With the same control performance between NPSS and CPSS, the controller output between these two controllers is compared in Figure 3.14. The comparison results show that the CPSS has a much higher actuator usage than NPSS to get the same performance. That is to say that the designed nonlinear compensator in NPSS can both improve the control performance and increase the efficiency of actuator usage.

Beside the transmission line fault, the mechanical input power of the generator also may have fault during the operation. Another case that indicate the step decrease and step increase of the mechanical input power are simulated for the SMIB power system. Figure 3.15 shows the control performance of the rotor angle, angular frequency, terminal voltage and output power of the generator during the mechanical power decrease and recovery. The NPSS has a faster recovery in oscillation and less overshoot in the rotor angle, angular frequency, and output power. If the rotor angle overshoot above 180 degree, the power system will become unstable. Therefore, the NPSS can increase the robustness of the SMIB power system.

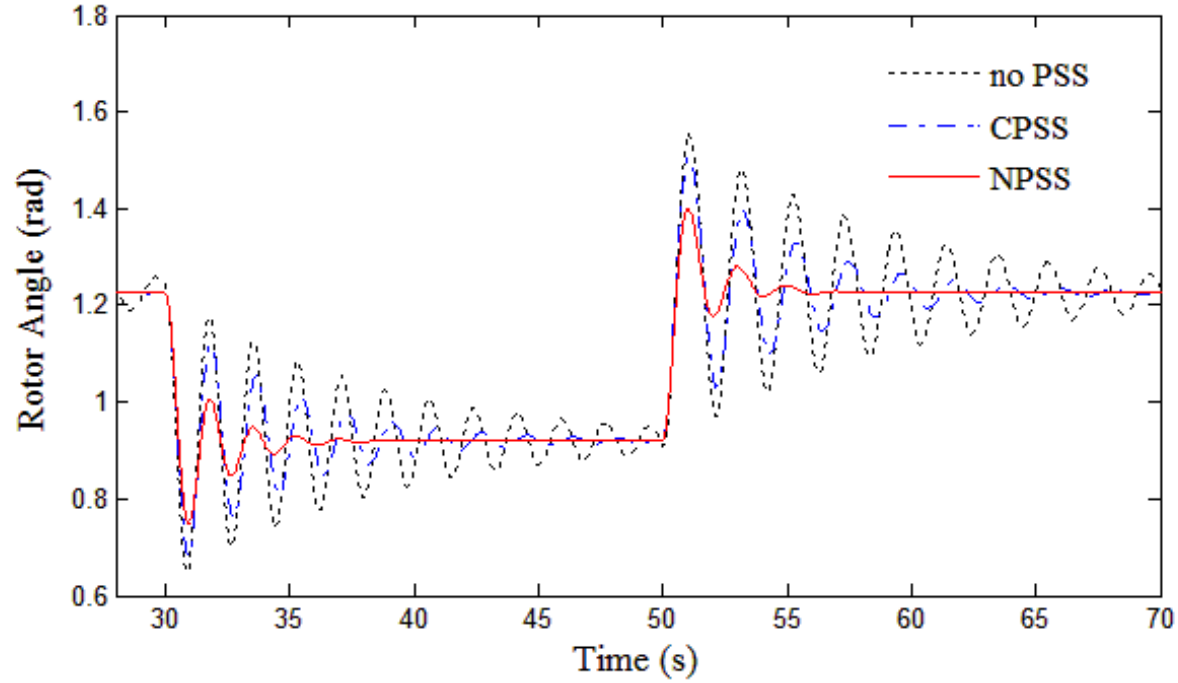
Rotor Angle (rad)
Time (s)
no PSS
CPSS
NPSS
1.8
1.6
1.4
1.2
1
0.8
0.6
30
35
40
45
50
55
60
65
70

(a)

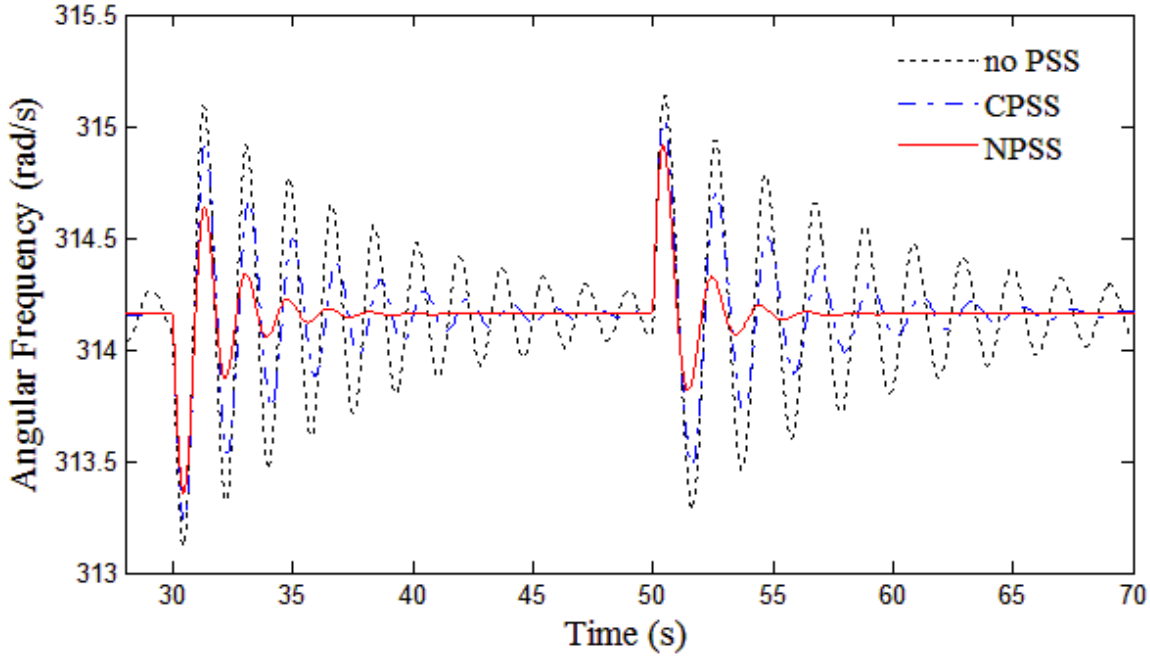
Angular Frequency (rad/s)
Time (s)
no PSS
CPSS
NPSS
315.5
315
314.5
314
313.5
313
30
35
40
45
50
55
60
65
70

(b)

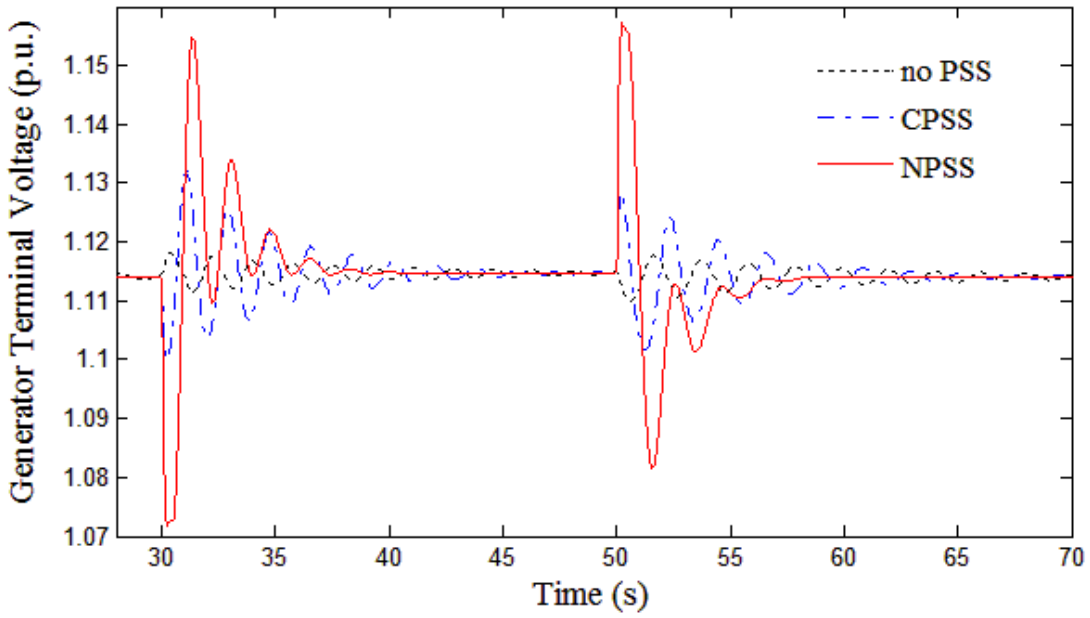

(c)

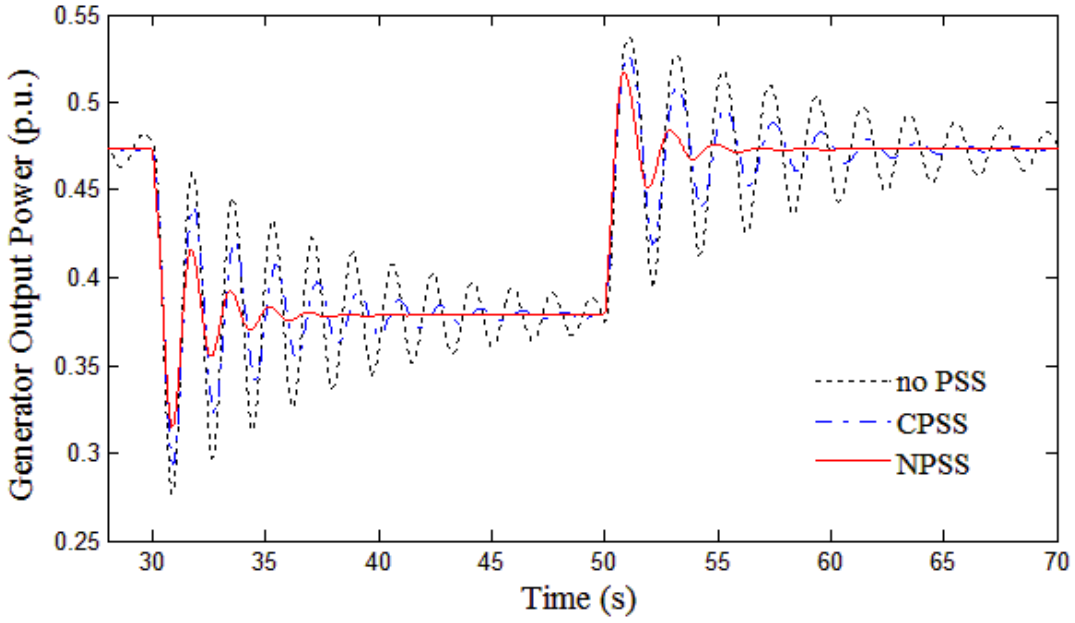

(d)

Figure 3.15: Simulation results comparison between different PSS under generator power drop and recovery (a) Rotor angle in rad, (b) Angular frequency in rad/s, (c) Generator terminal voltage in p.u., and (d) Generator output power in p.u.

3.8 Conclusion

This chapter has investigated the design of nonlinear PSS based feedback linearizing control and extend-order perturbation observer, based on the 4^{th}-order model of a SMIB system. The main difference of this chapter with reference [97] is that the PSS contributed its output to the input of the AVR, together with the terminal voltage deviation signal, rather than contribute the excitation voltage in parallel with the AVR in [1]. Comparison of the FLCPSS, ESOPSS with the CPSS have been carried out, to illustrate the advantages and disadvantages of the ESO based PSS.

Chapter 4 PSS based on Frequency Domain Unified Disturbance Estimator

4.1 Introduction

Time domain extend-state perturbation observer investigated in Chapter 3 requires a high-order observer which sometimes has very large gain and difficult to be implemented in practice. Frequency domain disturbance observer however only deal with the dynamic at the interested frequency range, usually the low frequency band such as the low frequency oscillation of power system. This chapter will investigate a frequency domain observer to estimate the disturbance and uncertainties, and pure derivative of state combining with the high-order low pass filter is used to replace the high-order state equation of the observer. The designed UDE-PSS is easily implemented but can still deal with the nonlinearities and uncertainties of the power system.

4.2 Uncertainty and Disturbance Estimator (UDE) based Control Method

This section will briefly recall the method of uncertainties and disturbance estimator proposed in frequency domain in [108-111]. The system to be considered is formulated as

$$\dot{x} = (A + F)x + Bu(t) + d(t) \tag{4.1}$$

where $\mathbf{x} = (x_1, x_2 \dots, x_n)^T$ is the state, $\mathbf{u(t)} = [u_1(t), \dots u_r(t)]^T$ is the control

input, A is the state matrix, F is the unknown state matrix, B is the control matrix having full column rank, and $d(t)$ is the unpredictable external disturbances.

Assume that the desired specification can be described by the reference model

$$\dot{x}_m = A_m x_m + B_m c(t) \tag{4.2}$$

where x_m, A_m, B_m are state, state matrix and control matrix of a reference model respectively. The control objective is to make the tracking error **e** between the system and the reference model converge to zero, that is

$$\mathbf{e} = (x_{m1} - x_1 \dots x_{mn} - x_n)^T = x_m - x \tag{4.3}$$

$$\dot{\mathrm{e}} = (A_m + K)\mathrm{e} \tag{4.4}$$

In other words, the error dynamics is stable, where ***K*** is called the error feedback gain.

Combining the equations above, we obtain

$$A_m x + B_m c(t) - Ax - Fx - Bu(t) - d(t) = Ke \tag{4.5}$$

Then the control action $u(\mathrm{t})$ is obtained as

$$u(\mathrm{t}) = B^+[A_m x + B_m c(t) - Ax - Fx - d(t) - Ke] \tag{4.6}$$

where $B^+ = (B^T B)^{-1} B^T$.

The control action $u(\mathrm{t})$ can be represented in the s-domain via Laplace transforms as

$$\mathrm{U(s)} = B^+[A_m X(s) + B_m C(s) - KE(s) - AX(s)] + B^+[-FX(s) - D(s)] \tag{4.7}$$

The second part, denoted hereafter by $U_d(s)$, includes the uncertainties and the external disturbance can be rewritten as

$$U_d(s) = B^+[-FX(s) - D(s)] = B^+[(A - sI)X(s) + BU(s)] \tag{4.8}$$

From system (4.1), we have

$$-FX(s) - D(s) = (A - sI)X(s) + BU(s) \tag{4.9}$$

Assume that $G_f(s)$ is a strictly proper low-pass filter with unity steady-state gain and broad enough bandwidth, then $U_d(s)$ can be accurately approximated to UDE, where

$$\text{UDE} = B^{+}[(A - sI)X(s) + BU(s)]G_f(s) \tag{4.10}$$

Hence, the control (4.7) can is

$$\text{U(s)} = B^{+}[A_m X + B_m C - KE - AX)] + \text{UDE} \tag{4.11}$$

That is

$$\text{U(s)} = B^{+}\left[A_m X + B_m C - KE - AX\left(1 - G_f\right) - sG_f X + G_f BU\right] \tag{4.12}$$

Then the UDE-based control law is derived as

$$\text{U(s)} = \left(I - B^{+}BG_f\right)^{-1}B^{+} \cdot \left[A_m X + B_m C - KE - AX\left(1 - G_f\right) - sG_f X\right] \tag{4.13}$$

The estimate error of UDE can be obtained as

$$\text{UDE}_{\text{error}} = \text{U}_\text{d}(s)\left(1 - G_f(s)\right) \tag{4.14}$$

As $G_f(s)$ is a low-pass filter, $G_f(s) = 1$ for $f < \omega_c$, where ω_c is the cut-off frequency of the linear system, thus the estimation error (4.14) will approximately approach zero at the interested frequency range of the system. A practical first-order low-pass filter is

$$G_f(s) = \frac{1}{T_s + 1} \tag{4.15}$$

where T=1/ω_f. Although this will cause some error in the estimation, the steady-state estimation error is always zero because $G_f(0) = 1$ can always be chosen to be zero for low frequency component. A high-order low-pass filter could be obtained by simply series connected the first-order filter (4.14).

4.3 Design of UDE-Based PSS

Based on the system (3.20) - (3.22), we have

$$\frac{d^4y}{dt^4} = a(x) + b(x)u_{pss}$$

where $z_1 = y,\ z_2 = \dot{y},\ z_3 = \ddot{y},\ z_4 = \dddot{y}$. Thus $y = \delta - \delta_0,\ \dot{y} = \omega_0(\omega - 1),\ \ddot{y} = \dot{\omega}, \dddot{y} = \ddot{\omega}$, and assume all four states are measurable (ie the up to second-order derivative of the speed) , we will design a full-state feedback UDE based PSS at first, in which the frequency domain UDE will be designed to replace the extended-order perturbation observer in the time-domain. Secondly, the rotor speed or the electrical power Pt (equivalent to the first-order of the rotor speed) will be chosen as the available output to design a UDE-PSS based on a third-order UDE (when rotor speed as the feedback input of the PSS) and a second-order UDE (when the electrical power as the feedback input of the PSS), respectively.

4.3.1 State-feedback UDE-PSS

By choosing the last state $y = z_4 = \dddot{y}$ as the input signal of the UDE, we have

$$\frac{d\ \ y}{dt} = a(x) + b(x)u_{pss}$$

Then a UDE with a third-order low pass filter $G_{f1}(s)$ as:

$$UDE_1 = \hat{A}(s) = G_{f1}(s)[s\ \ Y_1(s) - (B(s) - B_0)U_{pss}] \tag{4.16}$$

where $\hat{A}(s)$ is the estimate of *A(s)* in frequency domain, b_0 is the nominal value of b(x). $G_{f1}(s)$ is the first-order low-pass filter.

Choose different states as the outputs, i.e., $y_2 = z_3 = \ddot{y},\ or\ y_3 = z_2 = \dot{y}$ as the input of the UDE, we can have

$$UDE_2 = \hat{A}(s) = G_{f2}(s)[s^2Y_2(s) - (B(s) - B_0)U_{pss}] \tag{4.17}$$

$$UDE_3 = \hat{A}(s) = G_{f3}(s)[s^3 Y_3(s) - (B(s) - B_0)U_{pss}] \quad (4.18)$$

where $G_{f2}(s)$ and $G_{f3}(s)$ are second order and third-order low-pass filter respectively. Finally, the rotor angle can also be chosen as the input of the UDE and then a fourth-order low pass filter will be required.

Based on equation (3.41), we have the state feedback control as:

$$\begin{cases} u = \dfrac{v}{b_0} - \dfrac{UDE}{b_0} \\ v = -KZ \end{cases} \quad (4.19)$$

Where the *UDE* can be $UDE_1, UDE_2, UDE_1\ from$ (4.16 o (4.18). Note that the linear control *v* still requires the full state feedback and thus (4.19) is called the state-feedback UDE-PSS. The main purpose of the full-state feedback UDE-PSS is to verify the effectiveness and the equivalence between the time-domain ESPO and the UDE, in which UDE has merits such as: 1) the observer order is one-order less the ESPO; 2) doesn't require the direct derivative of the measurements; 3) and avoid the usage of the relatively high-gain in ESPO. 4) fewer tuning parameters as only one cut-off frequency required to be tuned in the UDE.

4.3.2 Output-feedback UDE-PSS

Control (4.19) requires the full-state feedback (, i.e., the linear controller requires all four states $z_1 = y,\ z_2 = \dot{y},\ z_3 = \ddot{y},\ z_4 = \dddot{y}$) and may have difficult in implementation in practice, this section will design an output feedback UDE-PSS. At first, a speed-type UDE-PSS based on the measurement of the speed only is designed as below:

$$u = \frac{v}{b_0} - \frac{UDE_3}{b_0}$$
$$v = -K_p * (\omega - 1.0) - K_p \int (\omega - 1.0)\mathrm{dt} - K_d \frac{d}{dt} \omega \quad (4.20)$$

Note that the control (4.20), together with *UDE₃* in (4.18) only require the measurement of rotor speed which is much easier than the rotor angle. The Integration part however still introduce the damping from the rotor deviation. Here the low pass filter could be chosen as

$$G_{f3}(s) = \frac{1}{T_f s + 1} * \frac{1}{T_f s + 1} * \frac{1}{T_f s + 1} \quad (4.21)$$

A power-type UDE-PSS is designed via using the acceleration power (Pm-Pt) of the generator as the feedback input of the UDE-PSS to design UDE (4.17):

$$u = \frac{v}{b_0} - \frac{UDE_2}{b_0}$$
$$v = -K_p * (\mathrm{Pm0} - \mathrm{Pt}) - K_p \int (\mathrm{Pm0} - \mathrm{Pt})\mathrm{dt} - K_d \frac{d}{dt} (Pm0 - Pt) \quad (4.22)$$
$$G_{f2}(s) = \frac{1}{T_f s + 1} * \frac{1}{T_f s + 1}$$

4.4 Simulation Results

Simulation studies have been undertaken based on the same SMIB system in Chapter 2 and Chapter 3 for a fair comparison.

4.4.1 State feedback UDE-PSS performance

The first-order low pass filter parameter $T_f = 0.001s$. Results of a first order UDE-PSS based on (4.18) are shown in Fig. 4.2, which show that almost same response than that of ESOPSS in Fig. 3.8. Estimate of the a(x) by the first order UDE (4.18) and the real a(x) calculated is shown in Fig. 4.3. Note that the estimate at the begging of the transient period is not accurate, and then converge to the real

estimate after 0.4 seconds. The effectiveness of the compensation of the estimated disturbance (or called perturbance in this thesis) can be shown in Fig. 4.4, in which the compensation (-UDE) is removed from the controller (4.20) and the response of the linear control v only is worse than that of the CPSS. This shows that the effectiveness of the compensation, even the estimate is not accurate, doesn't rely on the real-time compensation of all dynamic in time-domain, and may only depend upon the low-frequency domain dynamic. This will be further investigated in frequency domain.

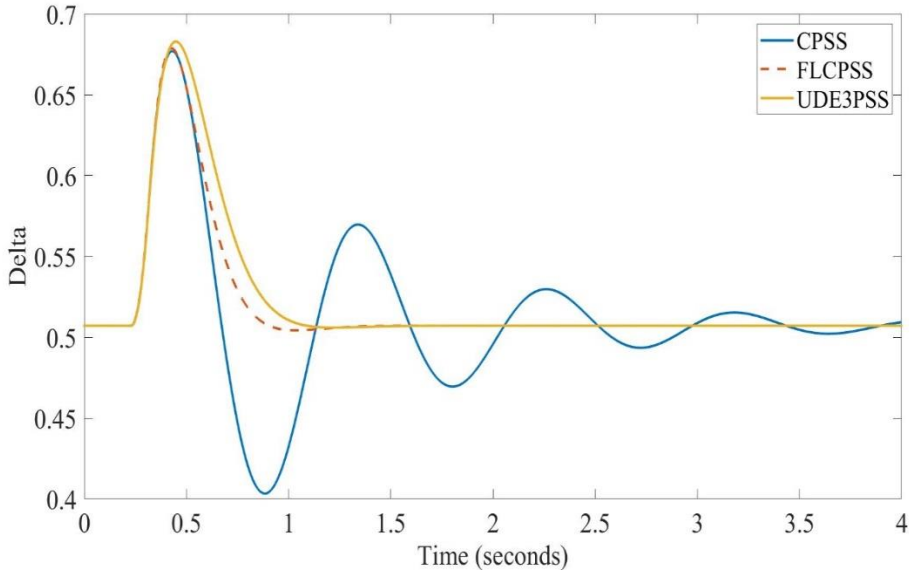

(a)

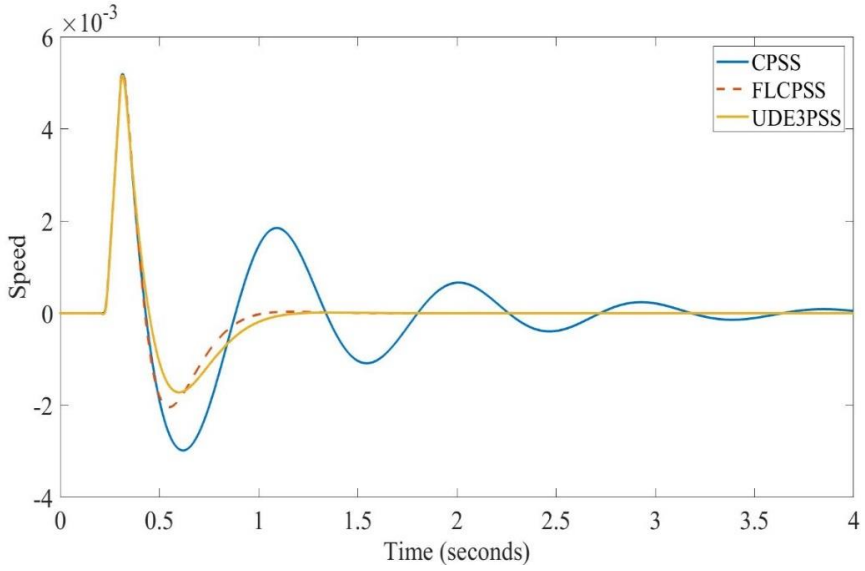
×10^-3
6
4
2
0
-2
-4
Speed
0
0.5
1
1.5
2
2.5
3
3.5
4
Time (seconds)
CPSS
FLCPSS
UDE3PSS

(b)

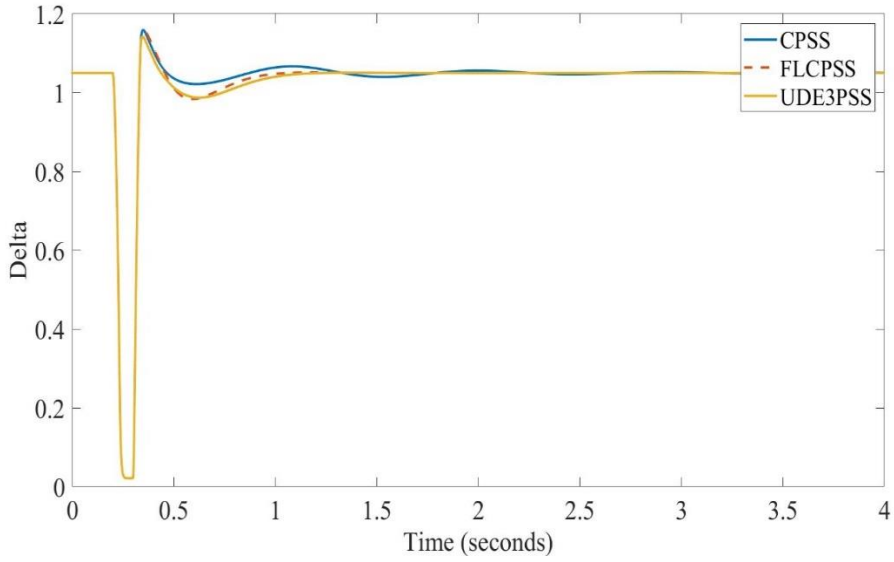
1.2
1
0.8
0.6
0.4
0.2
0
Delta
0
0.5
1
1.5
2
2.5
3
3.5
4
Time (seconds)
CPSS
FLCPSS
UDE3PSS

(c)

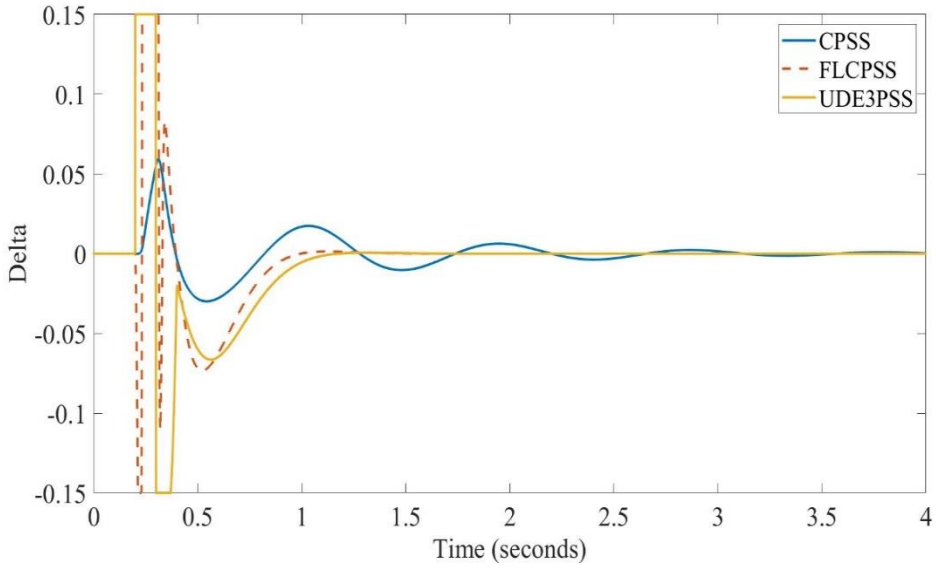

(d)

Figure 4.1 Response of UDE3-PSS with a first order UDE (a) Rotor angle; (b) Speed;

(c) Terminal voltage Vt; (d) Control

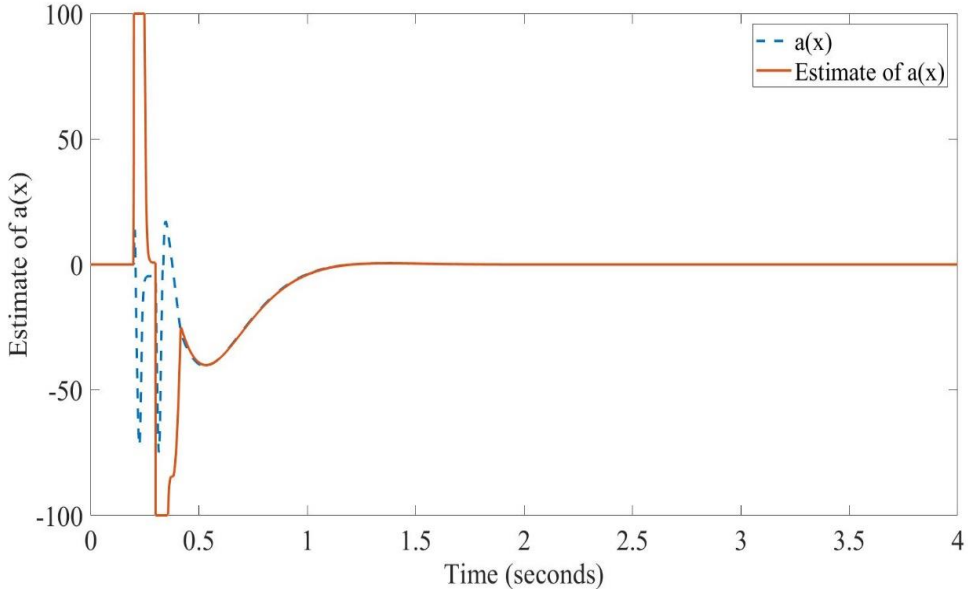

Figure 4.2 Estimate of a(x) via the first order UDE

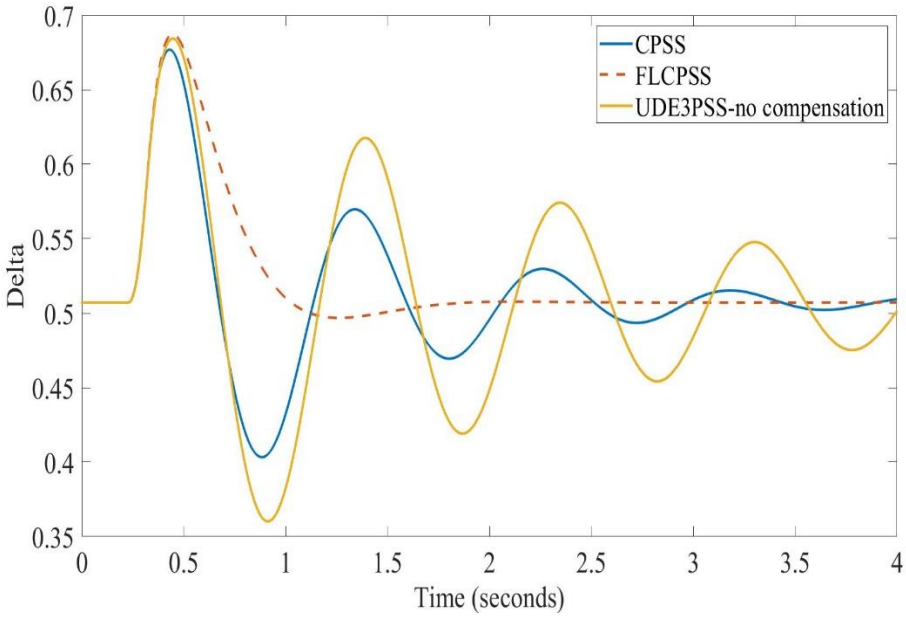

Figure 4.3 Effectiveness of the compensation of inaccurate estimate of a(x)

Design a third-order low pass filter (4.21) via setting parameter T_f=0.001s. Results of first order UDE-PSS based on (4.16) are shown in Fig. 4.5. Again, almost similar response with that of ESOPSS in Fig. 3.8 is obtained. Estimate of the a(x) by the third order UDE (4.16) and the real a(x) calculated is shown in Fig. 4.6.

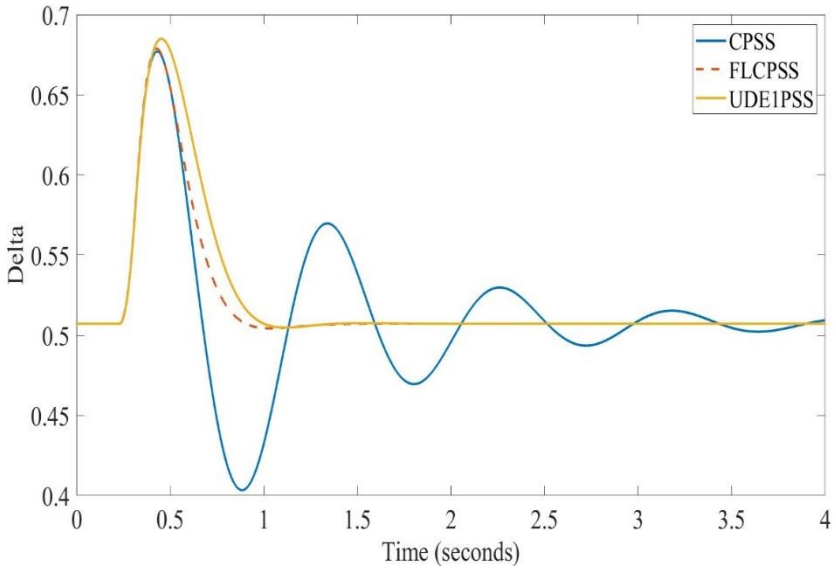

(a)

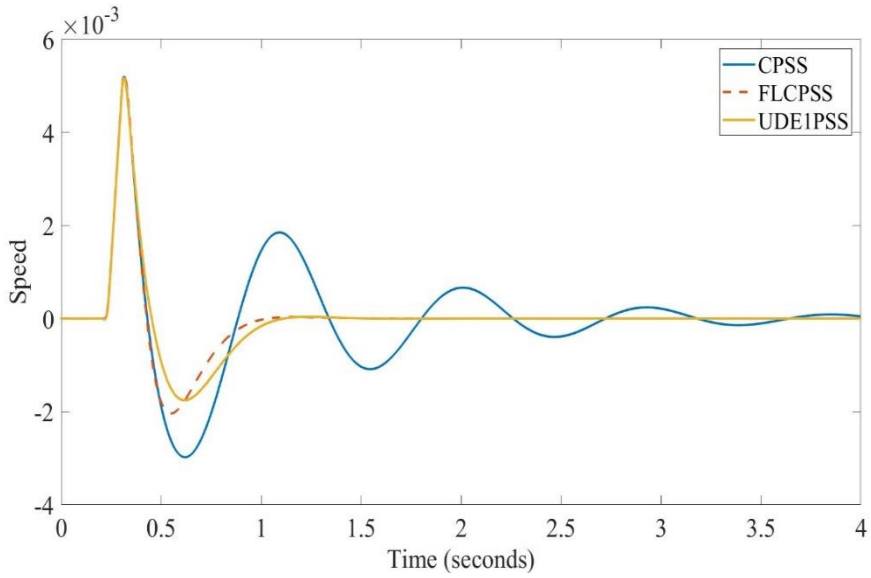
×10^-3
6
4
2
0
-2
-4
Speed
0
0.5
1
1.5
2
2.5
3
3.5
4
Time (seconds)
CPSS
FLCPSS
UDE1PSS

(b)

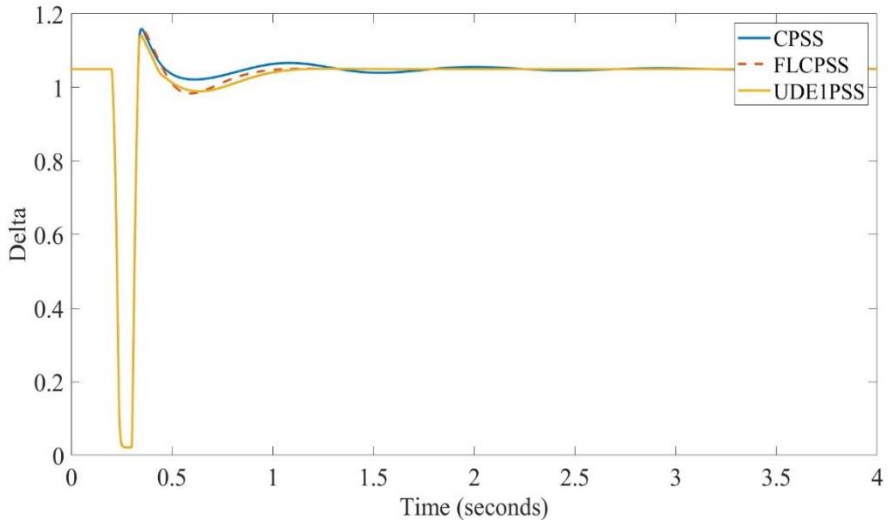
1.2
1
0.8
0.6
0.4
0.2
0
Delta
0
0.5
1
1.5
2
2.5
3
3.5
4
Time (seconds)
CPSS
FLCPSS
UDE1PSS

(c)

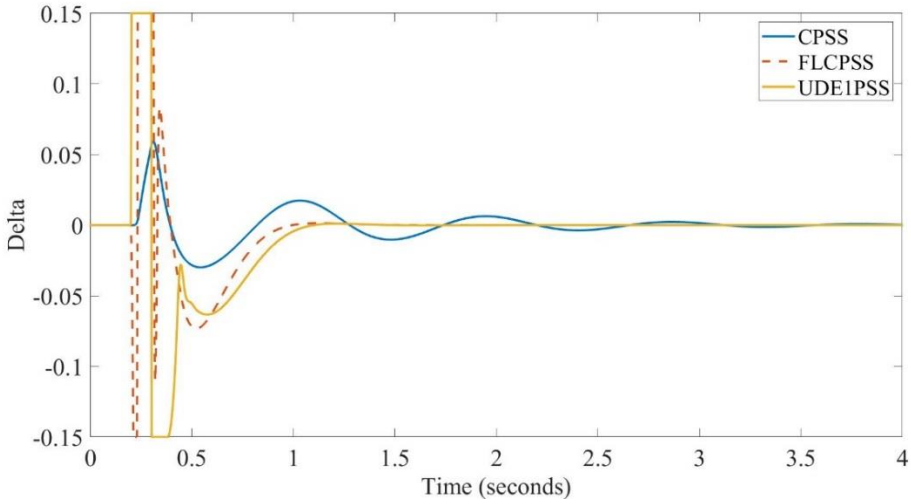

(d)

Figure 4.4 Response of full state PSS based on a third order UDE (a) Rotor angle; (b) Speed; (c) Terminal voltage Vt; (d) Control

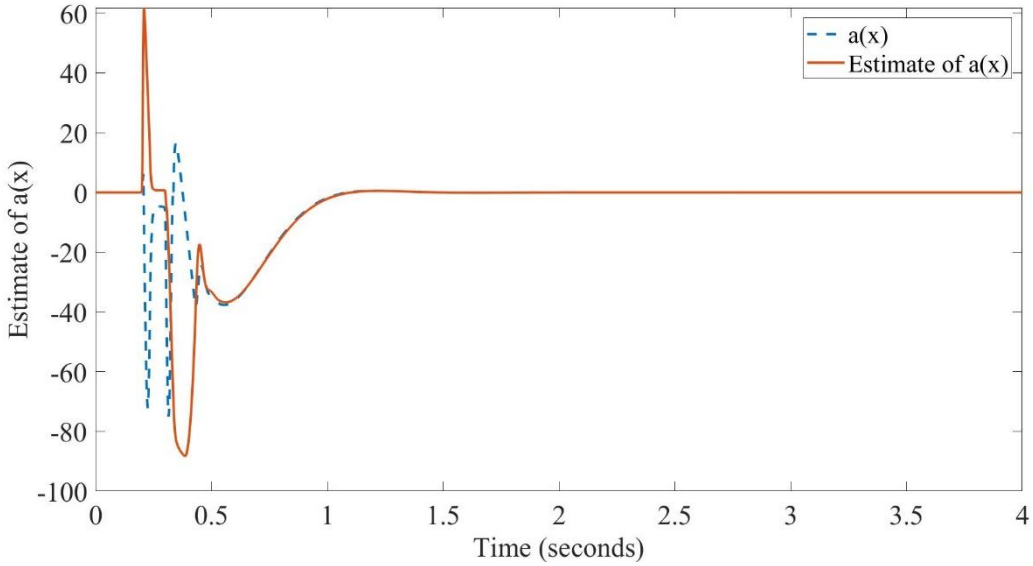

Figure 4.5 Estimate of a(x) via the third order UDE

4.4.2 Output feedback UDE-PSS

System output of a speed UDE-PSS based on UDE (4.16) and control (4.20) and (4.21) is shown in Figure and 4.6 and 4.7. Here a constant value of b(x) is used, i.e. b(x)=b0, where b0 =-459 is the nominal value of b(x). The Speed-type UDE-PSS only requires one measurement. Gains of the PID are tuned automatically by the tools provide by Matlab, and obtained as Kp=-23191, Ki=-20988; Kd=-1501. The output of the UDE is scaled down via being divided by b0.

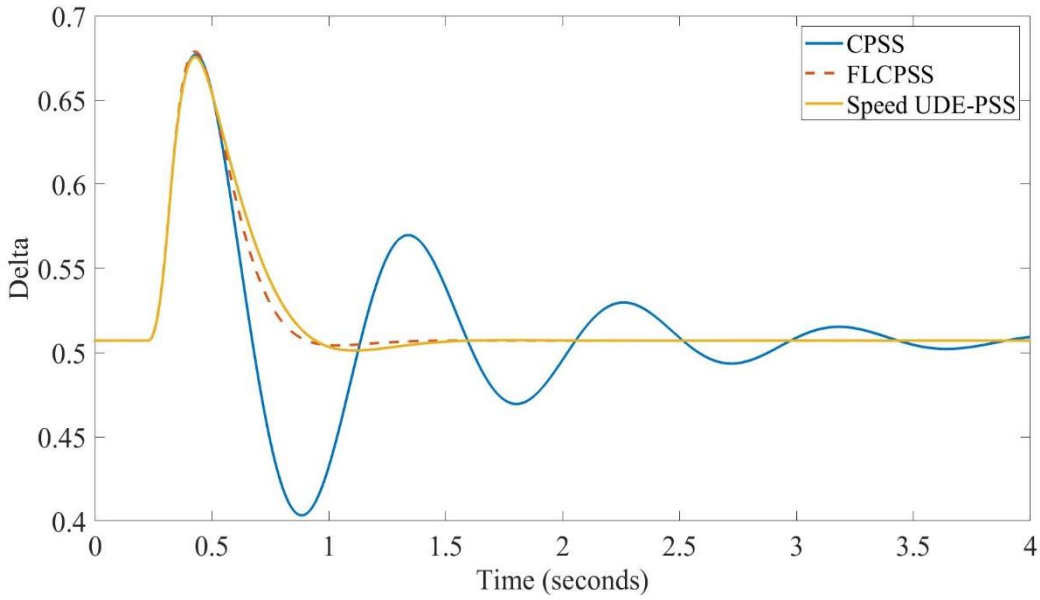

(a)

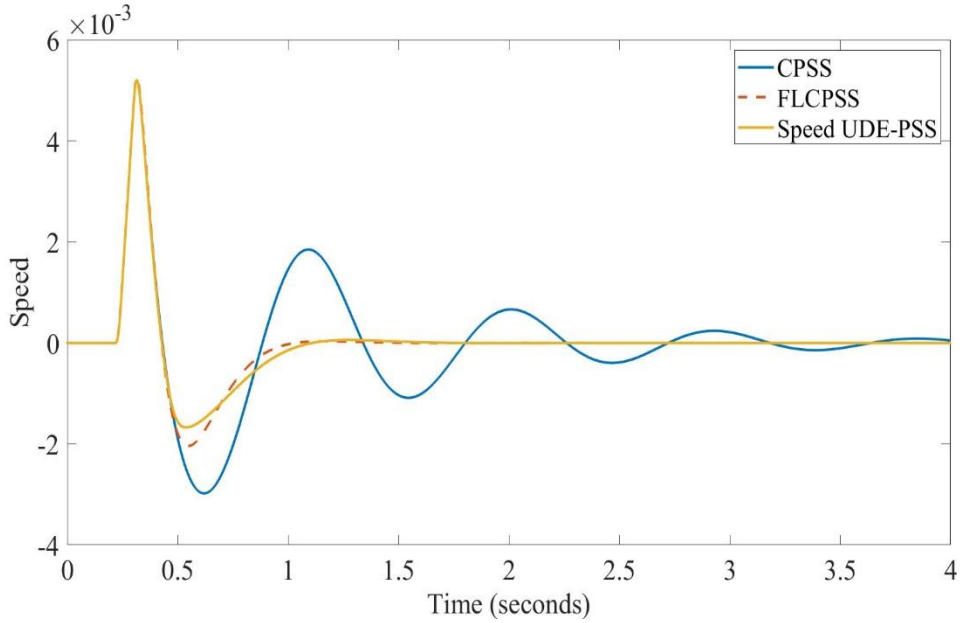
×10^-3
6
4
2
0
-2
-4
Speed
0
0.5
1
1.5
2
2.5
3
3.5
4
Time (seconds)
CPSS
FLCPSS
Speed UDE-PSS

(b)

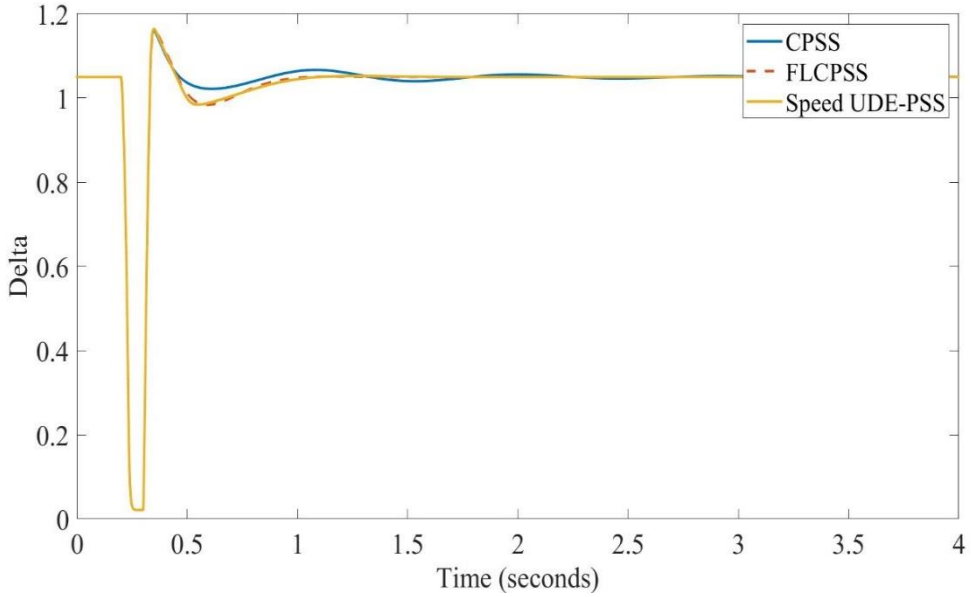
1.2
1
0.8
0.6
0.4
0.2
0
Delta
0
0.5
1
1.5
2
2.5
3
3.5
4
Time (seconds)
CPSS
FLCPSS
Speed UDE-PSS

(c)

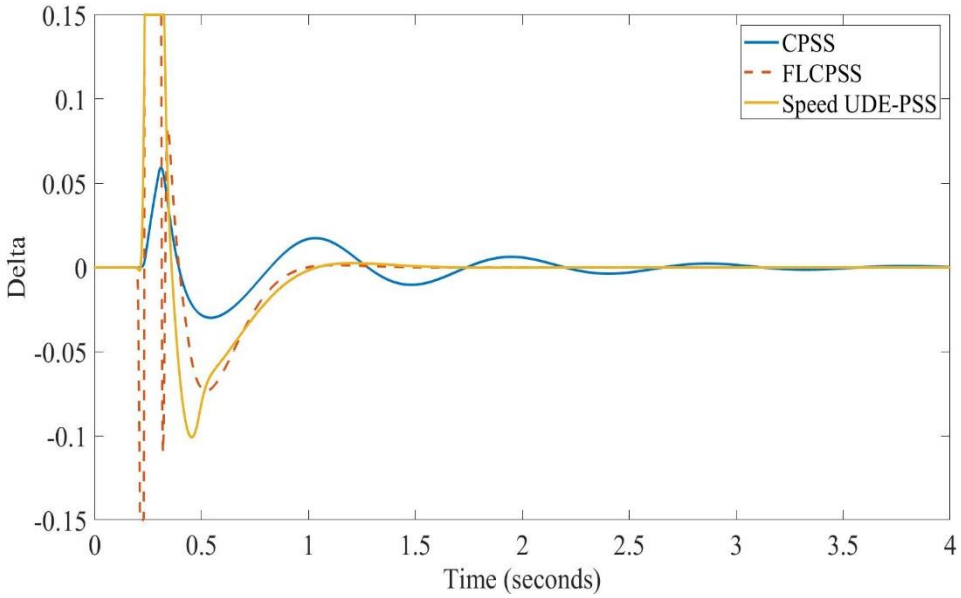

(d)

Figure 4.6 Response of Speed UDE-PSS based on a third order UDE (a) Rotor angle; (b) Speed; (c) Terminal voltage Vt; (d) Control

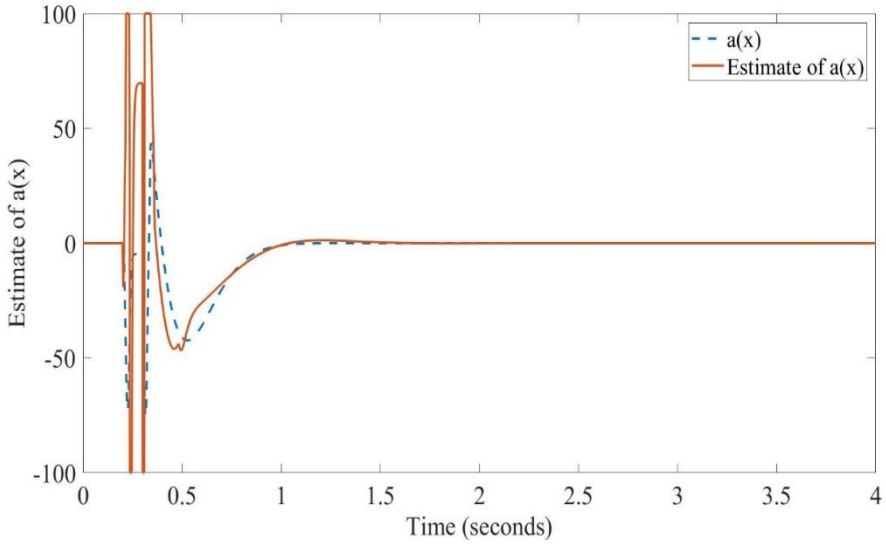

Figure 4.7 Estimate of a(x) via the third order UDE (speed-based)

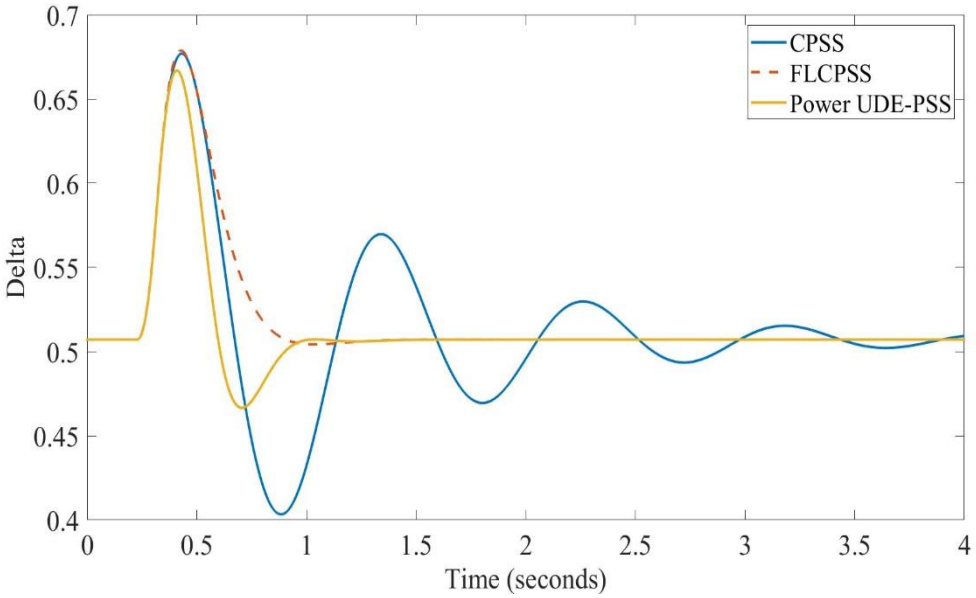
CPSS
FLCPSS
Power UDE-PSS
Delta
Time (seconds)
0.7
0.65
0.6
0.55
0.5
0.45
0.4
0
0.5
1
1.5
2
2.5
3
3.5
4

(a)

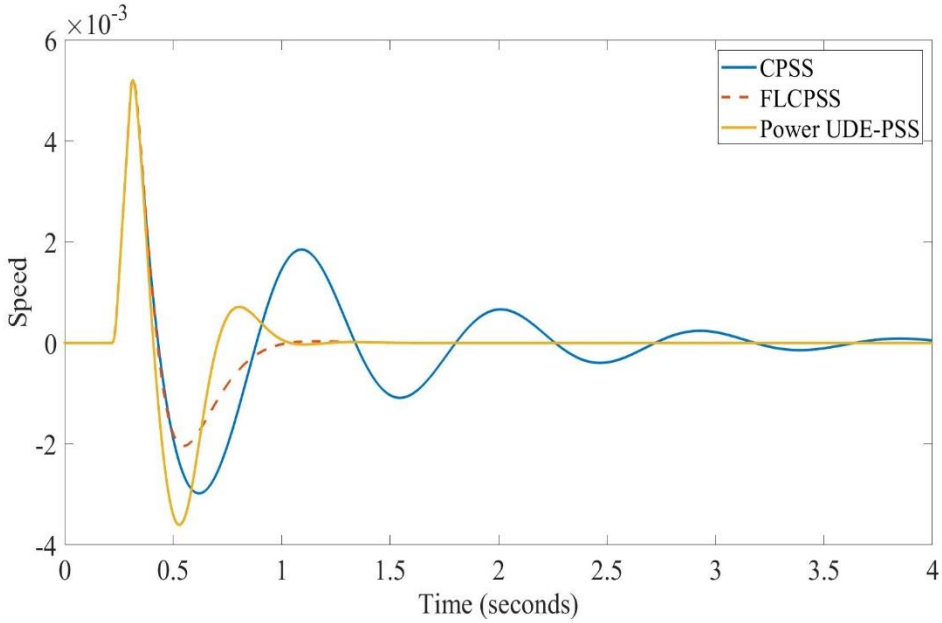
×10^-3
CPSS
FLCPSS
Power UDE-PSS
Speed
Time (seconds)
6
4
2
0
-2
-4
0
0.5
1
1.5
2
2.5
3
3.5
4

(b)

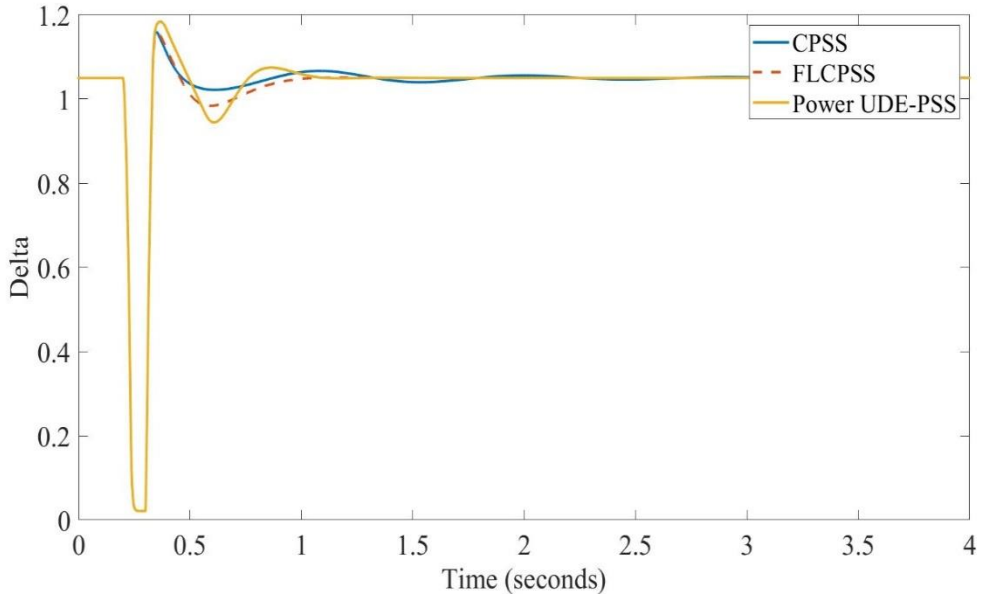

(c)

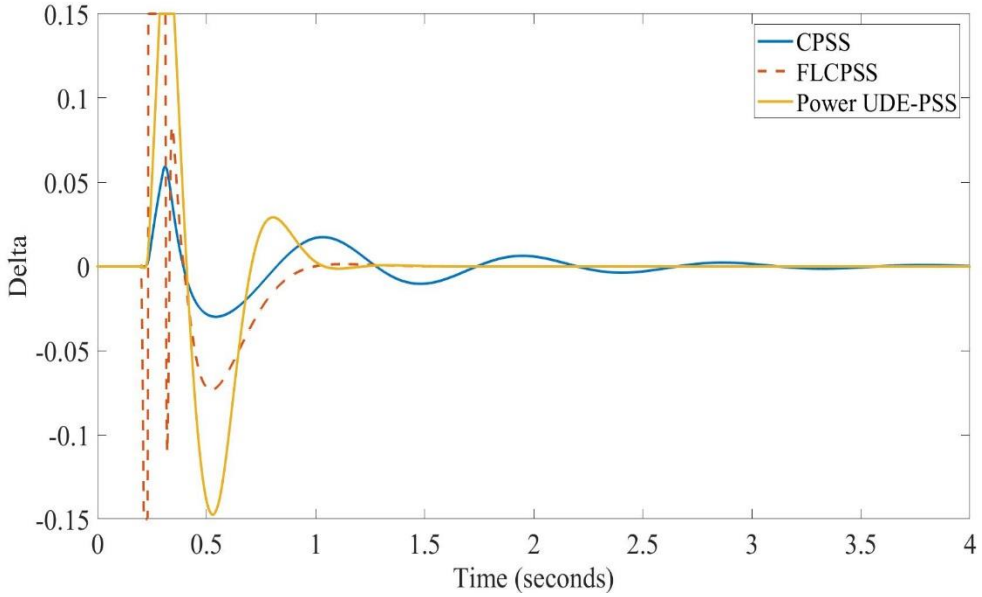

(d)

Figure 4.8 Response of Power UDE-PSS based on a second order UDE (a) Rotor angle; (b) Speed; (c) Terminal voltage Vt; (d) Control

Note that the rotor angle and the output power has been transferred to the new operation points smoothly, and UDE-PSS can provide better performance of the rotor

angle (output power), with the cost of a little worse terminal voltage performance. This is caused as both the rotor angle and the terminal voltage are controlled by the same control variable, excitation voltage, a better rotor angle performance will use more control effort among the excitation voltage. Based on simulation results, we can conclude that the UDE-PSS can provide better performance than the CPSS, based on the estimation and compensation of UD. The UDE is designed in frequency domain which makes it be easily analyzed and compared with the CPSS, the current industrial standard PSS.

4.5 Conclusions

Conventional lead-lag-type Power System Stabilizer (CPSS) developed in frequency domain has been recalled, and then a perturbation estimator designed in frequency domain has been augmented on to the CPSS, and results in a Nonlinear PSS which can deal with the model uncertainties originating from the shift of operation points, external disturbances from the grid faults, and parameters uncertainties. Initial simulation tests have been done to verify the performance of the proposed NPSS, compared with the CPSS.

Chapter 5 Performance evaluation in multi-machine power system

5.1 Introduction

The PSS's performance of damping local mode oscillation, i.e. single generator oscillates against the infinite bus system, has been verified in Chapter 4. This chapter will investigate the effectiveness of the PSS damping the inter-area oscillation which should be tested under multi-machine power system. The main challenges are that the existing of multi oscillation mode which are interacted and coupled each other. And, the interaction of the damping torque provided from PSSs to different modes and sometimes PSS designed for one mode may reduce the damping to another mode.

5.2 Multi-band PSS PSS2B and PSS4B

The system performance is tested with comparison of three Power System Stabilizer (PSS) as follows:

a) MB-PSS with simplified settings: IEEE® type PSS4B according to IEEE Std 421.5, called MB-PSS
b) Conventional Delta w PSS from P. Kundur (Ref. [1], pp. 814-815, and Ref. [2]), called Speed-PSS
c) Conventional Acceleration Power (Delta Pa) PSS, called Power-PSS

The diagram of those PSSs are shown in Figure 5.1.

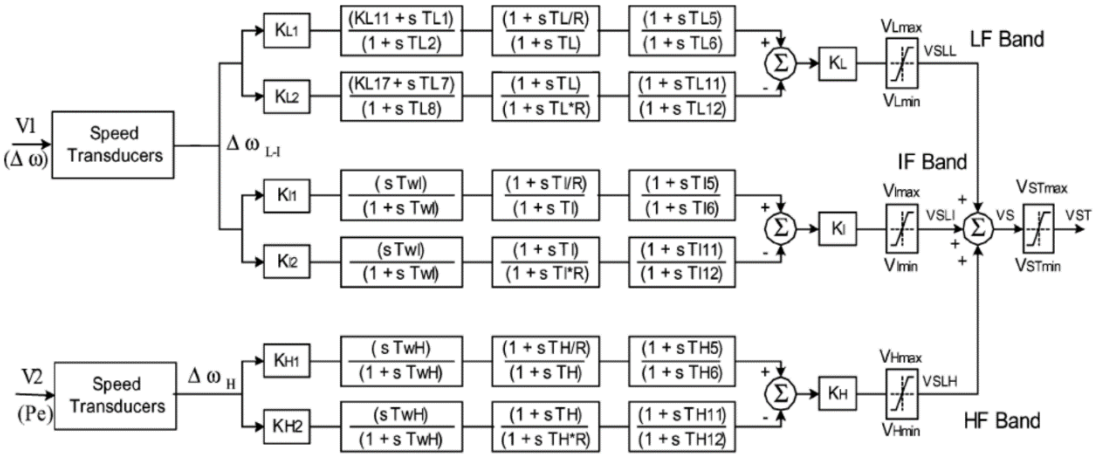

(a)

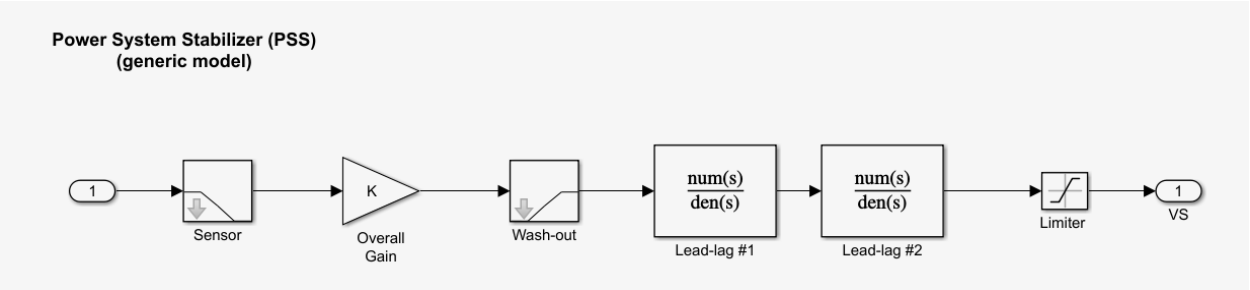

(b)

Figure 5.1 IEEE Standard PSS models, (a) MB-PSS (PSS4B); (b) Conventional Delta w PSS (Speed-PSS) and Acceleration Power (Delta Pa) PSS (Power-PSS)

In this chapter, contribution of damping of inter-area oscillation from the Speed-based UDEPSS (called Speed UDEPSS) and the Acceleration Power based UDEPSS (called Power UDEPSS) are tested respectively, compared with those PSSs mentioned above. For simplicity, those UDEPSSs use the same parameters obtained in Chapter 4 for a multi-machine case. Simulation results in the following part of this chapter show that they can still provide a satisfactory performance, which demonstrates the supreme robustness of the proposed UDEPSSs against different operation conditions

and also a much simpler tuning and design efforts than those conventional PSSs which suffer from the difficulty of optimal tuning. Of course, a fine tuning of those UDEPSSs will further improve their performance.

5.3 Verification of damping inter-area oscillation in a four machine two area system

The proposed PSS will be tested in a multi-machine power system based on Kundur's Four-Machine Two-Area Test System, which is a test benchmark for small signal stability and available on Matlab/Simulink/Simpowersystems Toolbox. The structure of this system as shown in Fig. 5.2. This system has been modified by adding the speed-type UDEPSS as type 4 PSS and the power-type UDEPSS Three PSS are compared using the same settings for all machines.

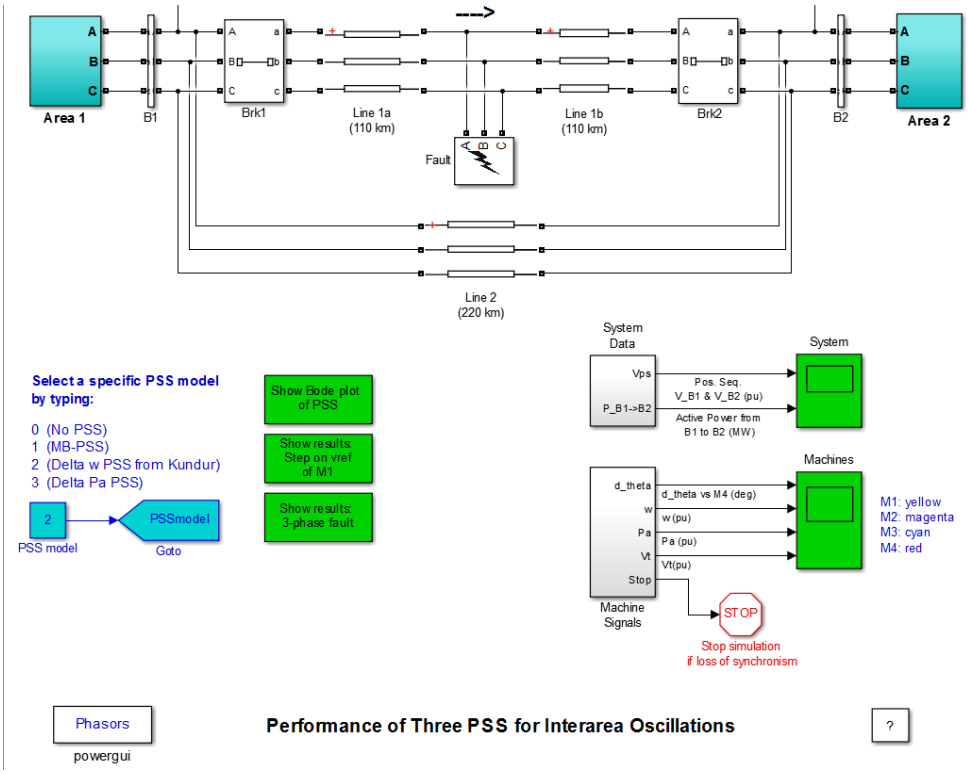

Figure 5.2 Kundur's Four-Machine Two-Area Test System [3]

The test system consists of two fully symmetrical areas linked together by two 230 kV lines of 220 km length. It was specifically designed in [1, 2] to study low frequency electromechanical oscillations in large interconnected power systems. Despite its small size, it mimics very closely the behaviour of typical systems in actual operation. Each area is equipped with two identical round rotor generators rated 20 kV/900 MVA. The synchronous machines have identical parameters [1, 2], except for inertias which are H = 6.5s in area 1 and H = 6.175s in area 2 [1]. Thermal plants having identical speed regulators are further assumed at all locations, in addition to fast static exciters with a 200 gain [1, 2]. The load is represented as constant impedances and split between the areas in such a way that area 1 is exporting 413MW to area 2. Since the surge impedance loading of a single line is about 140 MW [1], the system is somewhat stressed, even in steady state. The reference load-flow with M2 considered the slack machine is such that all generators are producing about 700 MW each. The results can be seen by opening the Powergui and selecting Machine Initialization. They are slightly different from [1], because the load voltage profile was improved (made closer to unity) by installing 187 MVAR more capacitors in each area. In addition, transmission and generation losses may vary depending on the detail level in line and generator representation.

5.3.1 Small-signal performance assessment

Small-signal performance assessment is simulated by setting a 5% step increase lasting for 12-cycle pulse on voltage reference of M1 at 1 second. Performance of this test are shown in Figure 5.3. The results show that all PSSs can provide very good

performance, while the proposed UDEPSS gives the best performance. Note that the UDEPSS has a simpler structure than the PSS4B and also provide a much better robustness as we directly use the designed EDEPSS for the SMIB system in Chapter 4. Also, the contribution of all PSSs to the damping of the inter-area oscillation has been well demonstrated.

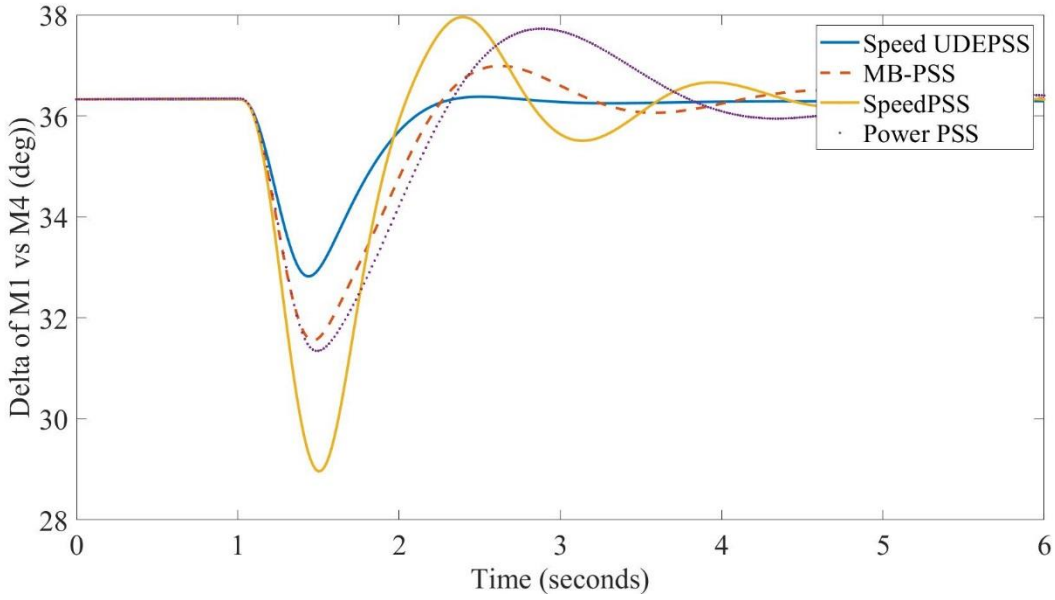

(a) Rotor angle of M1 vs M4;

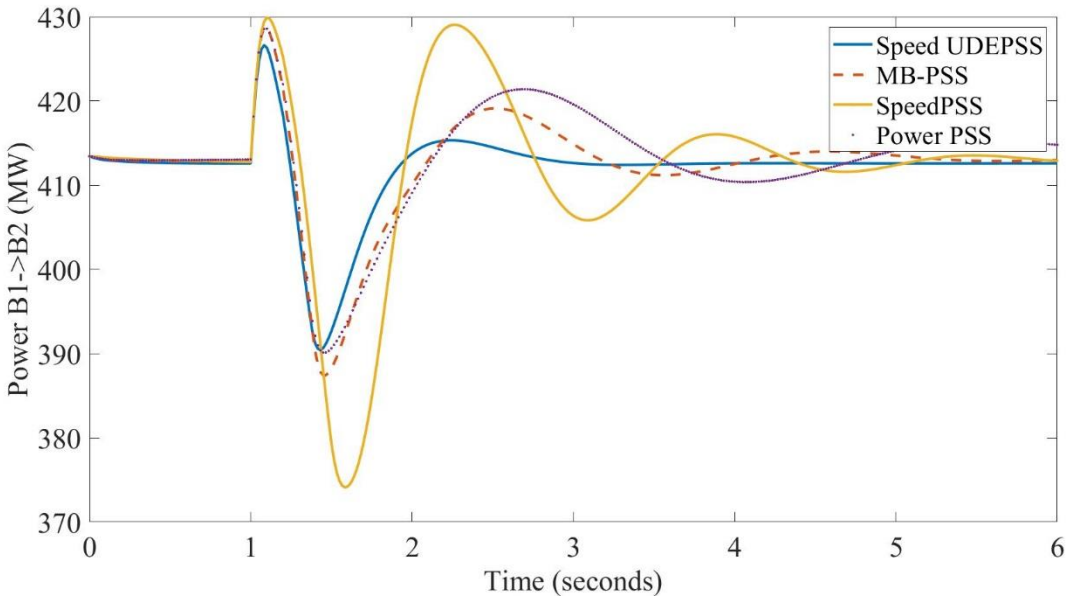

(b) Power transfer between B1 to B2

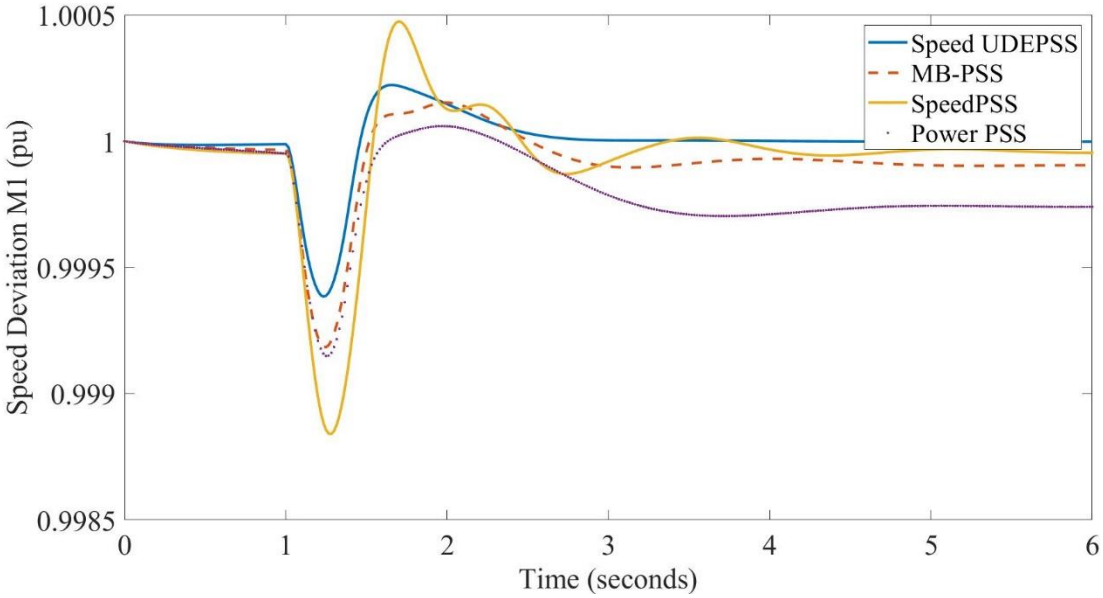

(c) Rotor Speed of M1

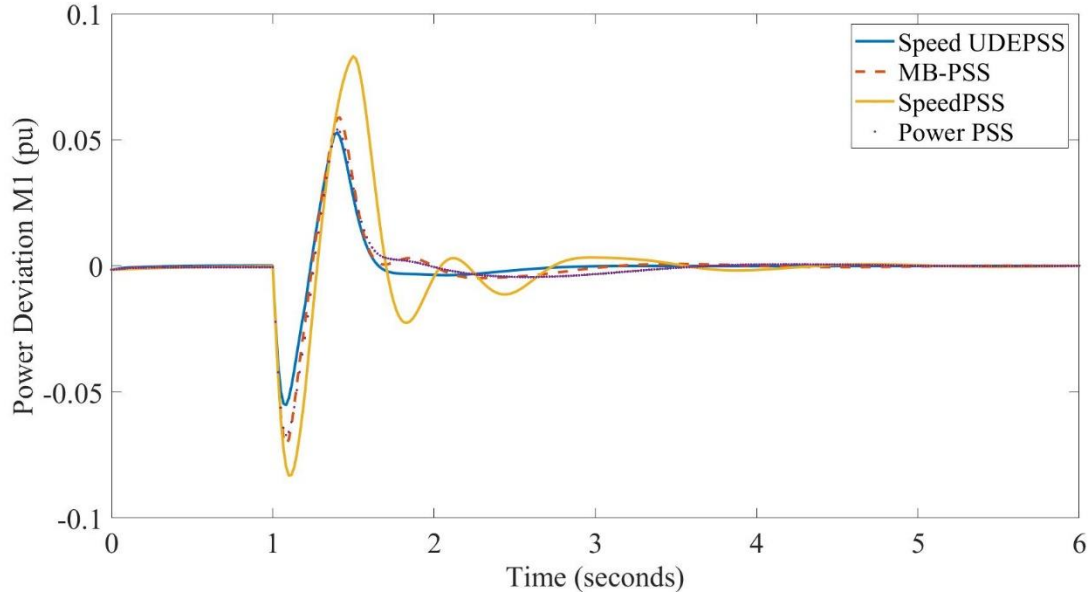

(d) Acceleration of Power of M1

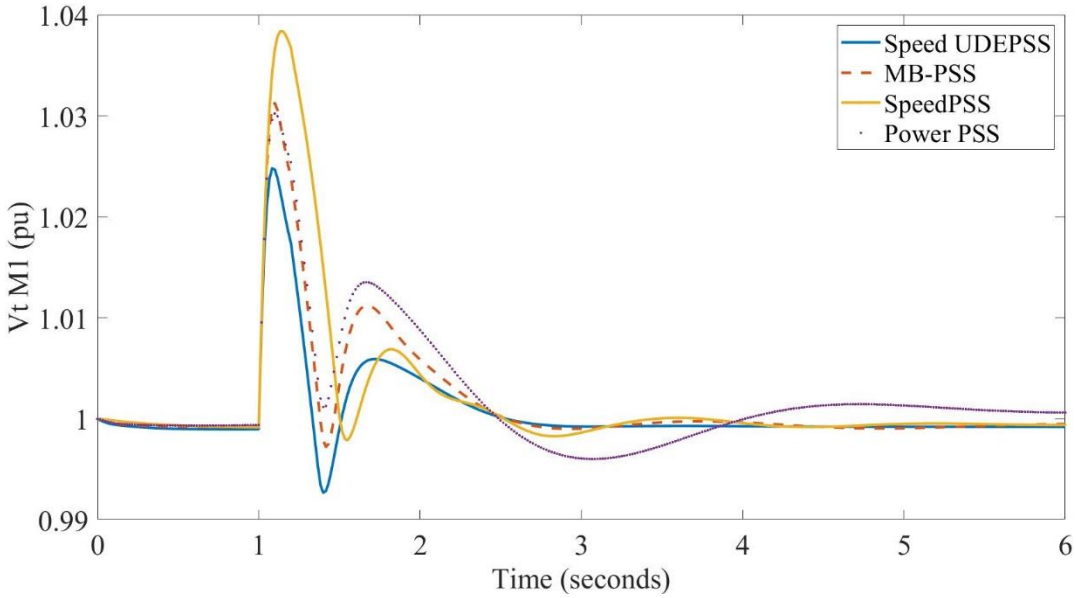

(e) Terminal voltage of M1

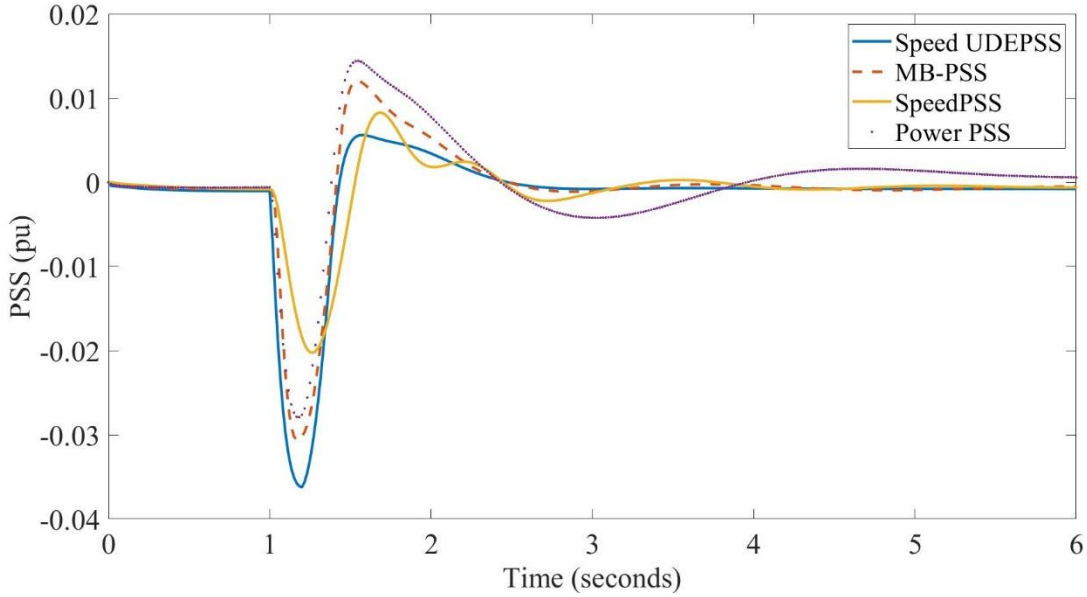

(f) Output of PSSs

Figure 5.3 Response of different PSSs under 5% step change of the terminal voltage of M1 for 12 cycles.

5.3.2 Large signal performance assessment

Performance of PSSs during the large perturbations and a good robustness with respect to changing operating conditions are other criteria of an equal importance for a PSS. To demonstrate and assess the PSS's performance, a three-phase to ground fault happens at 1 second at the middle of one of the two transmission lines and lasting 8 cycles (8/60 sec.) and then the fault line is tripped off by opening the breaker "Brk1" and "Brk2".

Results under 8 cycles fault: Simulation results of M1 is shown in Figure 5.4. Here three PSSs are compared: Speed UDEPSS, MB-PSS and Speed PSS. After one tie-line has been tripped off to clear the fault, the system can reach another stable operating point in steady-state, although not every PSS is able to ensure a smooth transition into this new highly stressed operating point, as shown in Figure 5.4(b). Once again, we can observer that the proposed UDEPSS can provide much better performance than the MB-PSS and Speed PSS. Note that the Power-type PSS cannot maintain the system stability under this type of fault, and its simulation results is not be included in the results.

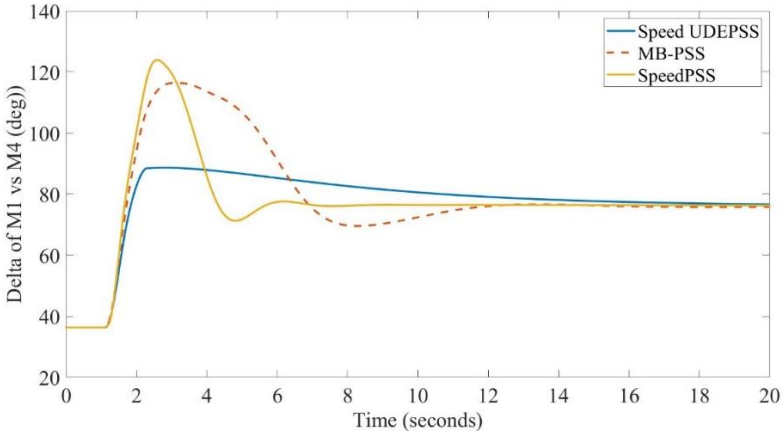

(a) Rotor angle of M1 vs M4

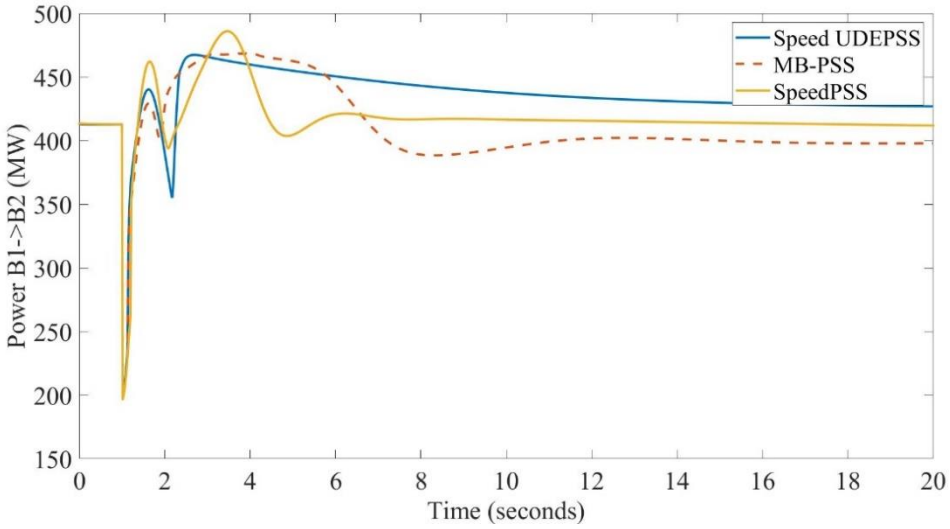

(b) Power transfer from B1 to B2

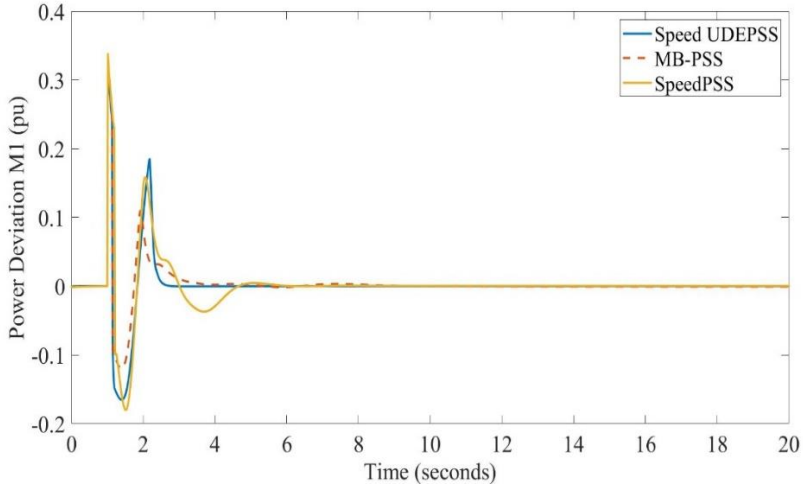

(c) Acceleration Power of M1

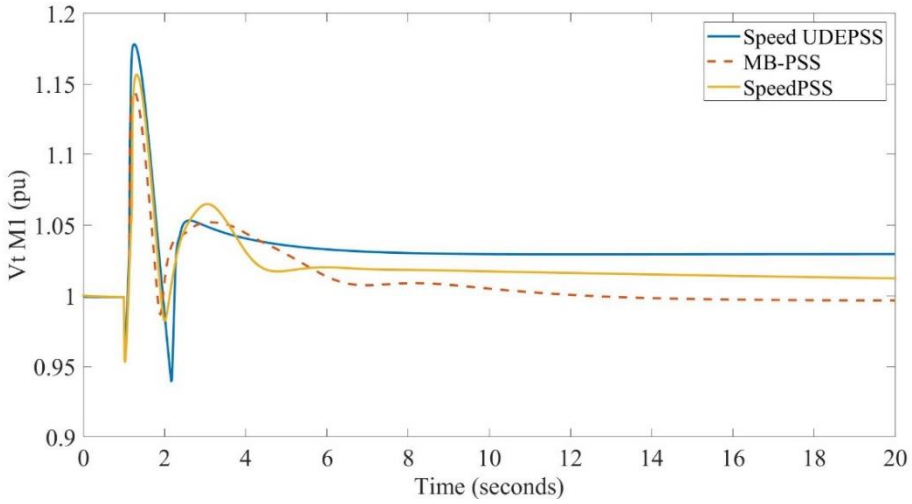

(d) Voltage of M1

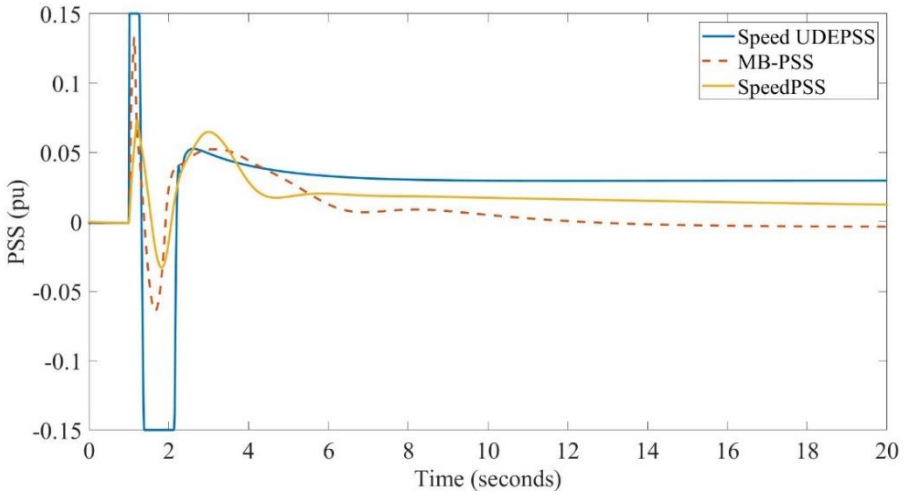

(e) PSS output

Figure 5.4 Response to three PSSs under three-phase to ground for 8 cycles

Results under 12 cycles faults: To further test the transient performance provided by the Speed UDE PSS, a 12 cycles three-phase to ground fault is simulated. Under this case, the MB-PSS will loss synchronism, and only the Speed PSS and the Speed UDEPSS can maintain the system stability. The simulation response is shown in Figure 5.5. From Figure 5.5, it can see that the proposed Speed UDEPSS can provide a

better response than the Speed PSS.

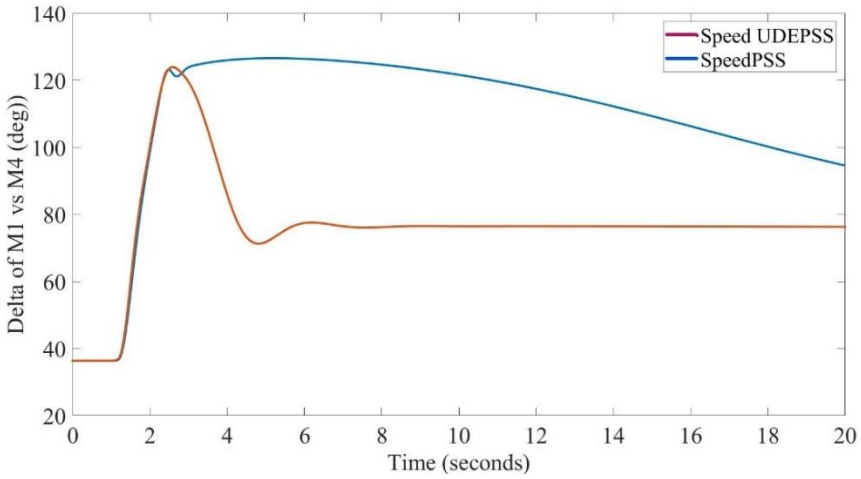

(a) Rotor angle of M1 vs M4

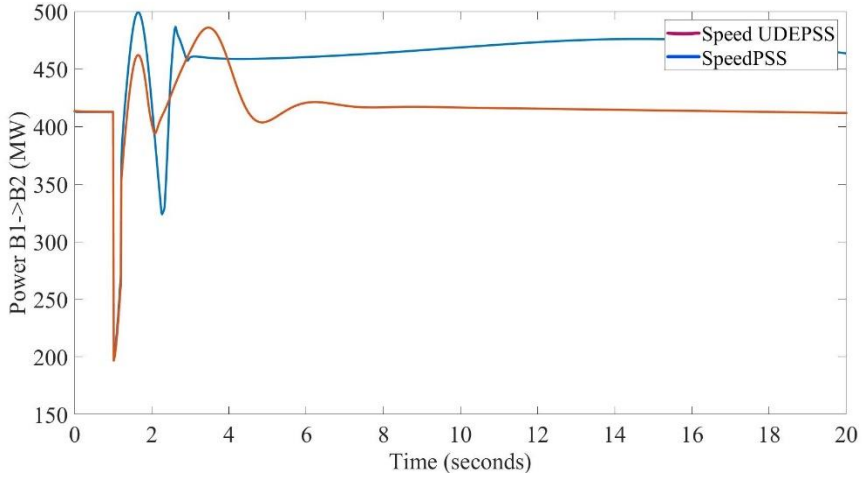

(b) Active power between B1 bus to B2 bus

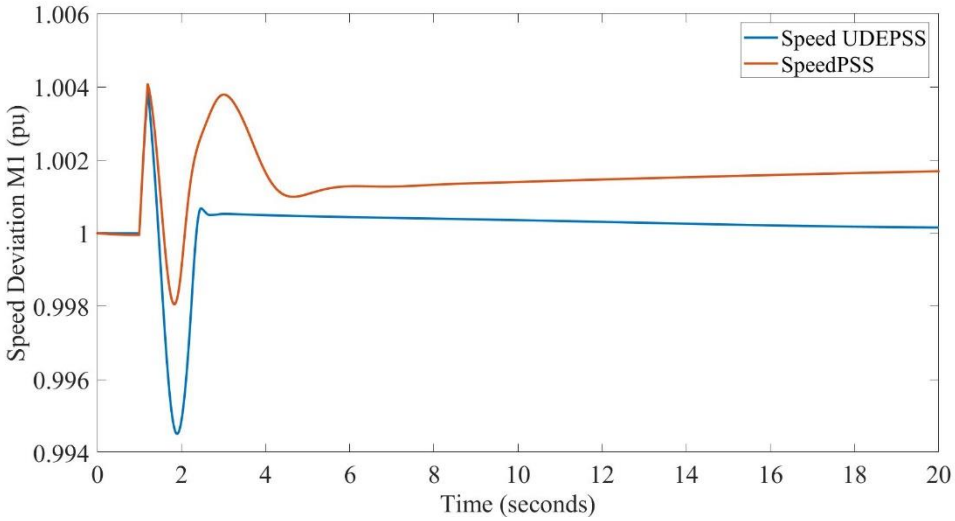

(c) Speed of M1

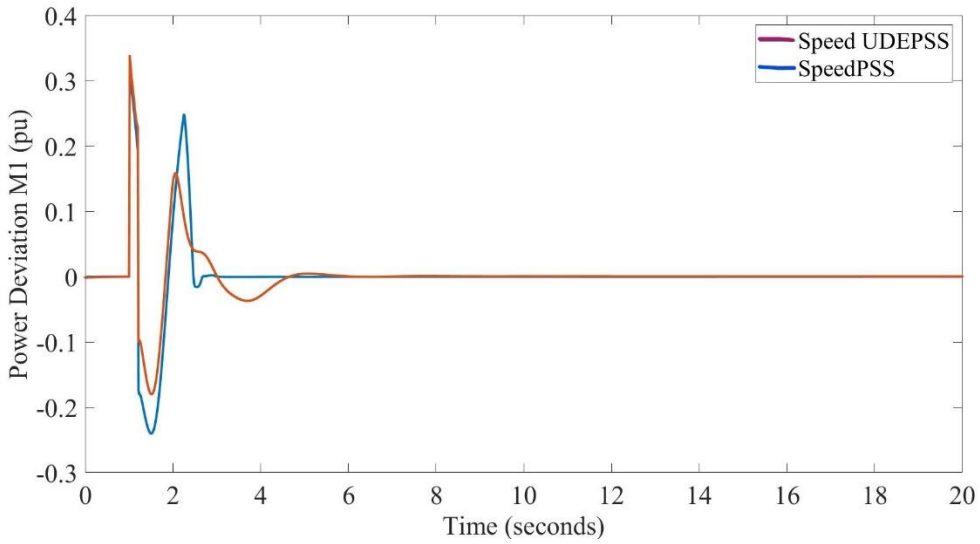

(d) Acceleration Power of M1

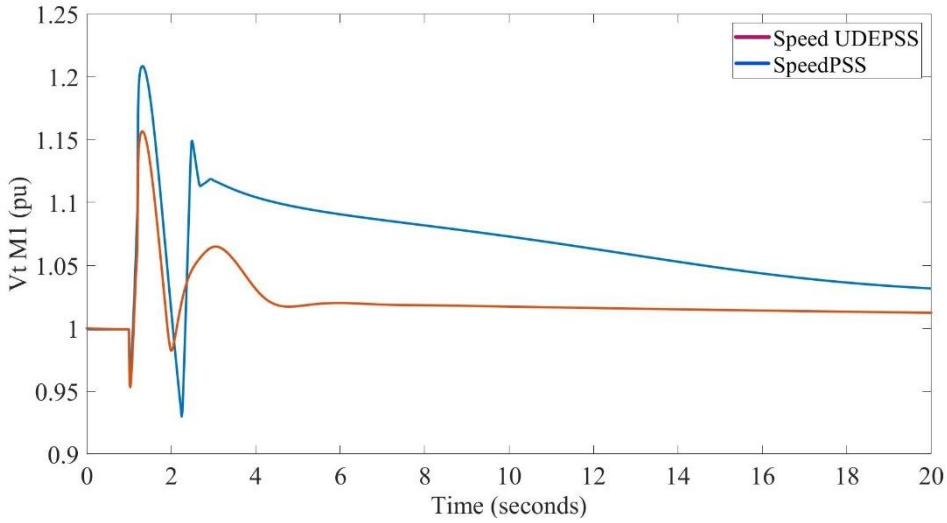

(e) Terminal Voltage of M1

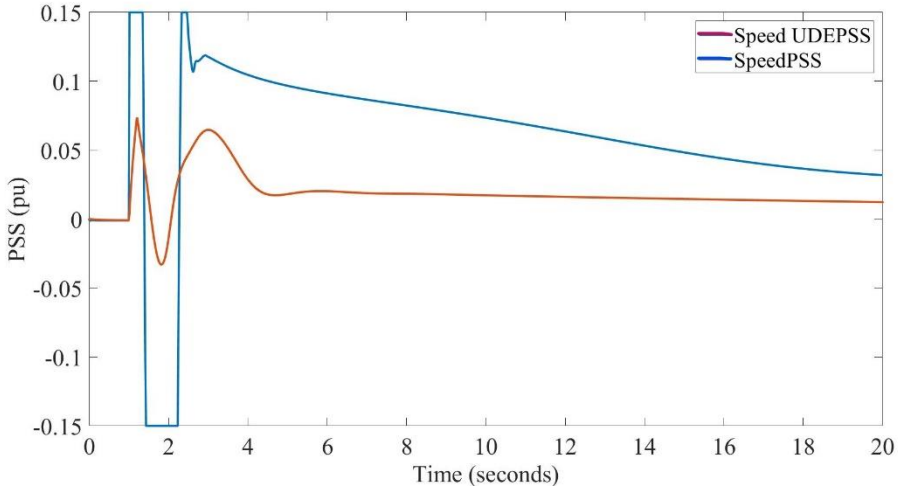

(f) PSS output

Figure 5.5 Response to different PSSs under three-phase to ground for 12 cycles, only Speed UDEPSS and Speed PSS can provide the stable response. MB-PSS and Power-PSS both cannot maintain the stability.

5.3.3 Power type UDEPSS large signal performance assessment

As discussed in the Section 4.3.2, a power type UDEPSS can be designed via using the acceleration power of the generator as the feedback input of the UDE (4.17) and design a PID type linear controller as shown (4.22). The structure diagram of a Power type UDEPSS is shown in Figure 5.6. Comparing with the Speed UDEPSS tested in previous section who uses a third-order low-pass filter, here a second-order low pass filter is used. Simulation results of Speed UDEPSS and Power UDEPSS under 12 cycles of fault are shown in Figure 5.7, which shows that both can maintain the system stability, while the Speed UDEPSS's performance is better and one possible reason is the Speed UDEPSS provide the damping torque from the direct feedback of the speed. Note that both of them are not fined tuned and use the designed PSSs for SMIB system in Chapter 4.

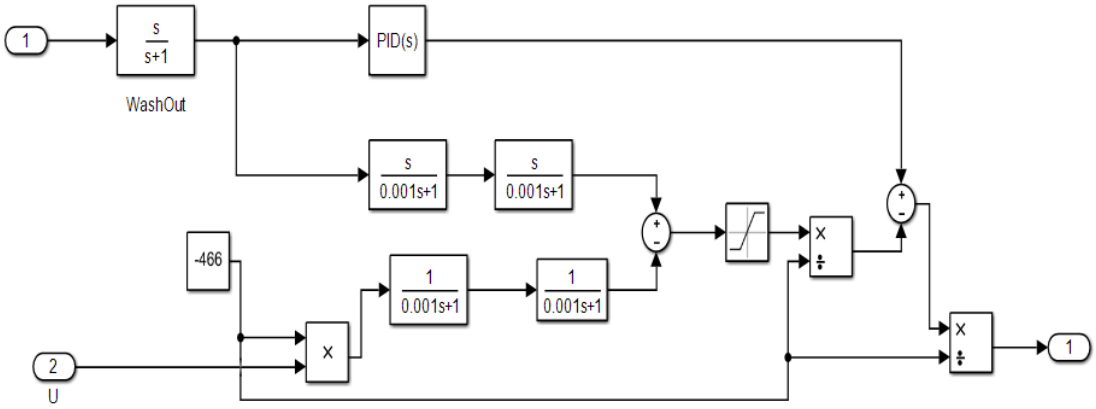

Figure 5.6 Structure of a Power type UDEPSS based on Eqn. (4.22)

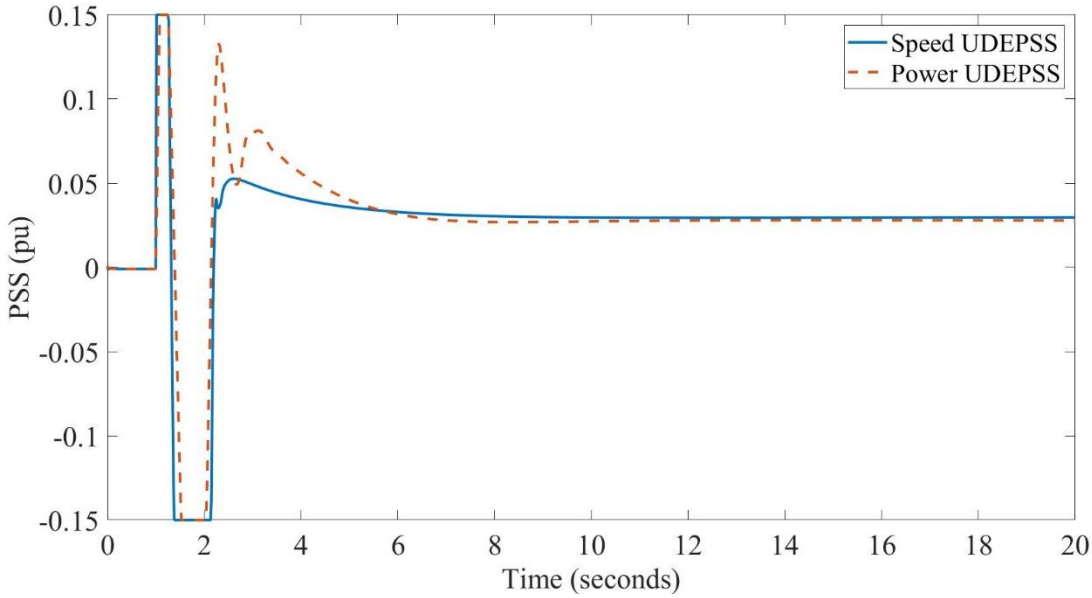

(a) PSS output

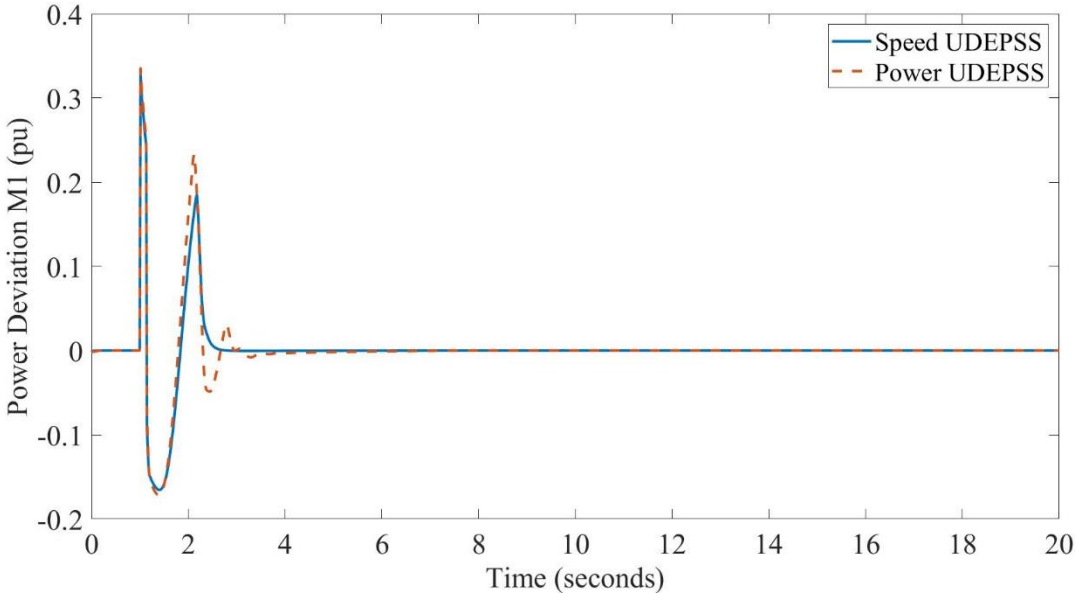

(b) Acceleration Power of M1

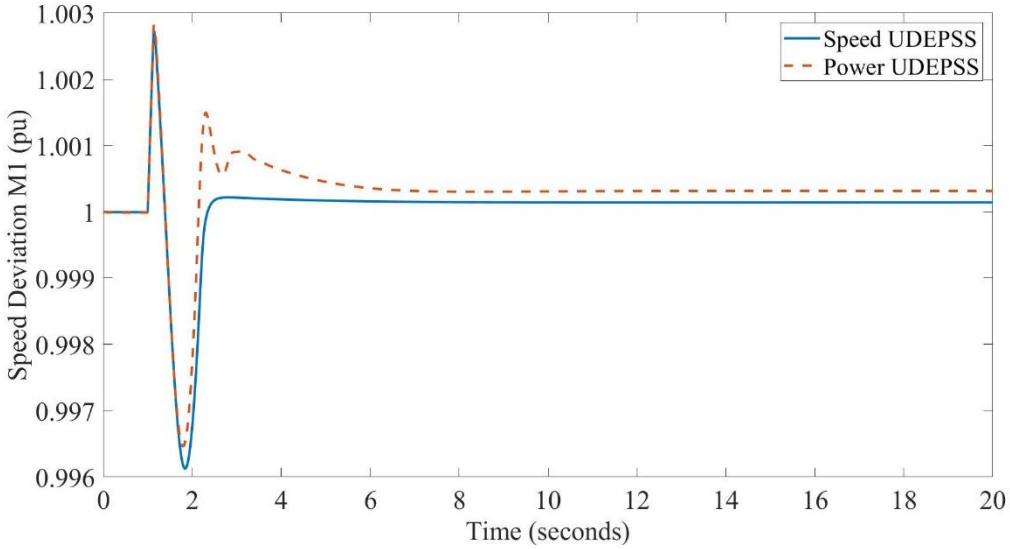

(c) Rotor speed of M1

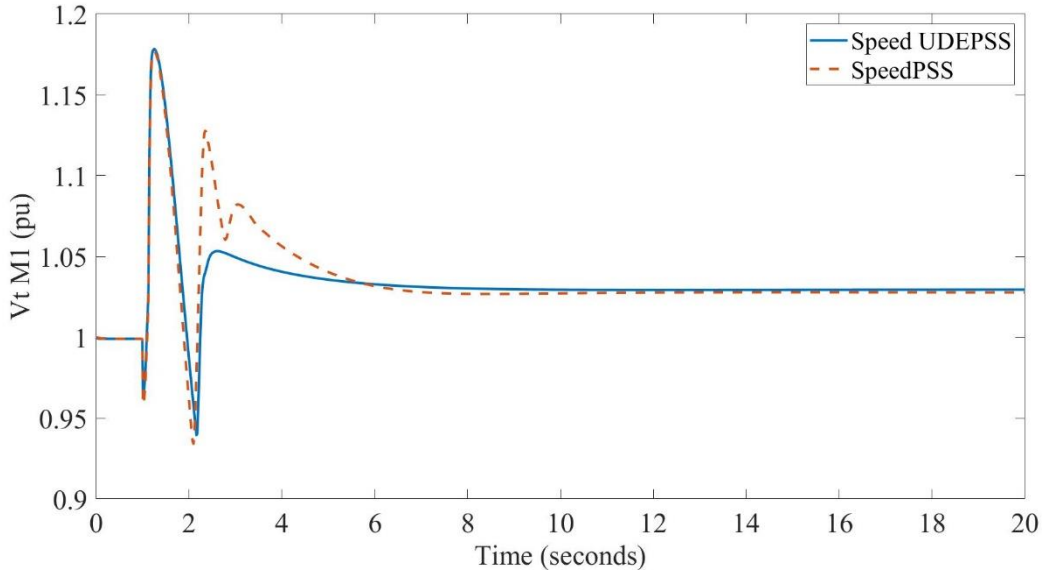

(d) Terminal voltage of M1

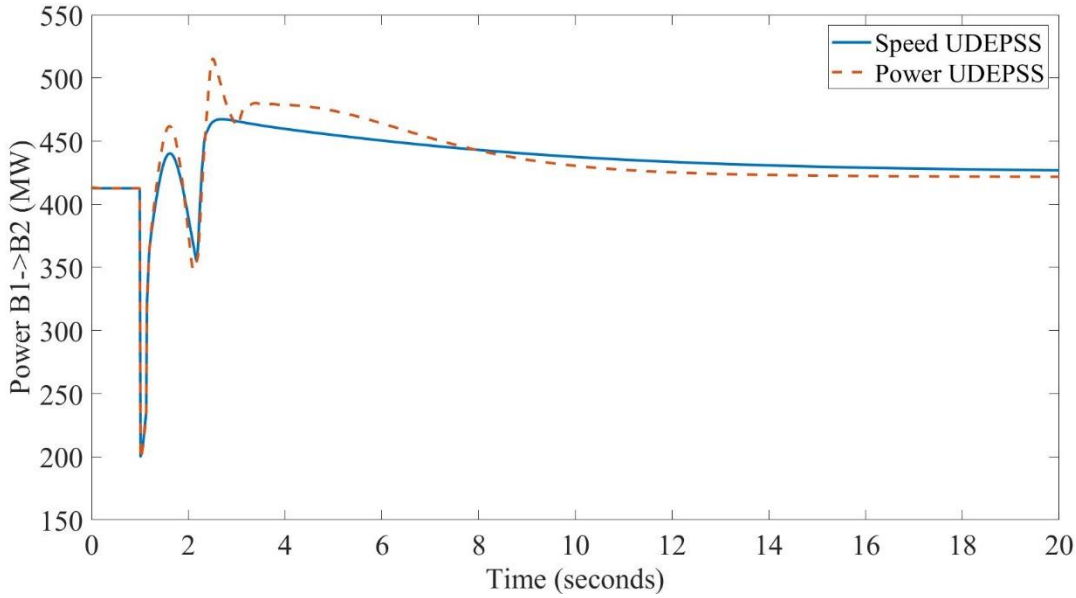

(e) Active Power from Bus 1 to Bus 2

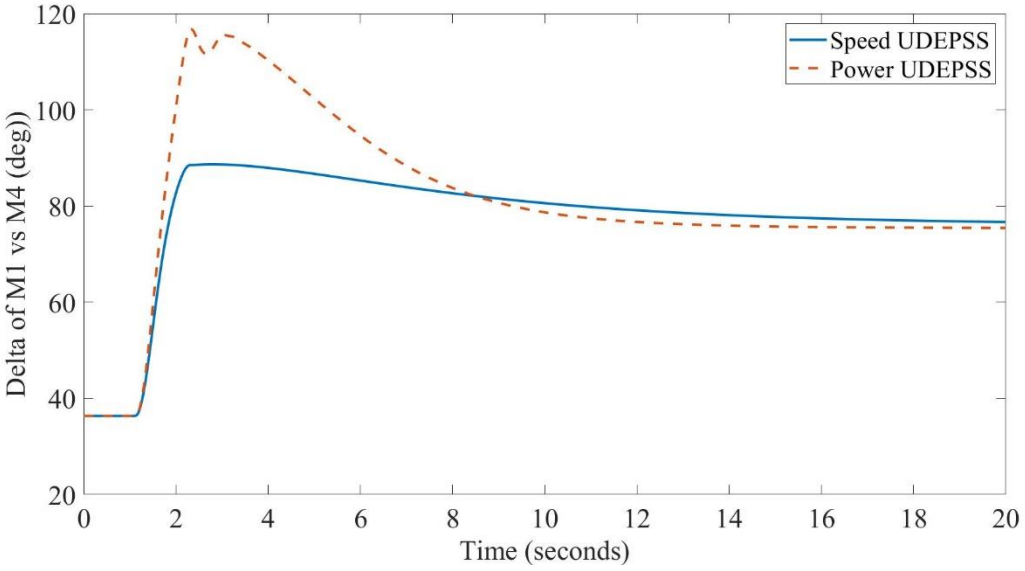

(f) Rotor angle of M1 vs M4

Figure 5.7 Response of Speed UDEPSS and Power UDEPSS under three-phase to ground for 12 cycles

5.4 Conclusions

Performance of the proposed UDEPSS has been tested in the multi-machine power system for their capability of damping of inter-area oscillation. IEEE standard multi-band PSS, PSS4B, and the classical speed type and acceleration power type PSSs are compared. The Speed type UDEPSS can provide better performance than all other PSSs which has much simpler structure than the PSS4B and very good robustness to system operation points and uncertainties due to the compensation of the disturbance and uncertainties. Moreover, it only requires one measurement which make it be more practical than those ESPO based PSS which requires rotor angle measurement and high-order derivatives of the rotor speed.

Chapter 6 Conclusions and future work

6.1 Conclusions

Control system plays a key role to maintain the stability of a modern power system which is a high nonlinear and large-scale interconnected system, subject to consistent load uncertainties and faults. The control of power system faces new challenges after the integration large-scale intermittent renewable power generations and flexible load at the demand-side. As synchronous generators still dominate the electricity generation and to its operation, all other new types of generation and control devices must cooperate with SG to achieve the whole system target, contribution of SG to maintain the whole system stability still is the most feasible and effective approach. Most large capacity synchronous generators have installed speed governing systems at the prime mover, automatic voltage regulator (AVR) and PSS at the generator side.

PSS's contribution to power system stability is desired more investigations due the following reasons. The first one is that their design and tuning are carried out based on the linearized model based on one operation point, their performance may be degraded when the power system operates at a different operation point caused either by load disturbances, dispatch command, and power system faults. Secondly, the conventional frequency domain-based design, such as lead-lag compensator type PSS, can only easily be designed and analyzed in a single machine infinite bus system (SMIB) and it is difficulty to extend them to multi-machine large-scale system. In

other words, the interaction between different generators cannot be handled effectively. Finally, with the increased development of renewable energy generation from wind and solar power, those intermittent and time-varying generations, together with demand-side response technology which include direct controllable load will further shift the whole power system operating at different operation points.

This thesis has investigated a nonlinear PSS mainly from the following three aspects:

1) A nonlinear PSS is designed based on the 4^{th}-order nonlinear model in which the output of the PSS is added into the terminal voltage deviation and together as the input of the AVR. This is different with most nonlinear excitation control reported in which the nonlinear excitation controller and the AVR is connected in parallel and both outputs are applied to field voltage. The reason of the proposed PSS is to improve the small signal stability, rather the transient stability in the nonlinear excitation controller. In fact, considering the saturation of the excitation field voltage, and also the regulation profile of the terminal voltage, a NPSS is designed for improving the damping of low-frequency oscillation.
2) Feedback linearization control and extended-order perturbation observer (ESO) based nonlinear adaptive control have been applied to design a nonlinear PSS and ESO-PSS respectively, based on the fourth order SMIB system. State feedback and output feedback control have been investigated respectively. The ESO-PSS employs an extend-order state and perturbation

observer to estimate the unknown states and the perturbation. It is found that a 5-th order ESO is not suitable even in simulation study due to the very high gain of the observer and the sensitivity to the noise. Also, a 5-th order ESO requires the rotor angle measurements, and the 2-roder ESO requires the second-order derivative of the speed, both variables are not easily measured. Simulation studies are carried out to illustrate the advantages and disadvantages of the time-domain ESO-PSS, and compared with the conventional speed-type PSS (CPSS),

3) An uncertain and disturbance estimator (UDE) designed in frequency domain has been proposed for a UDE-PSS. The UDE only requires same-order observer, equivalently represented as the pure derivate of states but its implementation difficulty has been removed by using the same order of low pass filter. The ESO in the time-domain is replaced by UDE for designing a full-state nonlinear PSS based on ESO. Then combining the conventional lead-lag-type PSS designed in frequency domain, the UDE is applied to design an UDE-PSS. The proposed UDE-PSS composes of a PID type controller and the cancellation of the estimated uncertainties and disturbance from the UDE. The UDEPSS only requires one measurement, speed type UDEPSS and the acceleration power type PSS are investigated respectively.
4) Performance of the proposed UDEPSS has been tested in the multi-machine power system for their capability of damping of inter-area oscillation. IEEE standard multi-band PSS, PSS4B, and the classical speed type and

acceleration power type PSSs are compared. The Speed type UDEPSS can provide better performance than all other PSSs which has much simpler structure than the PSS4B and very good robustness to system operation points and uncertainties due to the compensation of the disturbance and uncertainties.

6.2 Future Work

The following aspects of research have been identified to continue the design and test of disturbance observer-based PSS.

1) The analysis of the UDE-PSS in frequency domain and find out the relationship of the parameters of the PID and the gain and phase of the UDE-PSS. Further verification of the UDE-PSS based on the IEEE standard to tune the gains of the UDE-PSS, based on the procedure of reference [39].
2) Design a damping controller based on UDE-PSS for wind turbine such as DFIG-type and PMSG type wind power generation systems. The main motivation is to test the effectiveness of the time-varying operation points of a wind power generation system. Investigate the contribution of damping from a wind farm in multi-machine power system.
3) Continue the design a UDE-PSS in frequency domain: design an additional UDE for the forward compensation of the conventional lead/lag type PSS. The function of the UDE is to compensate the shift of the operation points.

REFERENCES

[1] P. Kundur, “Power System Stability and Control”. New York: McGraw-Hill, 1994.

[2] S. Chowdhury, S.P. Chowdhury and P. Crossley, “Microgrids and Active Distribution Networks”, IET, 2009.

[3] G. Rogers, “Power System Oscillations”. Boston, MA: Kluwer, 2000.

[4] H. F. Wang, W. J. Du, “Analysis and Damping Control of Power System Low-frequency Oscillations, Power Electronics and Power Systems”, Springer, 2016.

[5] G. Gurrala and I. Sen, “Synchronizing and Damping Torques Analysis of Nonlinear Voltage Regulators” IEEE Transactions on Power Systems, vol. 26, no. 3, pp. 1175-1185, Aug. 2011.

[6] S. H. Li, J. Yang, W.-H. Chen, and X. S. Chen, “Disturbance Observer Based Control: Methods and Applications”. CRC Press, 2014.

[7] R. C. Dorf and R. H. Bishop, “Modern Control Systems, 12th edition”. Englewood Cliffs, NJ, USA: Prentice-Hall, 2011.

[8] M.D. Ilic, H. Allen, W. Chapman, C.A. King, J.H. Lang, E. Litvinov, “Preventing Future Blackouts by Means of Enhanced Electric Power Systems Control: From Complexity to Order”, Proceedings of the IEEE, vol. 93, no. 11, pp. 1920-1941, 2005.

[9] P. Kundur, “Definition and classification of power system stability IEEE/CIGRE joint task force on stability terms and definitions”, IEEE Transactions on Power Systems, vol. 19, no. 3, pp. 1387-1401, Aug. 2004.

[10] “U.S.-Canada Power System Outage Task Force , Causes and Recommendations Final Report”, August 14, 2003

[11] “NERC interim report: Causes of the August 14th blackout in the United States and Canada” U.S.–Canada Power System Outage Task Force [Online]. Available: http://www.nerc.com/~filez/blackout.html

[12] “Recommended Practice for Excitation System Models for Power System Stability Studies”, IEEE Std 421.5™-2016.

[13] “NYISO final report on the 2003 blackout” Feb. 8, 2005 [Online]. Available: http://www.nyiso.com

[14] “DoE blackout report” [Online]. Available: http://www.doe.gov.

[15] M. L. Tuballa, M. L. Abundo, “A review of the development of Smart Grid technologies, Renewable and Sustainable Energy Reviews”, Volume 59, 2016, Pages 710-725.

[16] IEEE Digital Excitation Task Force of the Equipment Working Group of the IEEE/PES Excitation System Subcommittee, “Computer model for representation of digital-based excitation systems,” IEEE Trans. Energy Convers., vol. 11, no. 3, pp. 607–615, Sep. 1996.

[17] F. P. Demello and C. Concordia, “Concepts of Synchronous Machine Stability as Affected by Excitation Control”, IEEE Transactions on Power Apparatus and Systems, vol. PAS-88, no. 4, pp. 316-329, April 1969.

[18] E. V. Larsen and D. A. Swann, “Applying Power System Stabilizers Part I, II, III: General Concepts”, IEEE Transactions on Power Apparatus and Systems, vol. PAS-100, no. 6, pp. 3017-3024, June 1981.

[19] P. Kundur, M. Klein, G. J. Rogers, and M. S. Zywno, “Application of power system stabilizers for enhancement of overall system stability,” IEEE Trans. Power Syst., vol. 4, no. 2, pp. 614–626, May 1989.

[20] Impact of Interactions Among Power Systems Controls, Aug. 1998. CIGRÉ TF 38.02.16 (N. Martins, Convenor), CIGRÉ Brochure no. 166.

[21] S.K. Yee, J.V. Milanović, F.M. Hughes, “Phase compensated gas turbine governor for damping oscillatory modes”, Electric Power Systems Research, vol. 79, pp. 1192, 2009.

[22] R. Grondin, I. Kamwa, L. Soulières, J. Potvin, and R. Champagne, “An approach to PSS design for transient stability improvement through supplementary damping of the common low frequency,” IEEE Trans. Power Syst, vol. 7, no. 2, pp. 954–963, May 1993.

[23] A. Murdoch, S. Venkataraman, R. A. Lawson, and W. R. Pearson, “Integral of accelerating power type PSS. Parts I and II.,” IEEE Trans. Energy Convers., vol. 14, no. 4, pp. 1658–1672, Dec. 1999.

[24] M. Klein, G. J. Rogers, S. Moorty, and P. Kundur, “Analytical investigation of factors influencing power system stabilizer performance,” IEEE Trans. Energy Convers., vol. 7, no. 3, pp. 382–390, Sep. 1992.

[25] H. Vu and J. C. Agee, “Comparison of power system stabilizers for damping local mode oscillations,” IEEE Trans. Energy Convers., vol. 8, no. 3, pp. 533–540, Sep. 1993.

[26] D. Rimorov, I. Kamwa, G. Joós, “Quasi-Steady-State Approach for Analysis of Frequency Oscillations and Damping Controller Design”, Power Systems IEEE Transactions on, vol. 31, no. 4, pp. 3212-3220, 2016

[27] K. Bhattacharya, J. Nanda, and M. L. Kotari, “Optimization and performance analysis of conventional power system stabilizers,” Elect. Power & Energy Syst., vol. 19, no. 7, pp. 449–458, 1997.

[28] T. C. Yang, “Applying optimization method to power system stabilizer design: Parts 1 and 2,” Elec. Power & Energy Syst., vol. 19, no. 1, pp. 29–43, 1997.

[29] G. N. Taranto, J. H. Chow, and H. A. Othman, “Robust redesign of power system damping controllers,” IEEE Trans. Contr. Syst. Technol., vol. 3, no. 3, pp. 290–298, Sep. 1995.

[30] I. Kamwa, L. Trudel, and L. Gérin-Lajoie, “Robust design and coordination of multiple damping controllers using constrained optimization,” IEEE Trans. Power Syst., vol. 15, no. 3, pp. 1084–1092, Aug. 2000.

[31] N. Martins, A. A. Barbosa, J. C. R. Ferraz, M. G. dos Santos, A. L. B. Bergamo, C. S. Yung, V. R. Oliveira, and N. J. P. Macedo, “Retuning

stabilizers for the North-South Brazilian interconnection," in Proc. IEEE PES Summer Meeting, vol. 1, Jul. 1999, pp. 58–67.

[32] A. Fischer and I. Erlich, "Impact of long-distance power transits on the dynamic security of large interconnected power systems," Proc. 2001 IEEE Power Tech. Conf., vol. 2, p. 6, Sep. 2001.

[33] H. Breulman, E. Grebe, M. Losing, W. Winter, R. Witzman, P. Dupuis, M. P. Houry, T. Margotin, J. Zerenyi, J. Duzik, J. Machowski, L. Martin, J. M. Rodriguez, and E. Urretavizcaya, "Analysis and damping of inter-area oscillations in the UCTE/CENTREL power system," in Proc. CIGRE 2000, Paris, France. Paper 38-113.

[34] R. Castellanos B, J.G. C. G., D. Olguin, H. U. Sarmiento, A.R. Messina, "Use of power system stabilizers for damping inter-area oscillations in the south systems of the Mexican electrical grid", Electric Power Systems Research, vol. 76, pp. 169, 2006.

[35] R. Grondin, I. Kamwa, G. Trudel, J. Taborda, R. Lenstroem, L. GerinLajoie, J. P. Gingras, M. Racine, and H. Baumberger, "The multi-band PSS: A flexible technology designed to meet opening markets," in *Proc. CIGRÉ 2000*, Paris, France. Paper 39-201.

[36] R. Grondin, I. Kamwa, G. Trudel, L. Gérin-Lajoie, and J. Taborda, "Modeling and closed-loop validation of a new PSS concept, the multi-band PSS," presented at the 2003 IEEE/PES General Meeting, Panel Session on New PSS Technologies, Toronto, ON, Canada.

[37] I. Kamwa, R. Grondin and G. Trudel, “IEEE PSS2B versus PSS4B: the limits of performance of modern power system stabilizers” IEEE Transactions on Power Systems, vol. 20, no. 2, pp. 903-915, May 2005.

[38] D. Rimorov, A. Heniche, I. Kamwa, G. Stefopoulos, S. Babaei, B. Fardanesh, “Inter-area oscillation damping and primary frequency control of the New York state power grid with multi-functional multi-band power system stabilizers”, Power and Energy Society General Meeting (PESGM) 2016, pp. 1-5, 2016.

[39] L. Jia, X. Gao, Y. Xu, H. Xie, T. Wu, W. Su, J.H. Zhou, D. Q. Gan, H. H. Xin, “Application of PSS4B stabilizers in suppressing low frequency oscillations: A case study”, Power & Energy Society General Meeting 2015 IEEE, pp. 1-5, 2015.

[40] N Nikolaev, “Tuning of power system stabilizer PSS3B and analysis of its properties”, Electrical Apparatus and Technologies (SIELA) 2018 20th International Symposium on, pp. 1-5, 2018.

[41] B. Ansari, S. Babaei, B. Fradanesh, D. Rimorov, A. Heniche, I. Kamwa, “Adaptive wide-area primary frequency controller for improving power grid dynamic performance”, Power & Energy Society General Meeting 2017 IEEE, pp. 1-5, 2017.

[42] L. Gérin-Lajoie, D. Lefebvre, M. Racine, L. Soulières, and I. Kamwa, ““Hydro-Québec experience with PSS tuning” panel on system reliability as

affected by power system stabilizers" IEEE PES Summer Meeting, vol. 1, Jul. 1999, pp. 88–95.

[43] A. Dysko, W. E. Leithead, J. O'Reilly, "Enhanced Power System Stability by Coordinated PSS Design", Power Systems IEEE Transactions on, vol. 25, no. 1, pp. 413-422, 2010.

[44] G. Gurrala, I. Sen, "Power System Stabilizers Design for Interconnected Power Systems", Power Systems IEEE Transactions on, vol. 25, no. 2, pp. 1042-1051, 2010.

[45] A. C. Padoan, B. Kawkabani, A. Schwery, C. Ramirez, C. Nicolet, J. J. Simond, F. Avellan, "Dynamical Behavior Comparison Between Variable Speed and Synchronous Machines With PSS", Power Systems IEEE Transactions on, vol. 25, no. 3, pp. 1555-1565, 2010.

[46] Z. Wang, C.Y. Chung, K.P. Wong, "Systematic approach to consider system contingencies in PSS design", Electric Power Systems Research, vol. 79, pp. 1678, 2009.

[47] D. P. Ke, C. Y. Chung, Y.S. Xue, "An Eigenstructure-Based Performance Index and Its Application to Control Design for Damping Inter-Area Oscillations in Power Systems", Power Systems IEEE Transactions on, vol. 26, no. 4, pp. 2371-2380, 2011.

[48] F. J. De Marco, N. Martins, J. C. R. Ferraz, "An automatic method for power system stabilizers phase compensation design", Power Systems IEEE Transactions on, vol. 28, no. 2, pp. 997-1007, 2013.

[49] J. Zhang, C. Y. Chung, Y. D. Han, "A Novel Modal Decomposition Control and Its Application to PSS Design for Damping Interarea Oscillations in Power Systems", Power Systems IEEE Transactions on, vol. 27, no. 4, pp. 2015-2025, 2012.

[50] N. Martins, T. H. S. Bossa, "A Modal Stabilizer for the Independent Damping Control of Aggregate Generator and Intraplant Modes in Multi generator Power Plants", Power Systems IEEE Transactions on, vol. 29, no. 6, pp. 2646-2661, 2014.

[51] R. Jalayer, B. T. Ooi, "Co-Ordinated PSS Tuning of Large Power Systems by Combining Transfer Function-Eigenfunction Analysis (TFEA) Optimization and Eigenvalue Sensitivity", Power Systems IEEE Transactions on, vol. 29, no. 6, pp. 2672-2680, 2014.

[52] A. Yaghooti, M. O. Buygi, M. H. M. Shanechi, "Designing Coordinated Power System Stabilizers: A Reference Model Based Controller Design", Power Systems IEEE Transactions on, vol. 31, no. 4, pp. 2914-2924, 2016.

[53] D. Rimorov, I. Kamwa, Géza Joós, "Model-based tuning approach for multi-band power system stabilisers PSS4B using an improved modal performance index", Generation Transmission & Distribution IET, vol. 9, no. 15, pp. 2135-2143, 2015.

[54] K. Sebaa, M. Boudour, "Optimal locations and tuning of robust power system stabilizer using genetic algorithms", Electric Power Systems Research, vol. 79, pp. 406, 2009.

[55] B. Sumanbabu, S. Mishra, B.K. Panigrahi, G.K. Venayagamoorthy, “Robust tuning of modern power system stabilizers using Bacterial Foraging Algorithm”, Evolutionary Computation 2007. CEC 2007. IEEE Congress on, pp. 2317-2324, 2007.

[56] Y. Li, K. W. Wang, C. T. Tse, “Design Dual-Band PSS by phase compensation based on the sixth-order machine representation”, Electric Utility Deregulation and Restructuring and Power Technologies 2008. DRPT 2008. Third International Conference on, pp. 1478-1483, 2008.

[57] T. C. Ou, T. P. Tsao, C. M. Hong, Ch. H. Chen, “Hybrid control system for automatic voltage regulator in smart grid”, Machine Learning and Cybernetics (ICMLC) 2013 International Conference on, vol. 03, pp. 1103-1108, 2013.

[58] N. R. Chaudhuri, S. Ray, R. Majumder, B. Chaudhuri, “Interaction between conventional and adaptive phasor power oscillation damping controllers”, Power and Energy Society General Meeting 2010 IEEE, pp. 1-7, 2010.

[59] R. Shah, N. Mithulananathan, Kwang. Y. Lee, “Design of robust power oscillation damping controller for large-scale PV plant”, Power and Energy Society General Meeting 2012 IEEE, pp. 1-8, 2012.

[60] J. L. Rueda, J. C. Cepeda, I. Erlich, “Probabilistic approach for optimal placement and tuning of power system supplementary damping controllers”, Generation Transmission & Distribution IET, vol. 8, no. 11, pp. 1831-1842, 2014.

[61] A. Khodabakhshian, “Pole-zero assignment adaptive stabilizer”, Electric Power Systems Research, vol. 73, pp. 77, 2005.

[62] S. Mishra, M. Tripathy, J. Nanda, “Multi-machine power system stabilizer design by rule-based bacteria foraging”, Electric Power Systems Research, vol. 77, pp. 1595, 2007.

[63] H. Shayeghi, H.A. Shayanfar, S. Jalilzadeh, A. Safari, “Multi-machine power system stabilizers design using chaotic optimization algorithm”, Energy Conversion and Management, vol. 51, pp. 1572, 2010.

[64] R. V. de Oliveira, R. A. Ramos, N. G. Bretas, “An algorithm for computerized automatic tuning of power system stabilizers”, Control Engineering Practice, vol. 18, pp. 45, 2010.

[65] H. Shayeghi, H.A. Shayanfar, A. Safari, R. Aghmasheh, “A robust PSSs design using PSO in a multi-machine environment”, Energy Conversion and Management, vol. 51, pp. 696, 2010.

[66] J. Ma, Hao J. Wang, K. L. Lo, “Clarification on power system stabilizer design., Generation Transmission & Distribution IET, vol. 7, no. 9, pp. 973-981, 2013.

[67] H. K. Abdulkhader, J. J. Abraham, T. Mathew, “Fractional-order lead-lag compensator-based multi-band power system stabilizer design using a hybrid dynamic GA-PSO algorithm”, Generation Transmission & Distribution IET, vol. 12, no. 13, pp. 3248-3260, 2018.

[68] M. Alizadeh, S. Shokri Kojori, S. Ganjefar, “A Modular Neural Block to Enhance Power System Stability”, Power Systems IEEE Transactions on, vol. 28, no. 4, pp. 4849-4856, 2013.

[69] D. Molina, G. K. Venayagamoorthy, J. Q. Liang, R. G. Harley, “Intelligent Local Area Signals Based Damping of Power System Oscillations Using Virtual Generators and Approximate Dynamic Programming”, Smart Grid IEEE Transactions on, vol. 4, no. 1, pp. 498-508, 2013.

[70] A Sallama, M Abbod, P Turner, “Neuro-fuzzy system for power generation quality improvements”, Universities Power Engineering Conference (UPEC) 2012 47th International, pp. 1-6, 2012.

[71] Y. F. Ma, S. Q. Zhao, X. P, Gu “Coordinated damping control of power systems based on on-line identification”, Electric Utility Deregulation and Restructuring and Power Technologies (DRPT) 2011 4th International Conference on, pp. 1355-1359, 2011.

[72] A.A. Gharaveisi, S.M.R. Rafiei, S.M. Barakati, “An optimal Takagi-Sugeno Fuzzy PSS for multi- machine power system”, Power Symposium 2008. NAPS '08. 40th North American, pp. 1-9, 2008.

[73] R. Shivakumar, R. Lakshmipathi, Y. Suresh, “Supplementary Excitation Controller design to enhance system Damping Ratio using an innovative swarm intelligence algorithm”, Power Systems 2009. ICPS '09. International Conference on, pp. 1-6, 2009.

[74] J. K. Mallik, “Reducing the effect of vortex rope oscillation on hydro units by power system stabilizer designed using Genetic Algorithm”, India Conference (INDICON) 2011 Annual IEEE, pp. 1-4, 2011.

[75] M. Ramirez-Gonzalez, R. Castellanos B., O. P. Malik, “Application of simple fuzzy PSSs for power system stability enhancement of the Mexican Interconnected System”, Power and Energy Society General Meeting 2010 IEEE, pp. 1-8, 2010.

[76] F. G. Nogueira, W. Barra, C. T. da Costa, A. R.B. de Moraes, M. C.M. Gomes, J. J. de Lana, “Design and experimental evaluation tests of a Takagi–Sugeno power system stabilizer”, Generation Transmission & Distribution IET, vol. 8, no. 3, pp. 451-462, 2014.

[77] M. Cloughley, K. M. Muttaqi, H, Du, “Damping of low-inertia machine oscillations using Takagi-Sugeno fuzzy stabiliser tuned by genetic algorithm optimisation to improve system stability”, Generation Transmission & Distribution IET, vol. 8, no. 2, pp. 339-352, 2014.

[78] P.R. Gandhi, S.K. Joshi, “GA and ANFIS based power system stabilizer”, Power and Energy Society General Meeting (PES) 2013 IEEE, pp. 1-5, 2013.

[79] N.C. Pahalawaththa, S.J. Cheng, O.P. Malik, G.S. Hope, “A Self-tuning Power System Stabilizer”, IFAC Proceedings Volumes, vol. 20, pp. 31, 1987.

[80] O.P. Malik, “Amalgamation of Adaptive Control and Ai Techniques: Applications to Generator Excitation Control”, IFAC Proceedings Volumes, vol. 36, pp. 1, 2003.

[81] J. Zhenhua, “Design of a nonlinear power system stabilizer using synergetic control theory”, Electric Power Systems Research, vol. 79, pp. 855, 2009.

[82] W Liu, G K. V, Donald C. Wunsch, “Design of an adaptive neural network-based power system stabilizer”, Neural Networks, vol. 16, pp. 891, 2003.

[83] C. Nicolet, B. Greiveldinger, J. J. Herou, B. Kawkabani, Philippe Allenbach, J. J. Simond, F. Avellan, “High-Order Modeling of Hydraulic Power Plant in Islanded Power Network”, Power Systems IEEE Transactions on, vol. 22, no. 4, pp. 1870-1880, 2007.

[84] P. C. O. Silva, C. Nicolet, P. Grillot, J. Drommi, B. Kawkabani, “Assessment of Power Swings in Hydropower Plants Through High-Order Modelling and Eigen analysis”, Industry Applications IEEE Transactions on, vol. 53, no. 4, pp. 3345-3354, 2017.

[85] R. Shah, N. Mithulananthan, K. Y. Lee, “Large-Scale PV Plant with a Robust Controller Considering Power Oscillation Damping”, Energy Conversion IEEE Transactions on, vol. 28, no. 1, pp. 106-116, 2013.

[86] C. Martinez, G. Joos, B.T Ooi, “Power system stabilizers in variable speed wind farms”, Power & Energy Society General Meeting 2009. PES '09. IEEE, pp. 1-7, 2009.

[87] R. V. de Oliveira, R. A. Ramos, N. G. Bretas, “A Mixed Procedure Based on Classical and Modern Control to Design Robust Damping Controllers”, Power Systems IEEE Transactions on, vol. 22, no. 3, pp. 1231-1239, 2007.

[88] C.W. Taylor, C. Erickson, K. E. Martin, R. E. Wilson, and V. Venkatasubramanian, "WACS wide-area stability and voltage control system: R&D and on-line demonstration," Proceedings of the IEEE, vol. 93, no. 5, pp. 892-906, May 2005.

[89] N. R. Chaudhuri, S. Ray, R. Majumder, B. Chaudhuri, "A New Approach to Continuous Latency Compensation with Adaptive Phasor Power Oscillation Damping Controller (POD)", Power Systems IEEE Transactions on, vol. 25, no. 2, pp. 939-946, 2010.

[90] I. Kamwa, S. R. Samantaray, G. Joos, "Compliance Analysis of PMU Algorithms and Devices for Wide-Area Stabilizing Control of Large Power Systems", Power Systems IEEE Transactions on, vol. 28, no. 2, pp. 1766-1778, 2013.

[91] I. Kamwa, S. R. Samantaray, G. Joos, "Optimal Integration of Disparate C37.118 PMUs in Wide-Area PSS with Electromagnetic Transients," Power Systems IEEE Transactions on, vol. 28, no. 4, pp. 4760-4770, 2013.

[92] I. Kamwa, J. Beland, G. Trudel, R. Grondin, C. Lafond, D. McNabb, "Wide-area monitoring and control at Hydro-Quebec: past present and future", Power Engineering Society General Meeting 2006. IEEE, pp. 12 pp., 2006.

[93] R. Goldoost-Soloot, Yateendra Mishra, Gerard Ledwich, "Wide-area damping control for inter-area oscillations using inverse filtering technique", IET Generation Transmission & Distribution, vol. 9, no. 13, pp. 1534-1543, 2015.

[94] M. Huong Nguyen, Tapan Kumar Saha, Mehdi Eghbal, "Input/output selection for wide-area power oscillation damper of hybrid multi-terminal high-voltage direct current to connect remotely located renewable energy resources", IET Generation Transmission & Distribution, vol. 9, no. 5, pp. 483-493, 2015.

[95] B.W. Bequette. “Process Control: Modeling, Design, and Simulation. Prentice Hall”, New Jersey, 2002.

[96] A. Isidori. “Nonlinear Control Systems: An Introduction, 3rd ed”, Springer-Verlag, 1995.

[97] L. Jiang, “Nonlinear Adaptive Control and Applications in Power Systems”, PhD Thesis, The University of Liverpool, March 2001.

[98] K. Youcef-Toumi, and O. Ito, ‘‘A Time Delay Controller for Systems with Unknown Dynamics,’’ ASME J. Dyn. Syst., Meas., Control, vol. 112, no. 1, pp. 133–142, 1990.

[99] W. Chen, H.G. Zhang, and C.W. Yin, ‘‘An Output Tracking Control for Nonlinear Systems with Uncertainties and Disturbances Using Time Delay Control,’’ Cybernetics, vol. 40, no. 3, pp. 229–23, 1997.

[100] S.M. Chin, C.O. Lee, and P. H. Chang, ‘‘An Experimental Study on the Position Control of an Electro-Hydraulic Servo System Using Time Delay Control,’’ Control Engineering. Practice., vol. 2, no. 1, pp. 41–48. Feb. 1994

[101] H. Elmali, and N. Olgac, , ‘‘Sliding Mode Control With Perturbation Estimation ~SMCPE: A New Approach,’’ Int. J. Control, 56~4, pp. 923–941, 1992.

[102] P. H. Chang, S.H. Park, and J. H. Lee, ‘‘A Reduced Order Time Delay Control for Highly Simplified Brushless DC Motor,’’ ASME J. Dyn. Syst., Meas., Control, 121~3, pp. 556–560., 1999.

[103] J. Han, “From PID to active disturbance rejection control,” IEEE Trans. Ind. Electron., vol. 56, no. 3, pp. 900–906, Mar. 2009.

[104] L. Guo and S. Cao, “Anti-disturbance control theory for systems with multiple disturbances: A survey,” ISA Transactions, vol. 53, no. 4, pp. 846–849, Jul. 2014.

[105] J. Han, “Extended state observer for a class of uncertain plants,” Control and Decision (in Chinese), vol. 10, no. 1, pp. 85–88, 1995.

[106] B. Z. Guo and Z. L. Zhao, “On the convergence of an extended state observer for nonlinear systems with uncertainty,” System Control Letters, vol. 60, no. 6, pp. 420–430, Jun. 2011.

[107] W. Chen, J. Yang, L. Guo and S. Li, “Disturbance-Observer-Based Control and Related Methods—An Overview,” IEEE Transactions on Industrial Electronics, vol. 63, no. 2, pp. 1083-1095, Feb. 2016.

[108] Q.-C. Zhong, A. Kuperman, and R.-K. Stobart, “Design of UDE based controllers from their two-degree-of-freedom nature,” Int. J. Robust Nonlinear Control, vol. 17, no. 21, pp. 1994–2008, 2011.

[109] R. K. Stobart, A. Kuperman, and Q. C. Zhong, “Uncertainty and disturbance estimator-based control for uncertain LTI-SISO systems with state delays,” Trans. ASME, J. Dynamic System, Measurement, and Control, vol. 133, no. 2, 2011, Art. ID. 024502.

[110] Z. Tian, Z. J. Lyu, J. Yuan, “UDE-based sliding mode control of DC-DC power converters with uncertainties”, Control Engineering Practice, vol. 83, pp: 116-128, Feb 2019.

[111] S. Y. Gadelovits, Q. Zhong, V. Kadirkamanathan and A. Kuperman, “Uncertainty and Disturbance Estimator-Based Controller Equipped with a Time-Delayed Filter to Improve the Voltage Quality of Inverters”, vol. 66, no. 1, pp: 459-469, Jan. 2019.

[112] H. Shim and N. H. Jo, “An almost necessary and sufficient condition for robust stability of closed-loop systems with disturbance observer,” Automatica, vol. 45, no. 1, pp. 296–299, Jan. 2009.

[113] Y. Huang and W. C. Xue, “Active disturbance rejection control: Methodology and theoretical analysis,” ISA Trans., vol. 53, no. 4, pp. 963–976, 2014.

[114] W.-H. Chen, “Disturbance observer-based control for nonlinear systems,” IEEE/ASME Trans. Mechatronics, vol. 9, no. 4, pp. 706–710, Dec. 2004.

[115] L. Guo and W.-H. Chen, “Disturbance attenuation and rejection for systems with nonlinearity via DOBC approach,” Int. J. Robust Nonlinear Control, vol. 15, no. 3, pp. 109–125, Feb. 2005.

[116] I. Aharon, D. Shmilovitz and A. Kuperman, “Phase Margin Oriented Design and Analysis of UDE-Based Controllers Under Actuator Constraints”, IEEE Transactions of Industrial Electronics, vol. 65, no. 10, pp: 8133-8141, OCT 2018.

[117] Yang, B. Jiang, L. Zhang, C. K, “Perturbation observer-based adaptive passive control for nonlinear systems with uncertainties and disturbances.” Transactions of the Institute of Measurement, 40(4):1223-1236, FEB 2018.

[118] Yang, B. Jiang, L. Yao, Wei. “Perturbation observer based adaptive passive control for damping improvement of multi-terminal voltage source converter-based high voltage direct current systems”, Transactions of the Institute of Measurement and Control, vol. 39, no. 9, pp: 1409-1420, SEP 2017.

[119] Y.A.R.I. Mohamed. “Design and implementation of a robust current-control scheme for a PMSM vector drive with a simple adaptive disturbance observer”. IEEE Transactions on Industrial Electronics, vol.4, no. 4, pp:1981–1988, 2007.

[120] M. A. Mahmud, H. R. Pota, M. Aldeen and M. J. Hossain, “Partial Feedback Linearizing Excitation Controller for Multimachine Power Systems to Improve Transient Stability,” IEEE Transactions on Power Systems, vol. 29, no. 2, pp. 561-571, March 2014.

[121] R. Yan, Z. Y. Dong, T.K. Saha, R. Majumder, “A power system nonlinear adaptive decentralized controller design”, Automatica, vol. 46, pp. 330, 2010.

[122] D. N. Kosterev, C. W. Taylor, and W. A. Mittelstadt, “Model validation

for the august 10,1996 wscc system outage," IEEE Transactions on Power Systems., vol. 14, no. 3, pp. 967–979, 1999.

[123] "1996 system disturbances, Review of Selected 1996 Electric System Disturbances in North America", North American Electric Reliability Council, Princeton, New Jersey, 08540-5731, August 2002. Available https://www.nerc.com/pa/rrm/ea/System%20Disturbance%20Reports%20DL/1996SystemDisturbance.pdf.